General Disclaimer

One or more of the Following Statements may affect this Document

- This document has been reproduced from the best copy furnished by the organizational source. It is being released in the interest of making available as much information as possible.

- This document may contain data, which exceeds the sheet parameters. It was furnished in this condition by the organizational source and is the best copy available.

- This document may contain tone-on-tone or color graphs, charts and/or pictures, which have been reproduced in black and white.

- This document is paginated as submitted by the original source.

- Portions of this document are not fully legible due to the historical nature of some of the material. However, it is the best reproduction available from the original submission.

Produced by the NASA Center for Aerospace Information (CASI)

(NASA-CR-143254) AN INVESTIGATION OF THE SNS JOSEPHSON JUNCTION AS A THREE-TERMINAL DEVICE Ph.D. Thesis (Stevens Inst. of Tech.) 150 p HC $5.75 CSCL 20I

N75-29907

Unclas
G3/76 15267

ATS-15267

SIT-P278 (6/73)

UNCLASSIFIED

DEPARTMENT OF PHYSICS

Proximity Effect Between Superconducting and Normal Metals

Second Technical Report

An Investigation of the SNS Josephson Junction as a Three-Terminal Device

June 1973

Hans Meissner

and

George P. Prans

NASA Grant No. NGL 31-003-020
Office of Research Grants and Contracts
Office of Space Science and Applications
National Aeronautics and Space Administration
Washington, D.C. 20546

STEVENS INSTITUTE OF TECHNOLOGY
CASTLE POINT STATION
HOBOKEN, NEW JERSEY 07030

AN INVESTIGATION OF THE SNS JOSEPHSON JUNCTION AS A THREE-TERMINAL DEVICE

by

George Paul Prans

A DISSERTATION

Submitted to the Faculty of the Stevens Institute of Technology in partial fulfillment of the requirements for the degree of

DOCTOR OF PHILOSOPHY

George Paul Prans, Candidate

ADVISORY COMMITTEE

Co-Chairman

Co-Chairman

STEVENS INSTITUTE OF TECHNOLOGY

Castle Point, Hoboken, New Jersey

1973

AN INVESTIGATION OF THE SNS JOSEPHSON JUNCTION AS A THREE-TERMINAL DEVICE

ABSTRACT

Following the discovery by H. Meissner and R.R. Rockefeller of the control of an SNS Josephson junction by a current entering the normal region and leaving through one of the superconducting regions, an investigation was initiated to study the phenomenon and to characterize the new device as a circuit element.

The effect of the control current on the junction current was described by an empirical parameter α_o. The resulting transistor-like output current-voltage characteristics support the findings of Rockefeller.

The value of α_o was typically 0.8, and it was discovered to depend upon the ratio of the resistances of the two halves of the N layer. In particular, α_o could be varied by introducing a thin oxide layer at one of the SN interfaces. In theory, α_o can be predetermined anywhere in the range $0 < \alpha_o < 1$ through variations in the thin-film deposition procedure.

A low-frequency, lumped, nonlinear model based on that of Stewart and McCumber was proposed to describe the electrical characteristics of the device. The three-terminal current-voltage characteristics

were in good agreement with those predicted by the model.

A method peculiar to the three-terminal device was developed to plot the dynamic junction resistance as a function of junction current. With this method it was demonstrated that the device was operable at signal frequencies of at least 9.7kHz, the limit of the lock-in amplifier.

The effective thermal noise temperature of the sample was determined to be ~20-30K. With the r.f. shielding of a screened room, it was found to be reduced markedly to ~3K.

A small-signal linearized analysis of the device suggests its use as an impedance transformer. However, due to the present geometry limitations, no transformer action was observed. In theory, with a suitable geometry to reduce the input lead resistance, transformer ratios as high as α_o^{-1} are possible under favorable conditions.

In the linear approximation the present device is reciprocal and no power gain is possible. It is felt that the device has promise to become a "superconducting transistor" with suitable metallurgical and geometrical improvements.

TABLE OF CONTENTS

I. INTRODUCTION

A. Preface 1

B. Superconductivity

1. Origins 2
2. Theoretical Background 4
3. The Pippard Non-Local Theory 7
4. The Ginzburg-Landau Theory 9
5. The Microscopic Theory 10

II. THEORY OF THE EXPERIMENT

A. The Theory of an SN Junction 13

B. The Josephson Effect 17

C. The Magnetic Properties of the Josephson Junction

1. Magnetic Field Dependence of the Josephson Supercurrent 22
2. The Josephson Penetration Depth 25

D. Electrical Characteristics of the Josephson Junction

1. The Current-Voltage Characteristics 27
2. The Effect of Fluctuations 31

III. DESCRIPTION OF THE EXPERIMENT

A. Introduction 33

B. The Evaporator/Cryostat 35

C. The Vapor-Deposition System 39

D. The Cryostat 40

E. The Magnetic Field Coils 41

F. The Substrate Holder and Thermometer 42

G. The Sample and Its Preparation 45

H. Measurements

1. Film Thickness 51

2. The Thin-Film Electronic Mean Free Path 52

3. The Experimental Arrangement for I_J vs V Characteristics 54

4. The Experimental Arrangement for I_J vs ΔV Curves 59

IV. EXPERIMENTAL RESULTS

A. The Samples 61

B. The Critical Current of the Tin Film 69

C. The Effect of External Magnetic Field 77

D. The Current-Voltage Characteristics of the Device

1. I_J vs V Characteristics with $I_N = 0$ 82

2. I_J vs V Characteristics with $I_N \neq 0$ 90

E. Characteristic Resistances 104

F. Fluctuation Effects 108

V. CHARACTERISTICS OF THE DEVICE AS A CIRCUIT ELEMENT

A. Linear Model, Twoport Characteristics 114

B. Improvements Necessary for Amplification 127

VI. CONCLUSIONS 135

BIBLIOGRAPHY

ACKNOWLEDGEMENTS

I. INTRODUCTION

I.A. Preface

Following the experiments by H. Meissner and Bedard[1] and by H. Meissner[2] on the properties of the two-terminal, superconductor/normal-conductor/superconductor (SNS) junction, H. Meissner and Rockefeller[3] invented the three-terminal, SNS Josephson junction device. Using an SNS mechanical-contact junction consisting of two crossed tin wires sandwiching an intermediate film of gold, they discovered that the introduction of a current directly into the center layer of the sandwich would modify the two-terminal electrical characteristics of the device.[4] The resulting current-voltage characteristics of the three-terminal device are not unlike the output characteristics of the bipolar junction transistor.

Since this new transistor-like phenomenon was observed in a device consisting of only three metals at cryogenic temperatures, it had the potential advantage over the semiconductor junction transistor of ease of fabrication, low thermal noise, and, due to the very small energies

---

1. H. Meissner and F. Bedard, Phys. Rev. 101, 126 (1956).
2. H. Meissner, Phys. Rev. 109, 686 (1958).
3. H. Meissner and R.R. Rockefeller, U.S. Patent No. 3,689,780, Sept. 5, 1972.
4. R.R. Rockefeller, Ph.D. thesis, Stevens Institute of Technology, unpublished (1970).

characteristic of superconductivity, greater sensitivity. In addition, because the SNS sandwich is a tunnel junction, the intrinsic frequency limit of the device might be as large as that corresponding to the energy gap in the superconductor.

The present investigation was initiated to (a) study the properties of the new device in thin-film form, (b) determine the physical mechanism of the phenomenon, (c) propose a circuit model for the device, and (d) determine its applicability as an amplifier.

I. B. Superconductivity

I. B. 1. Origins

The seeds of the science of superconductivity were planted in 1908 when H. Kamerlingh Onnes first succeeded in liquefying helium. Liquid helium boils at 4.2K under one atmosphere of pressure, and it serves as a liquid bath environment for the study of phenomena at low temperatures.

Superconductivity was discovered in 1911 when Onnes[5,6] found that the electrical resistance of a mercury wire drops quickly to an immeasurably small value as it is cooled below a critical temperature. Sub-

---

5. H. K. Onnes, Leiden Comm. 122b, 124c (1911).
6. H. K. Onnes, Leiden Comm., Suppl. No. 34 (1913).

sequently, it was discovered that many polyvalent metals had their resistance drop to an apparently zero value below a characteristic temperature called the transition temperature, T_C. These metals are called superconductors and the currents which pass through them without experiencing a measurable resistance are called supercurrents.

After the initial discovery of superconductivity, Onnes soon found that the resistive state of a superconductor would reappear if a magnetic field larger than a certain value, termed the critical field H_C, is applied to the superconductor. He also noticed that the superconducting state could be quenched if a current larger than a critical value, I_C, is passed through the sample. Later, it was proposed by Silsbee[7] that the critical current produces a magnetic field of value H_C at the surface of a bulk superconductor.

In 1933, Walther Meissner and R. Ochsenfeld[8] discovered that the superconducting state is not sufficiently described by perfect conductivity but that perfect diamagnetism is also fundamental to the phenomenon. This was demonstrated when they found that a cylinder of tin situated in an applied uniform magnetic field expels the magnetic flux when it is cooled below the critical temperature. This is known as the "Meissner effect." It implies that the transition from the supercon-

---

7. F.B. Silsbee, J.Wash.Acad.Sci. 6, 597 (1916).
8. W. Meissner and R. Ochsenfeld, Naturwiss. 21, 787 (1933).

ducting state to the non-superconducting (normal) state is thermodynamically reversible (i.e., the final state of the specimen is not dependent on its path of transition).

I.B.2. Theoretical Background

In 1935, H. and F. London proposed a phenomenological theory[9] of the electromagnetic properties of superconductors which has been found to be extremely useful. They proposed two equations to describe the supercurrent. The first relates the acceleration of the superconducting electrons to the force of the electric field $\vec{E}$ by*

$$d\vec{j}_s/dt = (c^2/4\pi\lambda_L^2)\,\vec{E}, \qquad \text{I.B.2.1}$$

where $\vec{j}_s$ is the supercurrent density, c is the speed of light, and λ_L is a characteristic length, called the superconducting penetration depth, given by Eq. I.B.2.2 at absolute zero temperature.

$$\lambda_L(0) = (mc^2/4\pi n_s e^2)^{1/2} \qquad \text{I.B.2.2}$$

The quantities m and e are the effective mass and charge of the electron, respectively, and n_s is the density of superconducting electrons in the

---

* c.g.s. units will be used throughout this work unless otherwise specified.

9. F. London and H. London, Proc. Roy. Soc. (London) A149, 71 (1935).

metal.* Typically, $\lambda_L(0)$ is of the order of 10^{-5} to 10^{-6} cm. The variation of λ_L with temperature may be represented satisfactorily by the empirical relation

$$\lambda_L(t) = \lambda_L(0)\,(1 - t^4)^{-1/2}, \qquad \text{I.B.2.3}$$

where $t \equiv T/T_C$ is the reduced temperature.

The second London equation is phenomenological and is given by

$$\vec{j}_s(x) = -(c/4\pi\lambda_L^2)\,\vec{A}\,, \qquad \text{I.B.2.4}$$

where $\vec{A}$ is the vector potential defined by $\nabla \times \vec{A} = \vec{H}$. The simultaneous solution of Eq. I.B.2.4 with Maxwell's equation for the static magnetic field penetration into a superconductor filling the half-space $x > 0$ is

$$H(x) = H(0)\,\exp(-x/\lambda_L)\,, \qquad \text{I.B.2.5}$$

where x is the distance into the superconductor and H(0) is the mag-

---

* implicit here is a phenomenological two-fluid model of superconductivity[10] where it is assumed that a certain fraction of the electrons are in a superconducting state which does not contribute to the entropy of the system, and the remaining electrons are in the normal state. Although not rigorously correct in the light of the current microscopic theory, this model is helpful in depicting many aspects of superconductivity.

10. C. Gorter and H.B.G. Casimir, Physica 1, 306 (1934).

netic field at the surface of the superconductor. Thus, the theory predicts that the magnetic field does not disappear at the surface of a superconductor but falls off exponentially with distance into the metal with a characteristic length called the London penetration depth λ_L. The predicted field penetration was first confirmed by Shoenberg[11] in 1940. The London theory provides a useful approximate description of a superconductor where changes occur slowly over a distance λ_L (i.e., for low frequencies and long electronic mean free paths). The next section will introduce a theory which accounts for these short-range disturbances.

In the absence of a magnetic field, the superconductor experiences a second-order transition in returning to the normal state. However, in a magnetic field, the transition occurs when $H = H_C$ (for $T < T_C(H=0)$ and is a first order transition. The variation of H_C with temperature is described to within a few percent by

$$H_C(t) = H_C(0)(1 - t^2). \qquad \text{I.B.2.6}$$

---

11. D. Shoenberg, Proc. Roy. Soc. (London) A175, 49 (1940).

I.B.3. Pippard Non-Local Theory

In 1953, Pippard[12,13] found that the penetration depth was dependent upon the size of the normal electronic mean free path, ℓ. Such a dependence of $\lambda(0)$ on ℓ is incompatible with the original London model. Using the analogy of the anomalous skin effect in normal metals, and other arguments, Pippard proposed that the London equation (Eq. I.B.2.4) be replaced by a non-local relation where the supercurrent density at a point should be determined by an integral of the field over a distance of the order of $\xi(\ell)$, the Pippard coherence length. $\xi(\ell)$ is a characteristic length of the superconductor describing the distance over which perturbing effects are important. Experimentally, Pippard found that $\xi(\ell)$ obeyed the relationship

$$1/\xi(\ell) = 1/\xi_o + 1/0.8\,\ell \,, \qquad \text{I.B.3.1}$$

where ξ_o is a constant of the superconductor and is identified with the range of coherence of the pure superconductor at $T = 0$. Equation I.B.3.1 indicates that $\xi(\ell)$ is smaller than ξ_o and decreases with decreasing ℓ.

ξ_o has been determined from the microscopic theory[14] (and

---

12. A.B. Pippard, Proc.Roy.Soc. (London) A216, 547 (1953).
13. A.B. Pippard, Proc.Roy.Soc. (London) A203, 210 (1950).
14. J. Bardeen, L.N. Cooper, and J.R. Schrieffer, Phys.Rev. 108, 1175 (1957).

experimentally by Pippard), and it is given by

$$\xi_o = 0.18\hbar v_f / kT_C , \qquad \text{I.B.3.2}$$

where v_f is the electron velocity at the Fermi surface and h is Planck's constant. ξ_o is approximately the minimum size of a localized ensemble of electrons at the Fermi surface with the energy kT_C, where k is Boltzmann's constant.

The effect of Pippard's theory was to make the theory non-local and to replace the London penetration depth with one dependent upon the mean free path. For short mean-free-path superconductors (i.e., $\xi(\ell) << \lambda$, termed the "London limit"), the penetration depth is given by[15]

$$\lambda = [\xi_o / \xi(\ell)]^{1/2} \lambda_b , \qquad \text{I.B.3.3}$$

where λ_b is the empirical penetration depth for a bulk sample and takes the place of the London value. The experimental values of these intrinsic parameters for tin are $\lambda_b = 510\text{Å}$[16] and $\xi_o = 2100\text{Å}$.[17]

---

15. E.A. Lynton, Superconductivity (Methuen, London, 1964), p. 46.
16. Ibidem, p. 38.
17. e.g., T.E. Faber and A.B. Pippard, Proc. Roy. Soc. (London) A231, 336 (1955).

I.B.4. The Ginzburg-Landau Theory

In 1950, Ginzburg and Landau introduced a non-local phenomenological theory[18] which provided a powerful intuitive insight into superconductivity years before the development of the microscopic theory. They proposed the existence of a complex wave function $\psi(x)$ to characterize the superconducting state, where a normalization was chosen such that $\psi^*(x)\psi(x)$ represented the density of superconducting electrons. Using a free-energy approach, they arrived at two equations,

$$\alpha\psi + \beta|\psi|^2\psi + (1/2m)(-i\hbar\nabla - 2eA/c)^2\psi = 0 , \qquad \text{I.B.4.1}$$

$$\vec{j}_s = (e\hbar/im)(\psi^*\nabla\psi - \psi\nabla\psi^*) - (4e^2/mc)\psi^*\psi\vec{A} , \qquad \text{I.B.4.2}$$

called the Ginzburg-Landau equations. α and B are two coefficients from the expansion of the free energy. In pure metals for weak fields, where $\nabla\psi$ is small, Eq. I.B.4.2 reduces to a form of London's equation (Eq. I.B.2.4).

For the case where the currents and the magnetic fields are sufficiently small such that $\psi(x)$ (hereafter referred to as the "order parameter") suffers only perturbations from the field-free state and the vector potential can be neglected, Eq. I.B.4.1 reduces in the one-dimensional case to

---

18. V.L. Ginzburg and L.D. Landau, Sov. Phys.-JETP 20, 1064 (1950).

$$\xi_{GL} d^2\Psi/dx^2 + \Psi - \Psi^3 = 0 , \qquad \text{I.B.4.3}$$

where $\Psi(x)$ is a reduced order parameter and ξ_{GL} is a characteristic length over which $\Psi(x)$ cannot vary rapidly. ξ_{GL} is called the Ginzburg-Landau coherence length, and near T_C it has the form[19]

$$\xi_{GL}(T) = 0.74\,\xi_o(1 - t)^{-1/2} \qquad \text{I.B.4.4}$$

(for a "clean" metal)

$$\xi_{GL}(T) = 0.85\,(\xi_o \ell)^{1/2}(1 - t)^{-1/2} \qquad \text{I.B.4.5}$$

(for a "dirty" metal).

A "dirty" metal is one for which the electronic mean free path ℓ is much less than the coherence length ξ_{GL}.

I.B.5. The Microscopic Theory

A brief sketch of the microscopic theory is presented here as an aid to understanding the physical operation of the three-terminal Josephson junction device to be described in later chapters.

In 1956, Bardeen, Cooper, and Schrieffer proposed a quantum-mechanical theory[14] of superconductivity based on the interaction of electrons in a metal lattice. It is known as the "BCS" theory,

---

19. P.G. deGennes, Superconductivity of Metals and Alloys (Benjamin, N.Y., 1966), p. 225.

and it has been enormously useful in providing a derivation from first principles of the properties of superconductors.

Essentially, the theory depicts a superconductor as having a ground state composed of electron pairs (Cooper pairs). The electron pairs are formed through a mutual interaction with the lattice waves (phonons) which, for the proper values of electron spin and momentum, can effect an attraction between two electrons. This binding is extremely weak, however, and the "diameter" of the Cooper pair is as large as thousands of Angstroms ($\sim \xi_{GL}$). Thus, the electrons of each bound pair simultaneously range over a volume that contains millions of other electron pairs. This spatial overlapping of the pairs requires that the motion of all the pairs be correlated.[20] BCS showed that all the pairs in the superconductor may be described by a single macroscopic wave function or "order parameter" and have, in the absence of applied fields, identical quantum-mechanical phase. As will be seen later, this long-range coherence makes possible the Josephson effect.

The ground state of pairs is separated from the single-electron states by an energy gap $\Delta(T)$, where $\Delta(0) \sim kT_C$, which is essentially the energy necessary to break up a Cooper pair. The excited states consist of unpaired electrons and holes (vacant electron states in the

---

20. e.g., for a detailed explanation see D. J. Scalapino, Tunneling Phenomena in Solids, ed. by E. Burstein and S. Lundqvist (Plenum, N.Y., 1969), Ch. 32, p. 477-8.

Fermi sea) with energies at least $\Delta(T)$ above the ground state of pairs. These excited electrons or holes, which carry the normal current in nonequilibrium superconductors, are called "quasiparticles."[21]

Gorkov[22] has demonstrated that the Ginzburg-Landau equations (Eqs. I. B. 4. 1-2) are derivable from the microscopic theory. Pippard's intrinsic coherence length (ξ_o) is also confirmed by the BCS theory.

---

21. for a discussion of the quasiparticle concept see C. Kittel, Quantum Theory of Solids (J. Wiley, N. Y., 1963), p. 84.

22. L. P. Gorkov, Sov. Phys. - JETP 10, 593, 998 (1960).

II. THEORY OF THE EXPERIMENT

II.A. The Theory of an SN Junction

If a normal conductor N is in good electrical contact with a superconductor S, Cooper pairs can "leak" from S to N. The result of this transfer of pairs to the N metal (and quasiparticles to the S metal) is a lowering of the degree of "order" (i.e., degree of superconductivity) in S near the SN boundary. Experimental evidence of this effect in the form of a depressed transition temperature of S is documented in the pioneering work of H. Meissner.[1,2,23] As will be shown, this phenomenon, known as the "proximity effect", is strongly dependent upon the thicknesses of both the S and N metals and their respective coherence lengths ξ_{GL} and ξ_N.

In a metal near an SN boundary where the degree of order of the superconductor varies spatially, the BCS theory is no longer applicable.[24] For this case, deGennes[25] introduces a spatially-dependent degree of order called the "condensation amplitude," F(x), where $|F(x)|^2$ is proportional to the probability of finding a Cooper pair at x (i.e., it represents the superfluid density). F(x) is equivalent to the Ginzburg-Landau order parameter $\Psi(x)$, and it is related to the pair potential $\Delta(x)$ by $\Delta(x) = V(x)\,F(x)$, where V(x) is the electron-electron interaction

23. H. Meissner, Phys. Rev. 117, 672 (1960).
24. J. Clarke, Proc. Roy. Soc. A308, 447 (1969).
25. P. G. deGennes, Rev. Mod. Phys. 36, 224 (1964), p. 227.

potential. $\Delta(x)$ is analogous to the energy gap Δ of the BCS theory. It is the fact that the condensation amplitude cannot change abruptly at an SN boundary, but only over a distance of the order of a coherence length, which gives rise to the proximity effect.

Consider the one-dimensional problem of a normal metal (occupying the half-space $-\infty < x < 0$) in contact with a superconductor (occupying the half-space $0 < x < \infty$) at the plane $x=0$. According to Deutscher and deGennes,[26] the spatial variation of the condensation amplitude in the N metal is given by

$$F_N(x) \propto \exp(-k_N x) \qquad \text{II.A.1}$$

for $k_N x > 1$, where

$$k_N^{-1} = \xi_N [1 + 2/\ell n(T/T_{CN})] \qquad \text{II.A.2}$$

represents the depth of penetration of pairs into the normal metal. T_{CN} is the transition temperature of the normal metal (here a normal metal is defined as a metal above its transition temperature which, in some cases, may be absolute zero), and ξ_N is the coherence length in the normal metal, where

---

26. Superconductivity (Marcel Dekker, Inc., N.Y., 1969), ed. by R.D. Parks, p.1006.

$$\xi_N = \hbar v_N / 2\pi kT \qquad \text{II.A.3}$$

(in the clean limit, $\xi_N \ll \ell_N$)

$$\xi_N = (\hbar v_N \ell_N / 6\pi kT)^{1/2} \qquad \text{II.A.4}$$

(in the dirty limit, $\xi_N \gg \ell_N$) ,

where v_N and ℓ_N are the Fermi velocity and mean free path in the normal metal. The Ginzburg-Landau equations cannot be used to determine the coherence length ξ_N in the normal metal.[27]

In the superconductor, the condensation amplitude (or order parameter) is considerably depressed near the SN boundary by the presence of the normal metal. Its value as a function of distance into the superconductor is given by the solution to Eq. I. B. 4. 3 as

$$F_s(x)/F_s(\infty) = \Psi(x) = \tanh[(x-x_o)/2\xi_{GL}] , \qquad \text{II.A.5}$$

where $F_s(\infty)$ is the equilibrium value of the condensation amplitude in S far from the SN interface. If the electrical contact between S and N is good, if the density of states in N is comparable to that in S, and if N is thick compared to ξ_o, then the value of x_o in Eq. II. A. 5 is approximated[28] by $-x_o \approx b \sim \xi_o$ for temperatures near T_C where $\xi_o \ll \xi_{GL}$. The parameter "b" is the "extrapolation length" of $F_s(x)$ into the N

27. P. G. deGennes and E. Guyon, Phys. Letters 3 , 168 (1963), p. 169.
28. see ref. 19, p. 233.

metal (see Fig. 1). The value of $F_s(x)$ at the interface in terms of b then becomes

$$F_s(0)/F_s(\infty) = b/\sqrt{2}\,\xi_{GL} \quad . \qquad \text{II. A. 6}$$

A plot of the variation of $F_s(x)$ with x near an SN boundary is shown in Fig. 1 for a value of $b=0.2\xi_{GL}$. As shown in Fig. 1, a reasonable

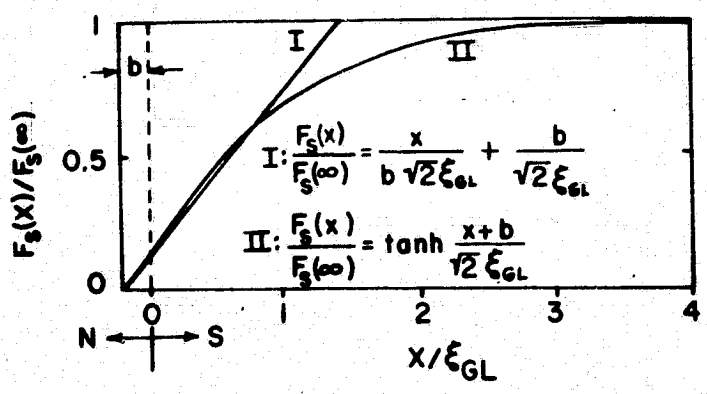

Fig. 1. $F_s(x)/F_s(\infty)$ vs x.

approximation to Eq. II. A. 5 is given by

$$F_s(x) = F_s(\infty)x/(b+\sqrt{2}\,\xi_{GL}) + F_s(\infty)b/\sqrt{2}\xi_{GL} \qquad \text{II. A. 7}$$

for $0<x<\sqrt{2}\xi_{GL}$, and

$$F_s(x) = F_s(\infty) \qquad \text{II. A. 8}$$

for $x > \sqrt{2}\xi_{GL}$. Then, from Eq. II.A.7 and the appropriate boundary conditions[29, 30] for a dirty metal, the extrapolation length is found to be

$$b = v_s \ell_s \xi_N(T) / v_N \ell_N \ , \qquad \text{II.A.9}$$

where v and ℓ are the respective Fermi velocity and mean free path in the S and N metals.

The value of the condensation amplitude in the N metal can be approximated from Eq. II.A.1 and Eq. II.A.6, with the boundary condition[29, 30] that $F_N(0) = F_s(0)$, to be

$$F_N(x) = [F_s(\infty) b / \sqrt{2}\xi_{GL}] \exp(-|x|/\xi_N) \ , \qquad \text{II.A.10}$$

where T_{CN} is assumed to be zero.

This concludes the discussion of the variation of the condensation amplitude in the vicinity of an SN boundary.

II.B. The Josephson Effect

The fact that a supercurrent can flow through a thin layer of non-superconducting metal which is sandwiched between two superconductors was experimentally discovered by H. Meissner.[2] Four years later, Josephson[31] proposed a theory predicting such a phenomenon

29. see ref. 25, p. 231.
30. N.R. Werthamer, Phys. Rev. 132, 2440 (1963).
31. B.D. Josephson, Phys. Letters 1, 251 (1962).

from the viewpoint of quantum-mechanical tunneling of Cooper pairs through a barrier layer. This phenomenon is now known as the "Josephson effect," and the superconductor/barrier/superconductor (SBS) sandwich is called a "Josephson junction."

Although the term "Josephson junction" had initially referred only to SBS sandwiches, it now includes a host of devices[32] wherein two superconductors are separated by a "weak link" which allows the passage of a limited supercurrent. The following development shall be restricted in particular to SBS devices, although, many of the following results will be applicable to all the "Josephson junction" devices.

As described in section I.B.5, all the Cooper pairs in a superconductor which is free of applied fields have the same quantum-mechanical phase. If two superconductors are brought together from a large separation, the relative phases of the condensation amplitude, $F_s = |F_s| \exp(i\theta)$, in the two superconductors will be arbitrary until, at a separation of the order of a coherence length, the phases of the two superconductors "lock in" to be equal to each other. This long-range order is similar to that of the bulk superconductor where order is a cooperative effect brought about by motion of the electrons from one part of the system to another. In the case of a thin barrier (i.e., a weak link) between two superconductors, Cooper pairs can tunnel

32. e.g., see J. Clarke, Proc. IEEE 61, 8 (1973).

through the barrier and provide this coupling. In practice, the tunneling barrier is usually either an insulating layer of thickness <30Å or a normal-metal layer of thickness up to several thousand Angstroms.

As described by Anderson[33], the phase θ of the condensation amplitude in a superconductor is given by

$$d\theta/dt = -\mu/\hbar \quad , \qquad \text{II.B.1}$$

where μ is the chemical potential of the Cooper pair. The application of Eq. II.B.1 to the phase difference, $\theta_2 - \theta_1 \equiv \phi$, across a weak link with a corresponding voltage difference of $V = (\mu_1 - \mu_2)/2e$ results in

$$d(\theta_2 - \theta_1)/dt = d\phi/dt = 2eV/\hbar \quad , \qquad \text{II.B.2}$$

which is known as the "Josephson frequency" relation, and

$$\omega_o \equiv 2eV/\hbar \qquad \text{II.B.3}$$

is defined as the Josephson frequency (corresponding to 483MHz/μV of junction voltage).

Consider now the SNS (superconductor/normal-metal/superconductor) junction shown in Fig. 2, where the two superconductors are assumed identical so that the bulk value, $F_s(\infty)$, of the condensation amplitude

---

33. P.W. Anderson, Rev. Mod. Phys. 38, 298 (1966).

is the same in each. Since the contribution to the condensation

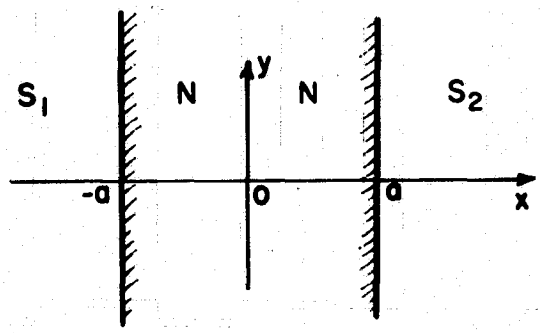

Fig. 2. An SNS sandwich with N-metal thickness 2a.

amplitude within the N region is now from two superconductors, Eq. II. A. 10 becomes

$$F_N(x)=[F_s(\infty)b/\sqrt{2}\xi_{GL}]\{\exp[-(x+a)/\xi_N+i\theta_1]+\exp[(x-a)/\xi_N+i\theta_2]\}, \qquad \text{II. B. 4}$$

where θ_1 and θ_2 are the values of the phase in the two superconductors, respectively. The Josephson supercurrent j_s may be found from Eq. I. B. 4. 2, and for negligible magnetic fields it becomes

$$j_s = (e\hbar/mi)(F^* dF/dx - F dF^*/dx). \qquad \text{II. B. 5}$$

Substituting the relation for $F_N(x)$ from Eq. II. B. 4 into Eq. II. B. 5, the x dependence drops out and j_s becomes

$$j_s = j_{Cm} \sin(\theta_2 - \theta_1) , \qquad \text{II. B. 6}$$

where

$$j_{Cm} = \frac{2 v_s^2 \ell_s^2 e\hbar \, |F_s(\infty)|^2 \xi_N}{v_N^2 \ell_N m \xi_{GL}^2} \exp(-t_N/\xi_N). \qquad \text{II. B. 7}$$

Equation II. A. 9 has been used here for b, and $t_N = 2a$ is the thickness of the normal metal. j_{Cm} is called the critical Josephson current density, and, as can be seen, it depends exponentially on t_N.

Equation II. B. 6 is the relation first derived by Josephson using a tunneling-Hamiltonian method.[31, 34] It describes the "d. c. Josephson effect," wherein a supercurrent up to some critical value j_{Cm} can pass through a Josephson junction with zero voltage drop across the junction. For currents above j_{Cm}, a voltage appears across the junction and the phase difference varies in time as described by Eq. II. B. 2. Substituting this time-dependent phase difference into Eq. II. B. 6 results in an alternating supercurrent. This is known as the "a. c. Josephson effect."

The temperature dependence of j_{Cm} may be approximated from the temperature dependence of the parameters in Eq. II. B. 7 to be[35]

---

34. B. D. Josephson, Rev. Mod. Phys. 36, 216 (1964).
35. e. g., see ref. 19, p. 238.

$$j_{Cm} \propto (1-t)^2, \qquad \text{II.B.8}$$

for $t \lesssim 1$, where $t \equiv T/T_{Csns}$ is the reduced temperature, and T_{Csns} is the transition temperature of the Josephson junction, defined as that temperature where j_{Cm} is zero (for H=0). Equation II.B.8 has been confirmed experimentally in the work of Clarke[24] and Rockefeller.[4]

II.C. The Magnetic Properties of the Josephson Junction

II.C.1. Magnetic Field Dependence of the Josephson Supercurrent

Thus far, the Josephson junction has been treated in the absence of magnetic fields. When magnetic fields are present, a term, $(-2e/\hbar c)\int_1^2 \vec{A}\cdot d\vec{\ell}$, must be added[34, 36] to the phase difference across the junction so as to make j_s gauge invariant.

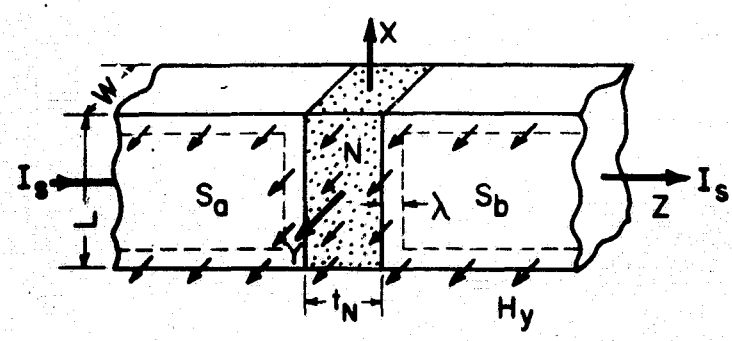

Fig. 3. The magnetic field penetration in an SNS junction. I_s is the Josephson supercurrent.

36. P.W. Anderson and J.M. Rowell, Phys. Rev. Letters 10, 230 (1963).

Figure 3 is a diagram of an SNS junction illustrating the penetration of an external magnetic field, $\vec{H}$, parallel to the plane of the junction. An expression for the total supercurrent I_s through the junction as a function of H can be obtained by integrating Eq. II. B. 6 (with the aforementioned addition to the phase difference to preserve gauge invariance) over the current-carrying area of the junction ($|x| \leq L/2$, $|y| \leq W/2$). The resulting expression for I_s is

$$I_s = I_C \sin(\theta_2 - \theta_1) , \qquad \text{II. C. 1. 1}$$

where.

$$I_C = I_{Cm} \sin(\pi\Phi/\Phi_o)/(\pi\Phi/\Phi_o) , \qquad \text{II. C. 1. 2}$$

$I_{Cm} = j_{Cm}WL$, Φ is the magnetic flux through the junction, and $\Phi_o = hc/2e$* is a quantum of magnetic flux. Thus, the maximum critical Josephson current, I_{Cm}, occurs for H=0; and, for non-zero values of H, the critical current is less than I_{Cm} and varies periodically with H.

For small values of I_s such that the field induced by I_s itself is small (see the following section for the alternate case), the magnetic flux penetrates the junction proper uniformly, and Φ is given by

$$\Phi = HL(t_N + 2\lambda) , \qquad \text{II. C. 1. 3}$$

---

* $\Phi_o = 2.07 \times 10^{-7}$ Gauss cm^2 in the c. g. s. system, and $\Phi_o = h/2e = 2.07 \times 10^{-15}$ Webers in the m. k. s. system.

where λ is the penetration depth into the superconductor (see Fig. 3).

At finite voltages, the current, I_J, through the Josephson junction is composed of both a supercurrent, I_s, and a quasiparticle (normal) current, I_{qp}. The supercurrent has both an alternating (a. c.) and constant (d. c.) component.[37] If a magnetic field, H, is applied to the junction in this finite-voltage region, the amplitude of the supercurrent would be expected to vary periodically with the number of flux quanta in the junction, perhaps somewhat like the variation expressed in Eq. II. C. 1. 2 (where a uniform supercurrent density was assumed*). If the total junction current, $I_J = I_s + I_{qp}$, is fixed at a constant value, then the effects of varying H can be observed as a change in the junction voltage, V. Rockefeller[4] has plotted V vs H and determined that the variation of the supercurrent with H is indeed given by the form of Eq. II. C. 1. 2 for the finite-voltage region. This plot provided a convenient method of measuring the junction diameter in the above work.

---

* the exact current distribution for finite voltages has been treated in reference 37.

37. J. Clarke, Phys. Rev. B 4, 2963 (1971).

II. C. 2. The Josephson Penetration Depth

When the Josephson supercurrent density, j_s, becomes sufficiently large (e.g., due to decreasing T for a thin barrier layer), the magnetic field due to j_s itself will tend to confine j_s to within a distance λ_J of the Josephson junction edges. λ_J is called the "Josephson penetration depth," and it has been shown by Ferrell and Prange[38] that λ_J is given by Eq. II. C. 2. 1 for the simple junction geometry of Fig. 4.

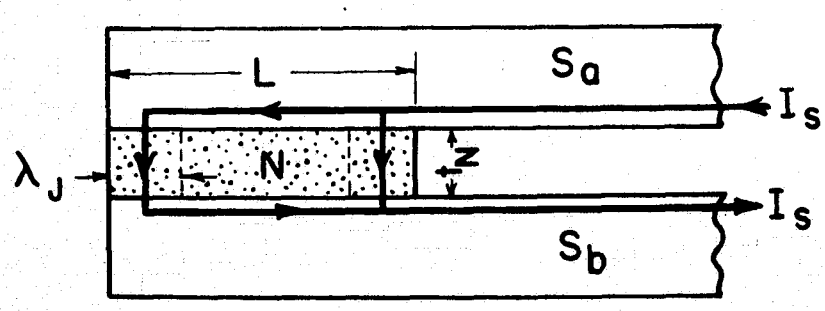

Fig. 4. One-dimensional junction model for $\lambda_J < L/2$ and $I_s < I_C$.

$$\lambda_J = [\hbar c^2 / 8\pi e j_s (t_N + 2\lambda)]^{1/2} \qquad \text{II. C. 2. 1}$$

If, for the model of Fig. 4, j_s is assumed uniform across the junction width, W (i.e., the direction into the paper in Fig. 4), then the total critical current, I_C, is limited by the size of λ_J and is given by

38. R.A. Ferrell and R.E. Prange, Phys. Rev. Letters 10, 479 (1963).

$$I_C \approx j_C 2\lambda_J W \ , \qquad \text{II. C. 2. 2}$$

where j_C is the critical current density. This restriction of the supercurrent to a distance $\sim\lambda_J$ within the edge of the junction is called "self-field limiting," and it is conventional[37] to approximate its onset for a value of j_s such that $\lambda_J \lesssim L/4$. Typically, λ_J is of the order of 0.1mm.

In essence, self-field limiting is a Meissner effect wherein flux is expelled from the center of the junction. In the presence of a small external field, a circulating supercurrent is set up to screen the applied field from the interior of the junction.[39] Thus, for the case of a self-field limited junction, the value of the flux, Φ, penetrating the junction for a given external magnetic field, H, becomes

$$\Phi \approx H2\lambda_J(t_N + 2\lambda) \ , \qquad \text{II. C. 2. 3}$$

where the simple model of Fig. 4 has been used.

---

39. A. M. Goldman and P. J. Kreisman, Phys. Rev. 164, 544 (1967).

II. D. Electrical Characteristics of the Josephson Junction

II. D. 1. The Current-Voltage Characteristics

When the current, I_J, passing through a Josephson junction is constant and less than the critical value, I_C, then the voltage, V, across the junction is zero. However, when $I_J > I_C$, a non-zero voltage appears across the junction and I_J may be composed of both a. c. and d. c. supercurrents and a quasiparticle (normal) current. In the following, an equation relating V to I_J is obtained from a lumped circuit model using the method of Stewart[40] and McCumber.[41]

That the Josephson junction could be approximated by the lumped circuit model shown in Fig. 5 was proposed independently by Stewart[40] and McCumber.[41] The total junction current, I_J, divides into three

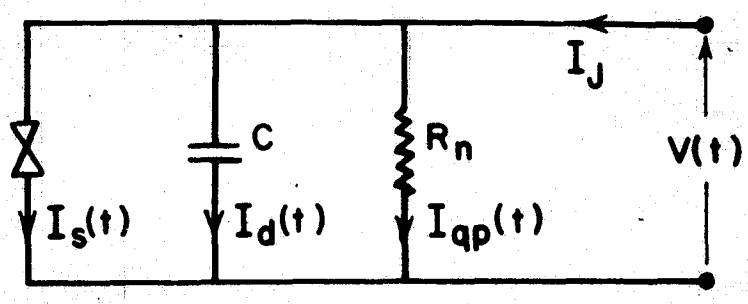

Fig. 5. A lumped, equivalent circuit for a Josephson junction.

components within the junction: a supercurrent $I_s(t)$, a displacement

40. W. C. Stewart, Appl. Phys. Letters 12, 277 (1968).

41. D. E. McCumber, J. Appl. Phys. 39, 3113 (1968).

current $I_d(t)$, and a quasiparticle current $I_{qp}(t)$. For an SNS junction the capacitance, C, can be neglected,[37] and the total junction current, $I_J = I_s(t) + I_{qp}(t)$, can be written as

$$I_J = I_C \sin \phi(t) + v(t)/R_n \ , \qquad \text{II.D.1.1}$$

where the instantaneous junction voltage, v(t), is related to $\phi(t)$, the condensation amplitude phase difference across the junction, by Eq. II. B. 2. If the current I_J is assumed fixed and independent of v(t) (i. e., a constant-current source), then a solution for the time-averaged (d. c.) voltage, V, in terms of I_J can be found from Eqs. II. D. 1. 1 and II. B. 2 to be[40]

$$V = R_n (I_J^2 - I_C^2)^{1/2}, \qquad \text{II.D.1.2}$$

where the quasiparticle resistance, R_n, which actually has a nonlinear voltage dependence[42], has been assumed independent of V. A plot of Eq. II. D. 1. 2 is shown in Fig. 6 for both polarities of I_J. The fact that for $I_J \gtrsim I_C$ the voltage does not jump to the value $I_J R_n$ is indicative of the persistence of d. c. supercurrents in the junction for finite voltages.

The shape of the I_J vs V curve may be changed by shunting the junction externally with a thin-film circuit element. Hansma et al[43] have

---

42. W. C. Scott, Appl. Phys. Letters 17, 166 (1970).

43. P. K. Hansma, G. I. Rochlin, and J. N. Sweet, Phys. Rev. B 4, 3003 (1971).

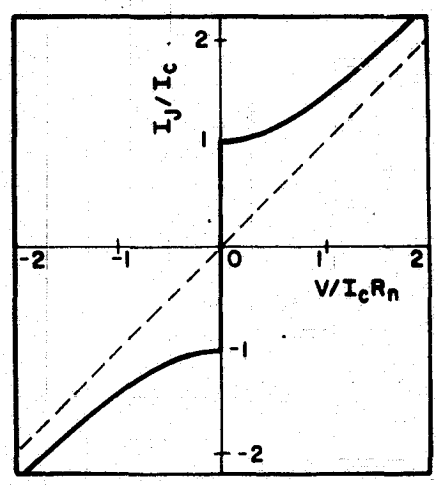

Fig. 6. Plot of Eq. II. D. 1. 2.

experimentally verified the theory of Stewart and McCumber for this case. These results are important here because the dynamic impedance of the SNS junction is then adjustable through proper fabrication techniques. For example, if a shunt capacitance is added to the junction, the initial slope at $I_J \gtrsim I_C$ becomes extremely small (i. e., the dynamic resistance becomes large) and quasi-linear. If the capacitance is sufficiently large, the voltage jumps instantly from zero to $I_C R_n$ as the critical current is exceeded, and the resulting I_J vs V curve exhibits hysteresis[40, 41]. Figure 7 shows the theoretical normalized I_J vs V curves of Stewart[40] illustrating the effects of increasing C.

The explanation for the increase of dynamic junction resistance with increasing values of C is that the corresponding larger values of

the R_nC time constant tend to smooth the variations in the junction voltage, v(t), and as a result make the supercurrent, $I_C \sin[(2e/h)\int_0^t v(\tau)d\tau]$ (Eqs. II. C. 1. 1 and II. B. 2), more sinusoidal in time. This reduces the d. c. supercurrent, which is the time average of the total supercurrent; and for a constant-current source, a decrease in the d. c. supercurrent implies an increase in the d. c. quasiparticle (normal) current and, hence, an increase in the d. c. voltage, V. The result is an increase in the dynamic resistance of the device for operating points near the critical-current "knee" of the I_J vs V characteristic.

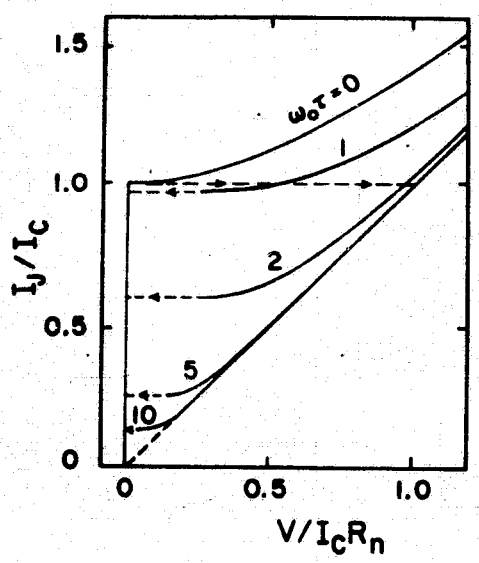

Fig. 7. Normalized d. c. theoretical junction characteristics (after Stewart[40]). The dimensionless parameter $\omega_0\tau$ is proportional to $\sqrt{C}$. Discontinuous jumps are indicated by dashed lines with arrows.

II. D. 2. The Effect of Fluctuations

At temperatures sufficiently close to the transition temperature thermal fluctuations can disrupt the coupling of the phases across the normal-metal barrier. In order to consider the effect of fluctuations in a Josephson junction, Ivanchenko and Zil'berman[44] and Ambegaokar and Halperin[45] have solved Eq. II. D. 1. 1, with the addition of a thermal noise current, for the time-averaged voltage.

Figure 8 represents the numerical solutions[45] for the normalized time-averaged voltage, $V/I_C R_n$, across the junction as a function of the normalized current, I_J/I_C (for a constant-current supply), for various values of the parameter

$$\gamma = \hbar I_C / ekT_{noise} \,. \qquad \text{II. D. 2. 1}$$

For the case $X \equiv I_J/I_C < 1$ and γ large, a solution is given in closed form by[45]

$$F(X) = 2(1-X^2)^{1/2} \exp\{-\gamma[(1-X^2)+X\sin^{-1}X]\}\sinh(\pi\gamma X/2), \qquad \text{II. D. 2. 2}$$

with $F(X) \equiv V/I_C R_n$.

---

44. Y. M. Ivanchenko and L. A. Zil'berman, Sov. Phys. -JETP 28, 1272 (1969).

45. V. Ambegaokar and B. I. Halperin, Phys. Rev. Letters 22, 1364 (1969).

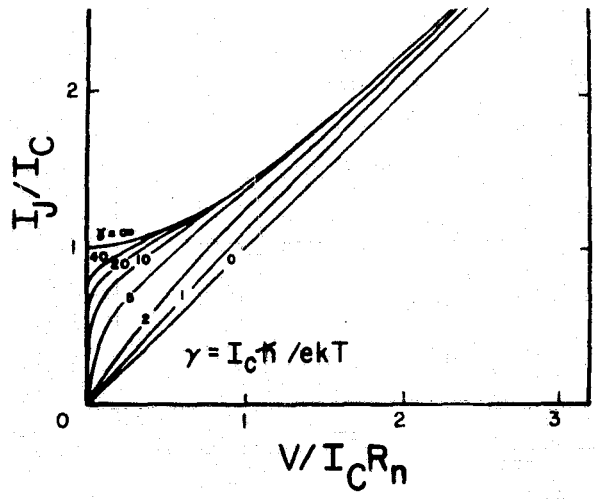

Fig. 8. Theoretical current-voltage characteristics of a Josephson junction for various levels of thermal fluctuations (after Ambegaokar and Halperin[45]).

In Fig. 8, the effects of thermal fluctuations are seen to be a rounding of the critical-current "knee." In the limit as $\gamma \rightarrow \infty$, the fluctuations become negligible and the normalized current-voltage curve becomes that described by Stewart for the absence of fluctuations (Eq. II. D. 1. 2).

III. DESCRIPTION OF THE EXPERIMENT

III. A. Introduction

The device studied in this experiment was a thin-film, SNS Josephson junction which was vapor-deposited in vacuo. Thin film junctions were preferred to the crossed-wire, mechanical-contact junctions investigated by Rockefeller[4] because (a) thin films are more definitive, rugged, and reproducible, (b) they allow larger junction areas than point contacts and, hence, larger currents and smaller fluctuation effects, and (c) it was hoped that the inherent capacitance of the thin-film junctions would increase the dynamic output resistance of the device as described in section II. D. 1.

Initially, in order to reduce interdiffusion between the S and N layers, the films were condensed on a single-crystal, sapphire substrate precooled to 4.2K, and the electrical characteristics were subsequently measured in situ. A hybrid evaporator/cryostat was designed and constructed for this purpose. During the course of the experiment, two limitations became apparent: (a) the proximity effect of the normal metal on the tin was so strong that at times the critical current of the tin was less than that of the junction, and (b) it was found that this could not be corrected by increasing the thickness of the tin, because there existed a maximum film thickness above which cracks would appear in the metal films. These films suffered severe

internal stresses due to the inability of the condensing metal atoms to migrate on a 4K substrate and reduce the lattice disorder. The cracks were a manifestation of stress relieval. Although for thicknesses exceeding a critical value the metal films would crack in small grain-like patterns, the resulting metal islands would still adhere to the sapphire substrate, thus illustrating that the adhesion of the film to the substrate was stronger than the metal-metal bond and testifying to the cleanliness of the system.

Consequently, to produce thicker, more reliable samples, the metals were then (a) vapor deposited onto a 273K substrate and (b) cooled in situ to liquid-helium temperatures within 20 minutes. These films experienced some annealing at 273K and, as a result, were macroscopically flawless even through cycling to 4.2K.

The early SNS films were maintained at cryogenic temperatures in the evaporator/cryostat by thermal contact with a liquid-helium reservoir through the single-crystal sapphire substrate, the copper substrate holder, indium washers, and the copper bottom of the helium vessel (see Fig. 11). Despite the high thermal conductivity and large contact areas which allowed the substrate holder never to be more than 0.15K above the temperature of the helium bath, when the Josephson critical current was exceeded in the thinner junctions (i.e., the junctions with larger critical current) heating effects became apparent

in the electrical behavior of the junction. For this reason and for the flexibility of using an eight-stage vapor-deposition system to fabricate more sophisticated junction geometries, it was decided to vapor deposit the later films onto a 300K substrate in a more conventional vacuum system and then transfer them immediately to an immersion cryostat where they could be cooled to liquid-helium temperatures within 30 minutes to minimize interdiffusion. These later samples were different also in that the normal-metal composition had been changed from pure gold to an alloy of gold/copper. The reason for the alloying will be discussed in section IV. B.

III. B. The Evaporator/Cryostat

The purpose of the dual evapor/cryostat was to provide an environment wherein a thin-film device could be vapor deposited at cryogenic temperatures and then electrically measured in situ. The primary advantage of the hybrid structure was the production of multi-layer films with well-defined laminae (i.e., distinct inter-layer boundaries), which was a result of the films never experiencing temperatures where appreciable diffusion might occur. A cross-sectional view of the evaporator/cryostat is shown in Fig. 9. The system consists of a 12-inch O.D. pyrex ring sitting on a collar and supporting a stainless-steel plate. Suspended from the top plate is a cylindrical liquid-nitrogen

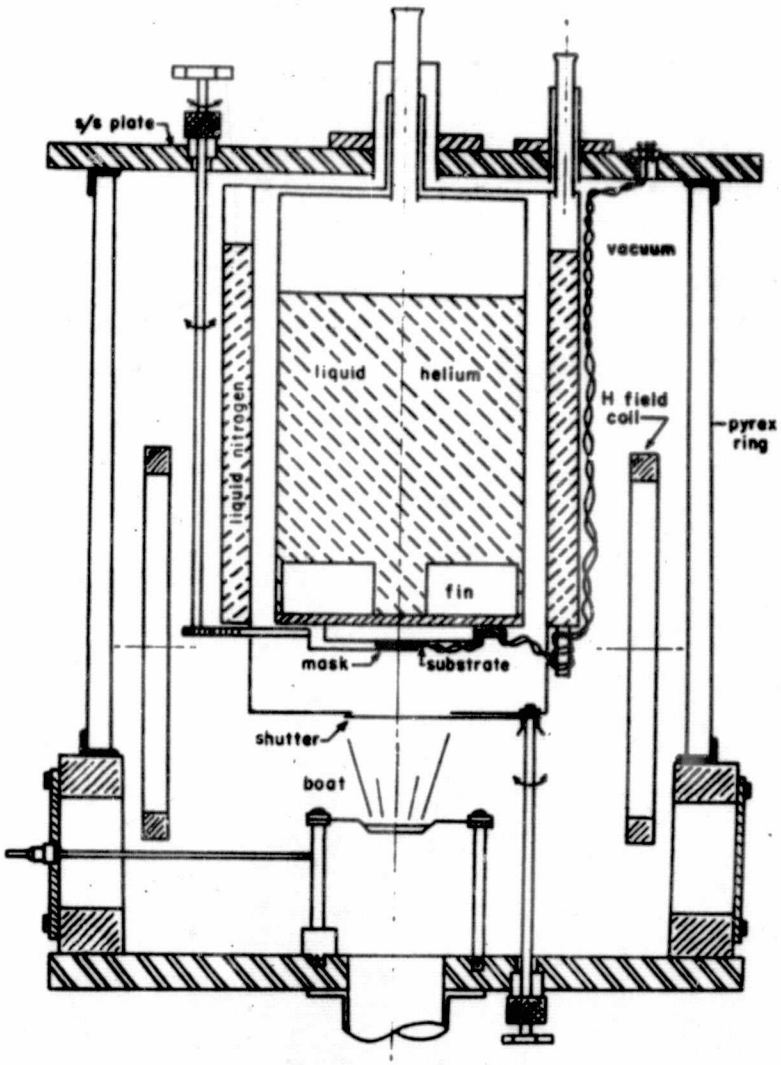

Fig. 9. Cross-section of evaporator/cryostat.

reservoir, inside of which is nested a liquid-helium vessel which serves both as a cryopump and a low-temperature reservoir to cool

the sample. The sample holder is mounted at the bottom of the helium vessel facing the heaters for the evaporation of the metals. The multiple-layer film patterns were created by the positioning of a mask manipulated by means of a mechanical feedthrough.

The non-magnetic metallic cylinders of the system allowed the unperturbed penetration of externally-applied, static magnetic fields while, at the same time, shielding the sample from some r.f. radiation.

The system was capable of maintaining temperatures from 4.2K to below 1.7K through pumping on the liquid-helium reservoir with a Consolidated Vacuum pump, model E70A (41 ft^3/min. rated capacity). Regulation of the vapor pressure (viz., the temperature) was accomplished through a needle valve in parallel with a Wallace and Tiernan FA-149 aneroid manostat. The helium vapor pressure was measured on a Wallace and Tiernan FA-135 precision mercurial manometer. The corresponding liquid-helium temperature was obtained from the table of the N.B.S. 1958 Helium Vapor Pressure-Temperature Scale[46]. With this method the temperature of the liquid helium could be determined to an accuracy of a few millikelvin. The temperature of the sample, on the other hand, was determined directly from the resistance of a calibrated carbon-composition resistor (see section III. F).

The liquid-helium vessel has interior fins to reduce the Kapitza[47]

46. National Bureau of Standards Monograph 10 (June, 1960).
47. P. L. Kapitza, Sov. Phys.-JETP 5, 59 (1941).

resistance between the copper and the helium II. It was designed to have a maximum 0.15K temperature difference between the liquid helium and the substrate holder. Experimentally, this temperature difference was found to be ~0.15K. This low thermal resistance is also evidenced in the short thermal time constants of the system: Any change in the helium vapor pressure would cause a corresponding change in the electrical resistance of the carbon resistor within a few seconds. Similarly, any Joule heating in the sample (when the sample current exceeded a critical value) was also sensed by the carbon resistor within a few seconds. Hence, the system thermal time constant from liquid-helium bath to sample was less than a minute. This was a result of the high thermal conductivity and small heat capacity of the cryostat components.

The system was evacuated by a Welch two-stage mechanical pump with a 5 ft^3/min. capacity in series with a Veeco three-stage diffusion pump capable of 85 ℓ/sec. The concomitant use of Convalex 10 diffusion pump oil and Apiezon type N grease for the seals assured a minimum vapor pressure of contaminant oils in the system.[48] In addition, all elastomer seals were fluorocarbon rubber (viton) because of their low outgassing rate and high outgassing temperature tolerance.[49]

48. L. I. Maissel and R. Glang, Handbook of Thin Film Technology (McGraw-Hill, N. Y., 1970), p. 2-10.

49. Ibidem, p. 2-53.

Typically, each metal film was vapor deposited for one minute, with the pressure reaching the low 10^{-7} Torr range during the evaporation. The evaporation sources (boats) were constructed from 0.005-inch molybdenum sheet and would conduct of the order of 60 Amperes for an indefinite number of evaporations. However, if some gold charge were to remain in a boat for a few days after an evaporation, that boat would most likely break upon reheating - possibly caused by the diffusion of the gold into the molybdenum.

III. C. The Vapor-Deposition System

The vapor-deposition system differs from the evaporator/cryostat in that (a) it is physically separate from its cryostat counterpart and (b) the substrate rather than the mask was manipulated to create the necessary thin-film patterns. It is a modified Veeco VE-400 vacuum system which utilizes a 15 ft^3/min. mechanical pump in series with a 4-inch, 400 l/sec. diffusion pump. A description with photographs of this multiple thin-film deposition system appears in the literature.[50] Five of the eight available mask positions were used: (1) Sn, (2) SiO, (3) Au/Cu, (4) Sn, (5) Sn. The masks were cut from 5-mil phosphor bronze. In essence, the boats were similar to those described above with the addition of a silicon-monoxide sublimation

50. P.M. Chirlian, V.A. Marsocci, H.W. Phair, and W.V. Kraszewski, Rev. Sci. Instr. 35, 1718 (1964).

source. The deposition time for each film was approximately two minutes except that of the Au/Cu alloy, which was less than one minute. During evaporations the vacuum pressure rose typically to $\sim 5 \times 10^{-6}$ Torr for the metals and to the low 10^{-5} Torr range for the SiO. The diffusion pump was operated with Dow Corning 704 oil, and there was a liquid-nitrogen cold trap between the bell jar and the diffusion pump to reduce the back streaming of pump-oil vapors.

III. D. The Cryostat

The sample is totally immersed in liquid helium inside a glass dewar which is supported within a thin-wall, stainless-steel cylindrical can. The top of the can has vacuum feedthroughs for electrical leads as well as a port leading to a mechanical pump. Except for a few inches at the top, the entire stainless-steel can is immersed in a brass dewar of liquid nitrogen. The helium-bath temperature could be varied from 4.2K to below 1.5K by pumping on the helium vapor. With the exception of one run, all pressure and temperature controls and measurements were similar to those described in section III. B.

One experiment was undertaken with the cryostat inside a screened room to reduce the effects of the r.f. radiation present in the metropolitan area. The results are discussed in section IV. F. Here, the helium temperature was controlled coarsely by adjusting a needle

valve in the pumping line (Kinney KS-47 mechanical pump). More accurate temperature stabilization was accomplished through a manganin-wire heater driven by an amplifier[2] phase-sensitive to the resistance variation of a carbon-composition resistor in the liquid helium. The helium vapor pressure was read digitally on a Texas Instrument precision pressure gage (accurate to ± 0.2mm Hg) and then converted to the bath temperature with the aforementioned table. No corrections were made for the hydrostatic pressure head of liquid helium.

III. E. The Magnetic Field Coils

There are two pairs of magnetic-field coils employed in this experiment. The first is a large Helmholtz coil surrounding the evaporator/cryostat and mounted with an azimuthal adjustment in order to negate the earth's magnetic field (of the order of 1/2 Gauss) in the vicinity of the sample to within a few milligauss. The second pair of coils is used to provide a known field up to 20G at the sample in the plane of the Josephson junction. Since this pair of coils was required to fit within the confines of the evaporator/cryostat (see Fig. 9), it was not constructed to the proportions of a Helmholtz coil. Later, for convenience, this latter pair of coils was also used to apply an external field to the sample in the cryostat (see Fig. 10). A Hewlett Packard 428B d.c. milliammeter with a 3529A probe was used to

confirm experimentally the field calculations for each coil and to assist in the alignment of the Helmholtz coil for negating the earth's field.

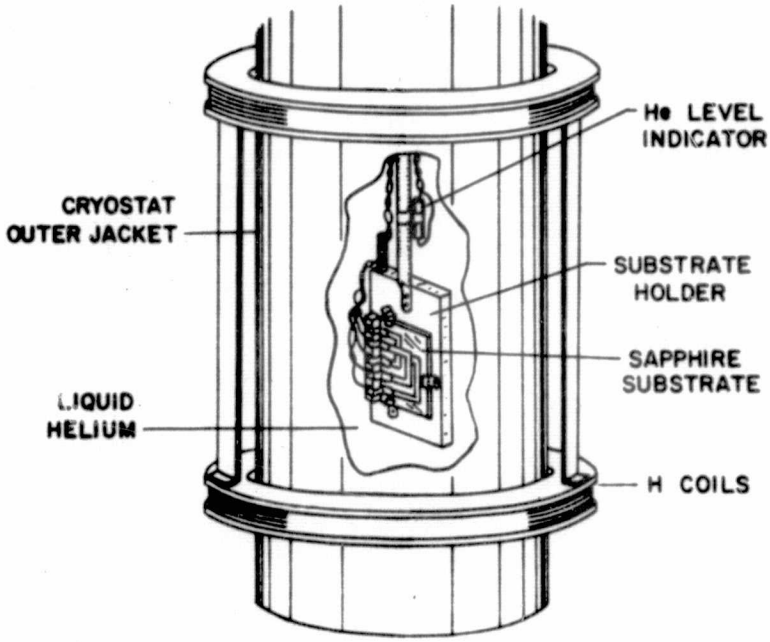

Fig. 10. Cutaway view of cryostat showing sample. Helmholtz coils to negate earth's magnetic field not shown.

III. F. The Substrate Holder and Thermometer

The purpose of the substrate holder is to support the single-crystal, sapphire substrate and make electrical contact to the thin films thereon. It is essentially an electrolytic-tough-pitch copper block

with a carbon-composition thermometer within it.

When the evaporator/cryostat was used, the substrate holder made electrical contact to preprinted gold islands via indium-tipped, phosphor-bronze leaf springs. The SNS films were then vapor deposited onto the sapphire making instant electrical contact to the gold islands and, hence, to the external measuring apparatus. Figure 11 illustrates the electrical connections of the substrate holder.

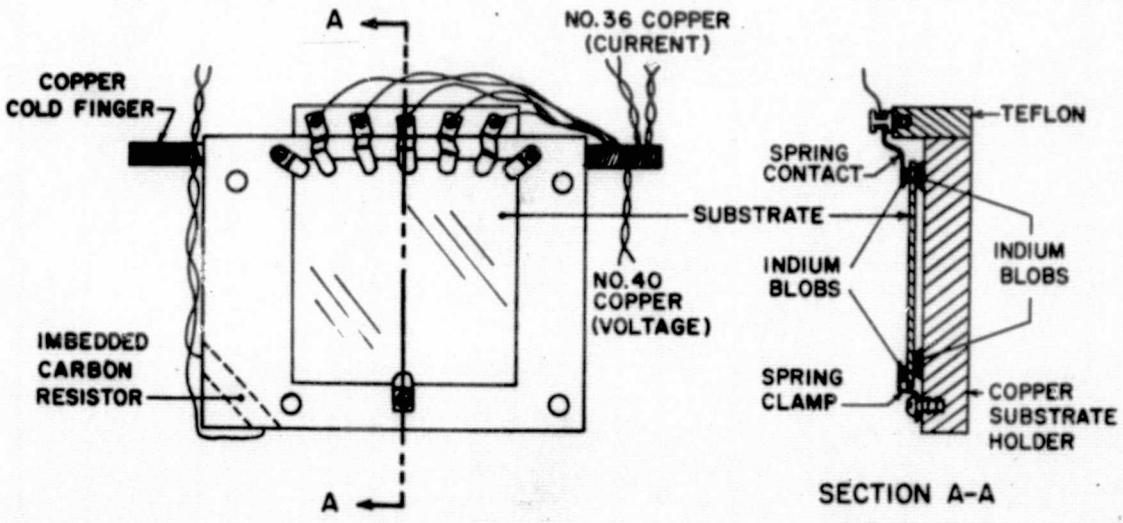

Fig. 11. Substrate holder with sapphire substrate.

The substrate holder was designed so as to present a low thermal resistance path from the sample to the liquid helium vessel in the evaporator/cryostat. The substrate was held down at three points by indium-tipped, phosphor-bronze spring clamps. Under each of the three points was a small blob of indium to increase the contact

surface area. Indium was chosen as the interfacial heat conductor because of its softness (at 290K, indium has a Brinell hardness two orders of magnitude less than copper[51] - which provides a larger thermal contact area for a given spring pressure) and its high thermal conductivity (at 4K, e.g. p. copper and indium have approximately equal thermal conductivity[52]). The copper block itself was clamped to the helium vessel against indium washers with phosphor-bronze lock washers used to maintain the pressure of the clamping screws after the contractions due to cooling to cryogenic temperatures.

The temperature of the copper block was obtained by measuring the resistance of a carbon-composition resistor imbedded within it and interpolating the temperature from a curve[53] fitted at three temperatures. From a few trial temperatures, the accuracy of the resistance-temperature curve was determined to be better than one percent. The resistor was a 100-Ohm, 2-Watt, Allen-Bradley carbon-composition resistor which had been stripped of its plastic protection and then imbedded within the copper block in Emerson and Cuming Stycast 2850FT high-thermal-conductivity epoxy. This epoxy was also used to enhance the thermal contact of the electrical leads to the

---

51. e.g., Metals Handbook (American Society for Metals, Ohio, 1961), Vol. 1.
52. Properties of Materials at Low Temperatures - A Compendium, ed. by V. Johnson (Pergammon, N.Y., 1961).
53. J.R. Clement, E.H. Quinnell, M.C. Steele, R.A. Hein, and R.L. Dolecek, Rev. Sci. Instr. 24, 545 (1953).

copper "cold finger" (see Fig. 11) and reduce the heat input to the sample.

The carbon-composition thermometer was used for experiments in both the evaporator/cryostat and immersion cryostat. Its resistance was measured on a d.c. bridge circuit which allowed a resolution of better than a millikelvin while producing only a few μWatts in the resistor.

III. G. The Sample and its Preparation

The Josephson junction device studied was a composite of superconductor and normal-metal thin-film layers forming an SNS sandwich. Each layer was vapor deposited in turn onto the substrate and previous layer. The superconductor, S, layers were formed from 99.999% pure tin, while the normal metal, N, was formed from either 99.99% pure gold or an alloy of gold containing 10wt.% of copper. The copper was stripped magnet wire.

All of the samples investigated in these experiments were "dirty", that is, the electronic mean free path was shorter than the coherence length in the N metal. This was desirable for the following reasons: (a) it allowed higher resistivity junctions with lower critical currents than clean samples with similar dimensions and smaller self-induced magnetic field effects (see sections II. C. 2 and IV. C), (b) these small-

er currents caused less sample heating, (c) it facilitated the separation of the Josephson and tin critical currents (see section IV.B), and (d) in the dirty limit the detailed atomic structure at the interface is less important and the large-scale motions of the superconducting electrons are ruled by a simple diffusion equation,[25] whereas in the clean case the reflection and transmission properties of the transmission region play an important role.

The earlier experiments carried out in the evaporator/cryostat used the sample geometry shown in Fig. 12. This sample was designed as a thin-film analogy to the crossed wires of Rockefeller[4] with a simplicity that allowed it to be vapor deposited in the constricted environment of the evaporator/cryostat. The Josephson junction proper was 0.25mm x 0.25mm.

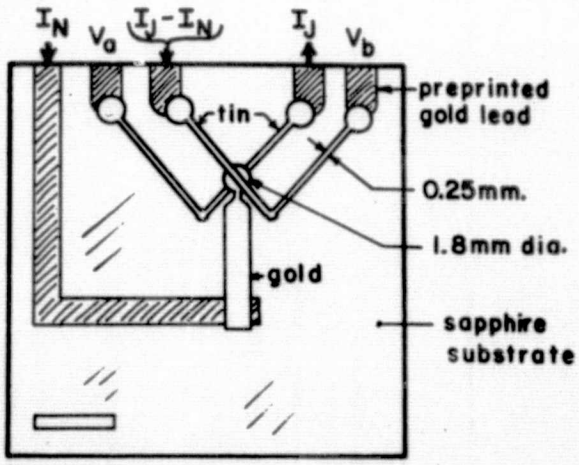

Fig. 12. Early sample geometry. I_N is the control current and I_J the junction current.

The later use of a separate thin-film deposition system and an immersion cryostat permitted the development of an improved sample geometry shown in Figs. 13 and 14. In order to reduce both the input impedance and the Joule heating in the control-current lead, the normal-metal film carrying the control current, I_N, into the N-layer tunneling barrier was replaced with a superconducting film of tin. Also, to insure complete injection of I_N into N, a thick insulating film of SiO was deposited both below and above the I_N lead, save for a 0.19mm slot which defined the width of the Josephson junction. The current-carrying area of the Josephson junction was 0.18mm x 0.19mm. Figure 14 illustrates the masking patterns and the sequence of deposition.

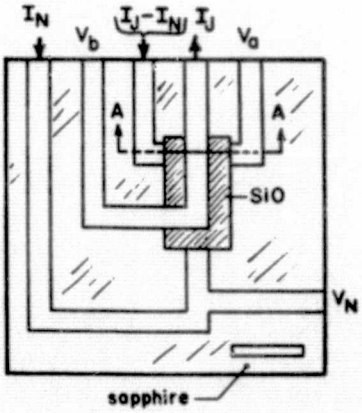

Fig. 13a. Substrate with improved sample. Tin films not labeled.

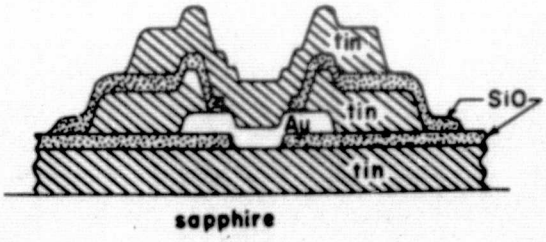

Fig. 13b. Section A-A with exaggerated scales for clarity.

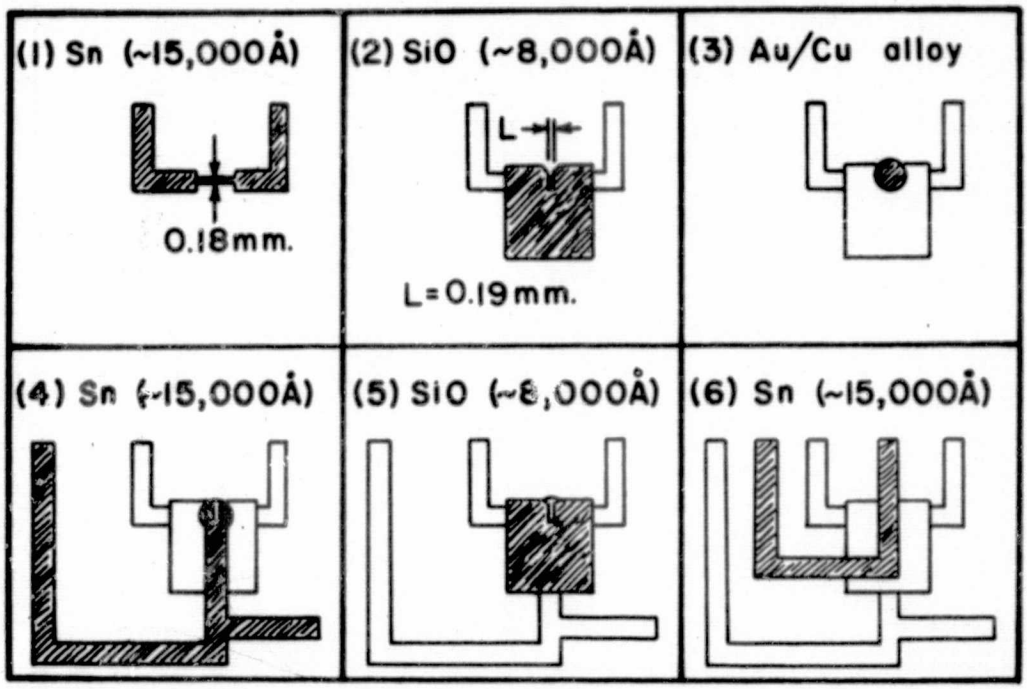

Fig. 14 Sequential construction of improved thin-film sample. (Shaded area is the material deposited during that step.)

The substrate was one of three 0.031" x 1.5" x 1.5" polished, single-crystal sapphire slabs (obtained from INSACO, Quakertown, Pa.) with a surface asperity of 10^{-6} inches. Single-crystal sapphire was chosen because at cryogenic temperatures its thermal conductivity is three orders of magnitude higher than that of glass.

The preparation of the substrate for vapor deposition initially involved the removal of films from a previous experiment. Metal films were readily removed by rubbing with a mixture of Linde B, 0.05-

micron, alumina abrasive and distilled water (sapphire is the crystalline form of alumina, Al_2O_3). The removal of SiO films, however, required the use of a buffing wheel and polishing rouge.* The substrate was then cleaned by hand with a glassware detergent (e.g., "Sparkleen" in distilled water) and a tissue. Next, the ultrasonic cleaner was employed: First, a wash in a detergent and distilled water solution, and then five successive rinses in distilled water. Finally, the substrate was cleaned ultrasonically in a beaker of reagent-grade methanol which was chosen both for its dissolution of water and sundry impurities as well as its volatility (for the next step). Drying was accomplished by withdrawing the substrate from the beaker after the methanol had been heated to its boiling point. The substrate was thoroughly dry after a few seconds in the hot methanol vapors. An indication of the effectiveness of the cleaning procedure was the uniformity of the evaporating methanol film over the substrate surface, for inter-

---

*Apparently, this treatment was not detrimental to the sample; for, although some small scratches could be seen in the sapphire using side-lighting and a 30x microscope, they disappeared when the usual 15,000Å initial layer of tin was deposited. The mechanism for this scratch filling is thought to be related to atomic migration and to the probability of some of the impinging metal atoms having sufficient energy for at least one reflection (i.e., one reflection in the scratch might direct the atom within the scratch, while one reflection on the flat would leave the substrate). The complex geometry of the evaporator/cryostat was replete with evidence that a fair proportion of the metal atoms suffered at least one reflection off a 300K substrate... and somewhat less off a 4.2K substrate.

ference fringes were observed in the evaporating methanol film across the entire surface. It is believed that the interference pattern was due mostly to the vertical position of the sapphire in the rising vapors (and the gravitational field) rather than being "grey-breath figures"[54] indicative of slight surface contamination.

After cleaning, the substrate was mounted in a holder particular to the vapor deposition being used. If it were the evaporator/cryostat system, the substrate would be placed first on a mask for pre-printing the gold islands. After this deposition, the substrate would be cleaned in successive beakers of xylene, methyl ethyl ketone, and methanol in order to remove traces of pump oil which may have condensed during deposition of the gold islands. The first two were recommended by the manufacturer as solvents for the Convalex 10 diffusion pump oil, and the methanol was used for the drying process. The dried substrate was then mounted on the substrate holder and placed in the evaporator/cryostat for final deposition and measurement in situ. Alternatively, if the conventional vacuum system were used, the substrate would be mounted in a holder which allowed it to be lifted and positioned over one of five masks. The vapor-deposited sample would then be removed and mounted in the immersion cryostat for study.

---

54. see ref. 48, p. 6-38.

III. H. Measurements

III. H. 1. Film Thickness

The thickness of the thin films was ascertained by optical methods using the principle of multiple-beam interferometry.[55, 56] For this method a thin film of aluminum was vapor deposited over the sample in order to improve the reflectivity of the SiO film and the sapphire. Each sample was used for just one experimental run, and the thickness measurement was made after the sample had been warmed to room temperature.

The computation of the thickness was computer assisted, and the accuracy of the measurements for the N film was usually better than 50Å. The measurement of the S (tin) and insulating (SiO) layer thicknesses was not required to such an accuracy; therefore, these films were measured to within ~ 1000Å (~ 1/3 of a fringe shift for sodium light) which corresponds to an accuracy of ~ 5 - 10% for these thicker films.

---

55. W. F. Koehler, J. Opt. Soc. Amer. 43, 739 (1953).
56. R. F. Duffy, Ph. D. thesis, Stevens Institute of Technology, 1964 (unpublished).

III. H. 2 The Thin-Film Electronic Mean Free Path

The electronic mean free path of the N metal is needed for the calculation of the coherence length in the tunneling barrier of the SNS Josephson junction. The ratio of coherence length to mean free path determines whether the clean or dirty limit of the theory should be applied to the sample.

At cryogenic temperatures the primary contribution to bulk electrical resistivity in metals is the scattering by lattice defects. In thin films the resistivity is increased by diffuse surface scattering. In order to obtain the desired bulk mean free path, ℓ_o, the contribution from surface effects must be segregated. The following method* for the calculation of ℓ_o was developed by Fuchs[57] and extended by Sondheimer[58].

If the surface scattering is assumed to be entirely diffuse (a good approximation for vapor-deposited films[59]), the equation relating the mean free path to other film parameters is given by

$$\sigma/\sigma_o = 1 - (3\ell_o/t)\int_1^\infty (1/\tau^3 - 1/\tau^5)[1 - \exp(-\tau t/\ell_o)]d\tau \ , \qquad \text{III. H. 2. 1}$$

---

*an excellent review of the subject is in ref. 48, ch. 13. 3.

57. K. Fuchs, Proc. Cambridge Phil. Soc. 34, 100 (1938).
58. E. H. Sondheimer, Adv. Phys. 1, 8 (1952).
59. H. Mayer, Structure and Properties of Thin Films (Wiley, N. Y., 1959), p. 225.

where σ_o is the bulk conductivity, σ is the total measured conductivity, and t is the thickness of the film. An equation defining the resistance of the film at 4.2K, $R_{4.2}$, along the length, L, of a film of width W is

$$\sigma/\sigma_o = [L/(R_{4.2} W t^2 \sigma_o/\ell_o)] (t/\ell_o). \qquad \text{III. H. 2. 2}$$

The quantity σ_o/ℓ_o is a constant for a given metal and independent of temperature. It can be determined from measurements of the anomalous skin effect. Values of $\sigma_o/\ell_o = 8.3\text{x}10^{10}\,\text{ohm}^{-1}\text{cm}^{-2}$ for gold and $\sigma_o/\ell_o = 9.5\text{x}10^{10}\,\text{ohm}^{-1}\text{cm}^{-2}$ for tin were obtained from the literature.[60] The value of σ_o/ℓ_o for gold was also used as an approximate value for that of the 90wt.%Au/10wt.%Cu alloy. The value of $R_{4.2}$ was determined from the resistance of the normal-metal film leading into the barrier in early samples. The simultaneous graphical solution of equations III. H. 2. 1 and III. H. 2. 2 yields values for ℓ_o and σ/σ_o. The experimental values for the mean free path are given in Tables 1-3 (section IV. A).

---

60. D. K. C. MacDonald, Encyl. Phys., XIV (Springer-Berlin, 1956), p. 188.

III. H. 3. The Experimental Arrangement for I_J vs V Characteristics

The time-averaged (d. c.) operating characteristics of an SNS Josephson junction can be displayed as a graph of the tunnel current, I_J, versus the voltage, V, across the junction. If a control current, I_N, is introduced via a third terminal directly into the N layer, the I_J vs V characteristics as a function of I_N resemble the output curves of a bipolar transistor.

The I_J vs V characteristics in this experiment were measured using two different techniques. The first was a d. c. method which had the advantage of (a) having only one voltage reference point (ground) in the circuit (at the voltage amplifier) and, hence, no ground loop currents or common-mode signals, and (b) no signal distortion due to lead and sample inductance. However, the tradeoff was that thermal e. m. f.'s could be detected as noise and the sensitivity of the amplifier was at best ~30nV, which was the "jitter" at the output of the amplifier measured over a few seconds with the input shorted. Consequently, this method was not adequate for the thicker samples where the interesting region (i. e., large dynamic resistance region) occurred for voltages below 30nV. Therefore, this d. c. method was used for the thinner samples (with correspondingly larger critical currents) and to check the second method at higher voltages. The d. c. circuit is shown in Fig.15. Both the I_J and I_N current supplies were 12-Volt lantern

batteries with a series transistor controlling the current. Both current supplies were floating, but both their cases were grounded at the d. c. amplifier through microphone cable shielding. The value of I_J was varied with a ten-turn potentiometer controlling the series transistor and was measured by the floating Y-input of a Hewlett Packard 135A X-Y recorder across a 1.05Ω resistor. I_N was measured with a Weston 931 milliammeter. The voltage across the sample was measured with a Keithley 149 milli-microvoltmeter, whose output drove the X axis of the X-Y recorder. The capability of either current source was ~900mA.

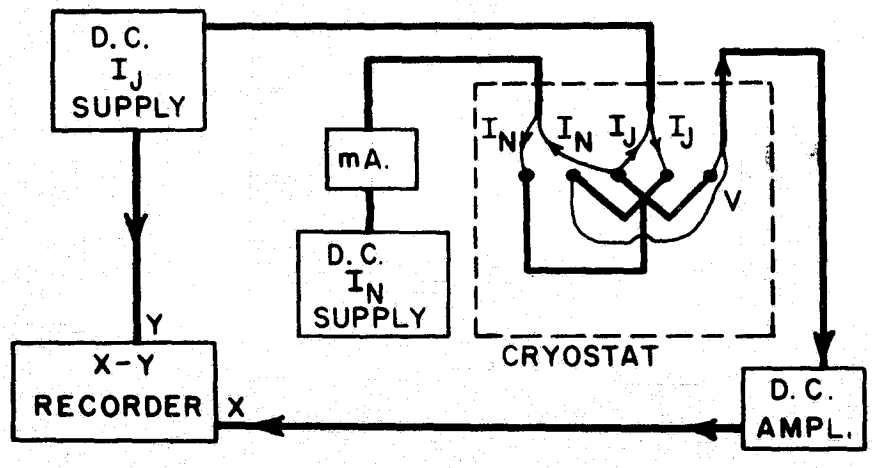

Fig. 15. The d. c. circuit to determine I_J vs V characteristics.

The second method of measuring the I_J vs V characteristics was to employ a lock-in amplifier - a technique which has the advantage

of permitting the detection of a signal buried many dB below the noise level. In essence, the lock-in amplifier is a narrow-band tunable amplifier which ignores all the noise outside a narrow frequency band about the signal frequency. A diagram of the experimental circuitry is shown in Fig. 16.

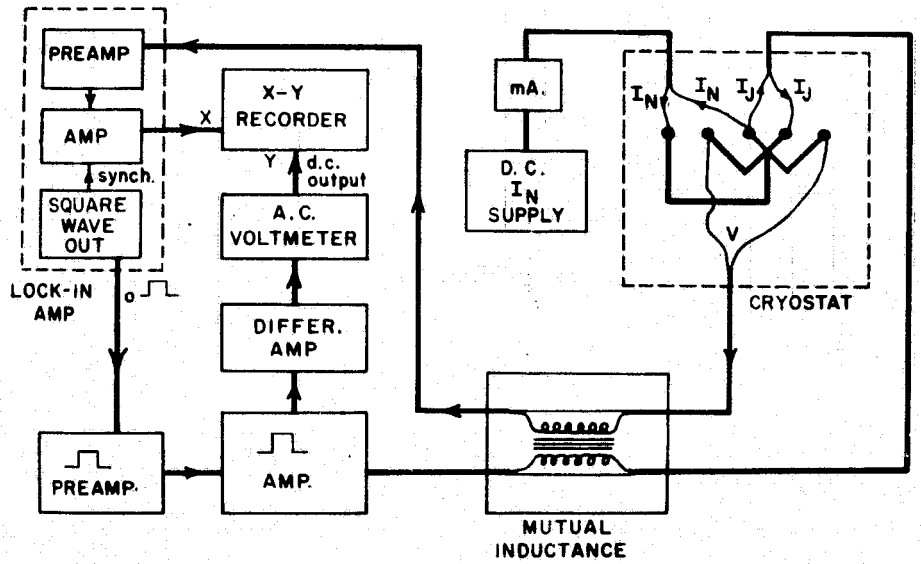

Fig. 16. Experimental setup for measuring I_J vs V characteristics with a lock-in technique.

A Princeton Applied Research HR-8 lock-in amplifier (hereafter denoted PAR) was used both as a signal source and as a detector and amplifier. The sample current was switched on and off at a fixed frequency (typically 5kHz) in square-wave fashion, and the resulting square-wave sample voltage was synchronously detected (locked-in) and amplified by the PAR. A square-wave current also has the ad-

vantage of heating the sample only about half as much as an equivalent direct current.

The PAR amplifies a signal which is the fundamental Fourier component of the square-wave voltage times a proportionality factor which is the cosine of the angle, φ, between the phase of the generated square wave fundamental and the detected signal fundamental. An internal phase adjustment, φ_o, is included in the PAR to determine which component of the incoming complex wave form is amplified.

A constant-amplitude, 5kHz square wave (switching from 0 to its peak value) was generated by the PAR and sent to a preamplifier, which consisted of two operational amplifiers and a ten-turn potentiometer for adjustment of the square-wave amplitude (i.e., I_J). The signal then was amplified further by a series transistor (with a 2-Ampere capacity) and applied to the sample. The value of I_J was determined by measuring the square-wave voltage across a series, 0.982-Ohm manganin wire. This voltage was amplified and isolated from the current-supply circuit by a Sanborn 8875A differential amplifier and fed into a Hewlett Packard 400E a.c. voltmeter. The d.c. output of this voltmeter, which was proportional to I_J, in turn drove the Y-axis of the X-Y recorder.

The sample impedance was both resistive and inductive, and since the current was a square wave (from a current source, switching from

0 to I_J), the resulting sample voltage contained terms proportional to both I_J and its derivative. Hence, the square-wave voltage detected by the PAR contained a voltage spike due to the differentiation of the square-wave current. This was remedied by including in the circuit a negative mutual inductance which would negate the effect of the sample inductance (see Fig. 16). The mutual inductance was inserted by diverting the sample current through a 0.17-0.27μHy, adjustable r.f. coil which had been coupled via its ferrite core to one turn of the voltage lead with the proper winding polarity. An optimum value of the mutual inductance was obtained by adjusting the position of the ferrite core while monitoring the square-wave voltage on an oscilloscope. After an optimum setting had been obtained, the mutual inductor was removed and its value ascertained to $\sim 2\times10^{-8}$ Hy. The effect of the mutual inductor was to cancel better than 90% of the voltage spike, which was more than sufficient; for the residual spike had a negligible Fourier component at the fundamental frequency of the square wave (i.e., its duration was an order of magnitude less than the width of the square wave at 5kHz).

The detected signal quality depended also upon the choice of the plug-in preamplifier for the PAR. Initially, a type B-1 preamplifier was employed because of its sensitivity (1nV full scale) and its availability. However, it had an isolating-transformer input with a small

impedance which was essentially inductive (~ 250μHy); and if the sample inductance were not cancelled by the mutual inductance, the desired resistive component of the junction voltage would have been difficult to discern due to the inductive loading of the B-1. Later, a type B pre-amplifier was obtained. It was preferred to the B-1, for it had the same sensitivity but with a much higher input inductance (~ 0.25Hy).

With the lock-in amplifier technique the noise voltage was as low as one nanovolt, and the I_J-V characteristics were in excellent agreement with those measured with d.c. methods.

III. H. 4. The Experimental Arrangement for I_J-ΔV Curves

In this part of the experiment the current, I_N, injected directly into the N layer of the SNS junction was a positive-going square wave and the Josephson junction current, I_J, was direct current. When the critical current of the junction was exceeded here, the junction voltage contained both a d.c. and a square-wave component ΔV. The operation was to fix the amplitude of I_N at a value smaller than the critical current of the junction and vary the direct current I_J in order that a graph of the junction square-wave voltage, ΔV, versus I_J could be obtained. The curve of I_J vs ΔV was repeated for different frequencies and amplitudes of I_N. The experimental arrangement is similar to that in the previous section and is shown in Fig. 17.

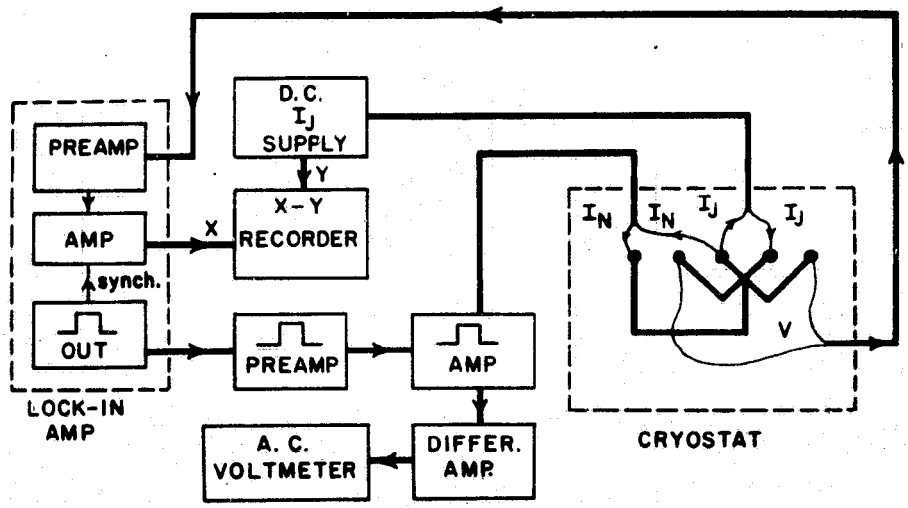

Fig. 17. Experimental setup for obtaining I_J vs ΔV curves.

IV. EXPERIMENTAL RESULTS

IV. A. The Samples

The operation of the SNS Josephson junction depends significantly upon its individual elements; therefore, the experimental characteristics of the separate thin films will be presented here first. Tables 1-4 are a summary of the film characteristics.

As was explained in section III. A, the samples fabricated during the course of this investigation may be divided into three categories: (a) pure metals vapor quenched on a 4.2K substrate (Table 1), (b) pure metals condensed on a 300K substrate (Table 2), and (c) pure tin and a Au/Cu alloy condensed on a 300K substrate (Tables 3 and 4). The following describes the normal-metal (N) films and the superconductor (S) films for these three cases.

N Films: As described in section II. A, the range of the proximity effect is ξ_{GL} and ξ_N in the S and N films, respectively, and decreases with decreasing electronic mean free path. The theory which explains this "leaking" of Cooper pairs from a superconductor to a normal metal is divided into two cases depending upon the ratio of the mean free path, ℓ_N, to the coherence length, ξ_N, in the normal metal. If $\ell_N/\xi_N(T) \gg 1$, then the SN junction is in the "clean" limit of the theory; and if $\ell_N/\xi_N \ll 1$, the junction is in the "dirty" limit. For this inves-

tigation, it was desirable to have the junctions in the "dirty" limit as explained in section III. G.

In general, metal films vapor deposited onto a substrate held at room temperature or below are in the dirty limit due to the large number of lattice dislocations formed during the deposition. As expected then, all of the metal films in this investigation were in the dirty limit; and, if the ratio $\ell_N/\xi_N(T)$ is used as an indicator, the N films may be divided into two groups: (a) pure gold films deposited on a 4.2K substrate having typical ratios of $\ell_N/\xi_N(3.5K) \approx 0.15$ and Au/Cu-alloy films deposited on a 300K substrate with $\ell_N/\xi_N(3.5) \approx 0.2$, and (b) pure gold films deposited on a 300K substrate with $\ell_N/\xi_N(3.5) \approx 0.5$. The former group of films is "dirtier" than the latter because of the increased number of electron scattering sites due to either impurity atoms (viz., copper) or vapor-quenched lattice dislocations.

The thickness, t_N, of the N layer was varied from 200Å to 5200Å, with the thinner samples deposited only on substrates at cryogenic temperatures in order to reduce the possibility of "pinholes" in the films. Warmer substrates permit the migration of condensing metal atoms to nucleation centers, thus leaving voids in the film (e.g., the minimum thickness for a continuous gold film deposited on a 300K substrate is[61] ~500Å). However, because the stresses in the gold

61. M.H. Jacobs, D.W. Pashley, and M.J. Stowell, Phil. Mag. 13, 129 (1966).

films deposited on the 4.2K substrate caused cracking for thicknesses above 2000-3000Å, it was decided to vapor deposit the films on a 300K substrate and restrict their thicknesses to be greater than 500Å to insure film continuity. The resulting films were structurally sound and exhibited the characteristics of a less disordered crystalline structure (see Table 2). Finally, to insure that the films were indeed in the dirty limit and for reasons given in section IV.B, the gold film was alloyed with copper, resulting in an increased lattice disorder once again (see Tables 3 and 4).

S Films: The superconducting (S) films in this investigation may be described in two categories: (a) the pure tin films vapor quenched on a 4.2K substrate (Table 1) and (b) the pure tin films condensed on a 300K substrate (Tables 2-4). As with the N films, the S films which were vapor quenched on a 4.2K substrate also experienced cracking for film thicknesses exceeding a minimum value ~2000Å. The S films which were condensed at 300K, though, were mirror perfect with thicknesses ranging to 15,000Å, which were well beyond the reported minimum thickness of a continuous film of tin on an ultra-clean substrate.[62]

The transition temperature, T_{Cs}, of the S film was obtained by

62. H.L. Caswell, J.Appl.Phys. 32, 105 (1961).

extrapolating the temperature-dependent tin-film critical current, I_{Cs} (see section IV. B), to zero current. The resulting values of T_{Cs} in Table 1 compare well with those of Buckel and Hilsch[63] who also vapor quenched their films of tin on a substrate cooled with liquid helium. In particular, the resulting enhancement of T_{Cs} over that of the bulk material, 3.72K, may be attributed to a combination of internal stress[64] and lattice disorder.[65] The electrical resistivity of the vapor-quenched tin film ($\sim 5 \times 10^{-6}$ ohm-cm for a 3000Å film) also agreed with the data of reference 63. The corresponding mean free path, ℓ_S, was ~200Å. Upon warming, the films annealed; and, at room temperature, their resistance was about one half of their low-temperature resistance. Later, when the sample was vapor deposited onto a 300K substrate and the thickness of the S layer was increased to ~15,000Å, the mean free path correspondingly increased to $\gtrsim$4000Å. The vacuum pressure during the deposition of these later samples rose to $\sim 5 \times 10^{-5}$ Torr for the SiO and $\sim 5 \times 10^{-6}$ Torr for the metals. Since it became desirable to dirty (viz., alloy) the N film, the additional impurities contributed from the condensation of the gaseous contamination were not detrimental to the desired characteristics

---

63. W. Buckel and R. Hilsch, Z. Physik 138, 109 (1954).
64. J. M. Lock, Proc. Roy. Soc. (London) A208, 391 (1951).
65. J. W. Garland, K. H. Bennemann, and F. M. Mueller, Phys. Rev. Letters 21, 1315 (1968).

of the N layer nor were their secondary effects[62] on the superconducting properties of the tin films deleterious to the investigation of the composite structure as a device*.

Tables 2-4 contain values for the critical temperature of the SNS device, T_{Csns}, which were determined by extrapolating the temperature dependence of the Josephson critical current to zero current. A possible explanation for the enhanced T_{Csns} in Table 4 is the stress experienced by the films of tin due to the differential contraction of film and substrate when cooled from room temperature to that of liquid helium[66]. On the other hand, those in Tables 2 and 3 are slightly suppressed due, most likely, to the proximity effect which depends on the coherence length, $\xi_N(T)$, in the N metal as well as the thickness of both the N and S layers, t_N and t_S.

The remaining parameters in Tables 1-4 are: $\rho_{N4.2}$, the N-metal resistivity at 4.2K; R_{in}, the resistance seen by the control current, I_N (see section IV.D.2); and R_n, the Josephson junction resistance for currents far exceeding the critical value.

---

* The overall effect of these layers is quantitatively described in section IV.D.1 by an empirical "effective coherence length."

66. see ref. 48, p. 22-9.

TABLE 1. CHARACTERISTICS OF FILMS DEPOSITED ON 4.2K SUBSTRATE

Sample	t_N	t_{S1}	t_{S2}	$\rho_{N_{4.2}}$	ℓ_N *	$\xi_{N_{theor.}}(3.5)$ [a]	R_{in}	T_{Cs}
No.	Å	10^3 Å	10^3 Å	10^{-6} Ω cm	Å	Å	Ω	K
7	1050	1.5	2	< 38	> 40	> 250	50	b
8	750	2	3	28	60	310	50	~3.8
9	200	2.5	2.5	27	40	250	300	3.85
13	900	3.3	5	< 65	> 30	220	100	[c] 4.1, 4.4
15	340	2.6	4.2	77	20	180	320	4.35
16	530	3	1.75	65	25	200	170	~4.3

* The mean free path of the tin is ~200Å.

a. obtained from Eq. II.A.4
b. very noisy near T_{Cs}
c. both films of tin became normal

TABLE 2. CHARACTERISTICS OF FILMS DEPOSITED ON 300K SUBSTRATE IN EVAPORATOR/CRYOSTAT

Sample	t_N	t_{S1}	t_{S2}	$\rho_{N_{4.2}}$	ℓ_N *	$\xi_{N_{theor.}}(3.5)$ a	R_{in}	ℓ_S	T_{Csns}
No.	Å	10^3 Å	10^3 Å	$10^{-6}\Omega$ cm	Å	Å	Ω	Å	K
19	550	2.8	2.9	6.0	230	600	15	10^3	-
20	750	4	5.7	4.3	350	750	8.0	10^3	~3.5
23	1450	6.5	9	4.4	500	900	4.5	-	3.62
24	1125	9.2	9.7	4.8	380	780	5.5	4×10^3	3.55

TABLE 3. CHARACTERISTICS OF FILMS DEPOSITED ON 300K SUBSTRATE IN EVAPORATOR/CRYOSTAT - GOLD ALLOYED WITH COPPER

Sample	wt.% Cu	t_N	t_{S1}	t_{S2}	$\rho_{N_{4.2}}$	ℓ_N *	$\xi_{N_{theor.}}(3.5)$ a	R_{in}	T_{Csns}
No.	%	Å	10^3 Å	10^3 Å	$10^{-6}\Omega$ cm	Å	Å	Ω	K
27	5.2	1700	8.2	9.6	9.0	160	500	4.5	3.6
28	9.1	780	8.9	9.7	11	130	450	12	3.66
29	9.9	595	8.9	10.7	11.5	120	430	16.5	3.75

* $\ell_S \sim 4\times10^3$ Å.

a. obtained from Eq. II. A. 4.

TABLE 4. CHARACTERISTICS OF FILMS DEPOSITED ON 300K SUBSTRATE, MEASURED IN CONVENTIONAL CRYOSTAT - GOLD ALLOYED WITH COPPER

Sample	wt.% Cu	t_N	t_{S1}	t_{S2}	R_{in}	R_n	T_{Csns}
No.	%	Å	10^3Å	10^3Å	Ω	10^{-6}Ω	K
30	9.4	5200	12	12	1.8	1.5	3.75
improved geometry begins here							
32	9.2	1290	12	15	a	14	3.76
34	8.9	1410	13	15	0.068	6.0	~3.70
35	8.6	1550	12	15	0.10	10	b
36	9.2	3000	12	13.5	0.057	32	b
37	10.0	2580	14	15.5	0.083	22.5	b
38	11.5	1225	13.5	15.5	0.22	370	3.52
39	9.8	540	15	15	--	<5	3.8

a. input lead open circuited.
b. critical currents too small to be determined near T_{Csns}.

$\rho_{N_{4.2}} \approx 11 \times 10^{-6}\,\Omega\text{cm}$

$\ell_N \approx 100$Å

$\xi_N(3.5\text{K}) \approx 500$Å

IV. B. The Critical Current of the Tin Film

A serious problem which arose during the early stages of this investigation was the transition of one or both of the superconducting tin films to the normal state whenever the junction current, I_J, or a combination of I_J and the control current, I_N, exceeded a critical value, I_{Cs}. The purpose of this section is to present (a) evidence of the phenomenon, (b) a feeling for the underlying mechanisms, and (c) a method for eliminating the effect. In the following, I_N is assumed to be zero for simplicity; no attempt is made to pursue the quantitative effect of I_N on I_{Cs}.

When an S layer became normal conducting near the junction, it destroyed the operation of the SNS Josephson-junction device and contributed an additional resistance of up to $10^{-3}\Omega$ to the junction resistance ($R_n \sim 10^{-5}\Omega$). In the early samples, this phenomenon was evidenced in the unexpected appearance of a large negative voltage in the junction I_J vs V characteristic. An example illustrating the effects of the transition of the tin film is shown in Fig. 18. As the junction current, I_J, is increased beyond the junction critical current, I_{Csns} (not shown on the scale of Fig. 18), the device exhibits ohmic behavior (with a slope equal to the junction resistance, $R_n = 1.5\mu\Omega$) up to a critical current I_{Cs}, whereupon the voltage begins to reverse with increasing I_J. As I_J is increased still further, V becomes negative and increases rapidly

in the negative direction until the junction again acts ohmic (for a value $I_J \gtrsim 350$mA, not shown in Fig. 18) but this time with a slope of 215μΩ, which is just the value of the junction resistance measured at 4.2K when both tin films are normal conducting. Thus, the reversal of the

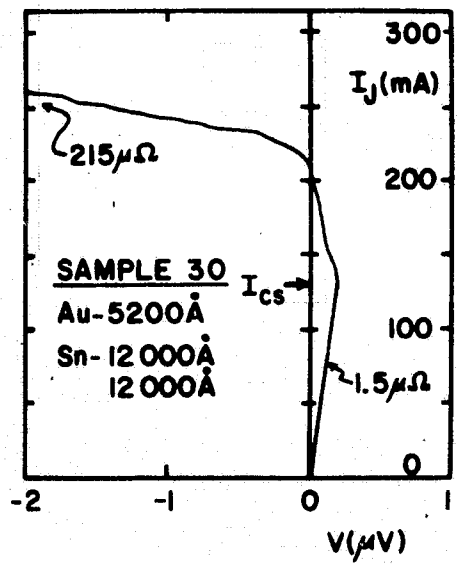

Fig. 18. I_J vs V showing a voltage reversal at I_{Cs} ($I_{Cs\,ns}$ not seen on this scale).

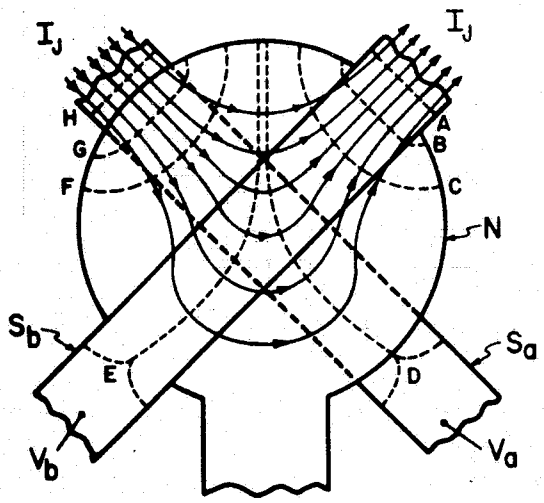

Fig. 19. An early sample showing the flow path of I_J for both S films normal and I_N=0. Equipotential lines A-H not incremented equally for emphasis.

junction voltage is caused by the value of I_J exceeding the critical current of both tin films. This may be explained using Fig. 19, which is a diagram of the early sample geometry illustrating the approximate flow patterns and equipotential lines when both tin films are normal conducting (e.g., $I_J \gg I_{Cs}$). The flow of I_J is shown heaviest in the

two tin (S) films because the S layers are thicker than the N film. The two-dimensional approximation assumed in Fig. 19 for the equipotential pattern is valid here because the thickness of the films is negligible compared with their other dimensions. The current is conventional, and the potential increases from lines "A" to "H" in varied increments for emphasis of illustration. The junction voltage, V, is defined as the difference of the potential measured between superconductors "a" and "b" sufficiently distant from the flow of I_J (i.e., $V = V_a - V_b$). When both tin films are normal, as shown in Fig. 19, the lead measuring V_a is at potential "D" and the one for V_b is at potential "E"; therefore, $V_a - V_b < 0$. On the other hand, when both tin films are superconducting (each tin film is then one equipotential), V_a is greater than V_b by the Josephson-junction voltage drop across the thickness of the N layer between the two superconductors, and $V_a - V_b > 0$. A further look at Fig. 19 suggests that the voltage reversal occurs only if both S films become normal conducting.

As the N layer was made thinner, the value of the critical current of the junction, I_{Csns}, approached the critical current of the tin, I_{Cs}. Figure 20 shows the I_J vs V characteristic for a sample at a temperature where I_{Cs} is slightly larger than I_{Csns}. It is thought that the critical current of only the thinner S layer is witnessed here, and, hence, no voltage decrease is expected. Figure 21 illustrates the

temperature dependence of I_{Csns} and I_{Cs} for this sample.

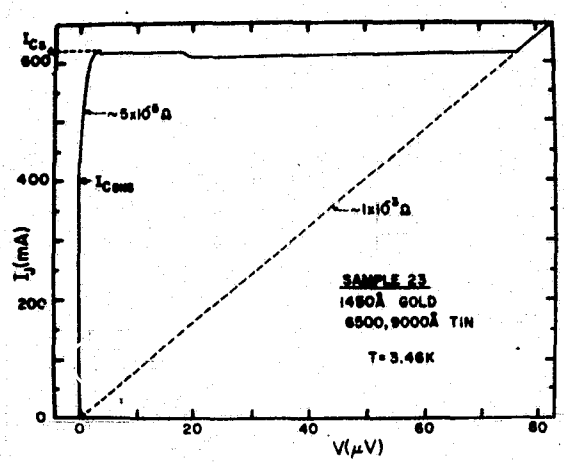

Fig. 20. I_J vs V plot showing the critical currents of both the tin and the sandwich. An expanded graph is used to determine I_{Csns}.

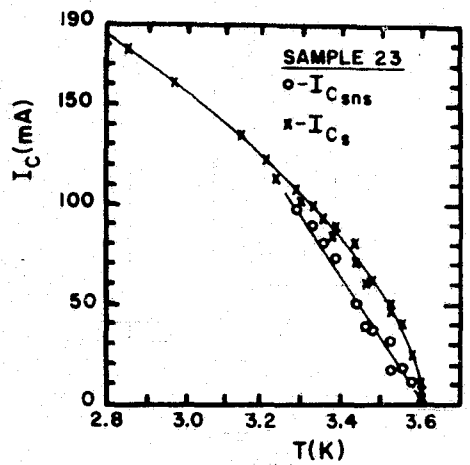

Fig. 21. Temperature dependence of the two critical currents.

Upon a closer inspection of Fig. 20, two negative differential resistance regions are noticed. They occur when the total sample resistance, V/I_J, increases rapidly due to the tin films changing to the normal state. Since the source resistance was ~50Ω, the increase in sample resistance corresponding to this current drop is of the order of 1/2Ω. This is in good agreement with ~0.35Ω for the measured resistance of a 9000Å tin film at 4.2K.

A plot of $\log(I_{Cs})$ vs $\log(1-t^2)$ for five different samples is shown in Fig. 22. One of the samples (15b) was fabricated with the N layer

omitted. The critical current dependence on $(1-t^2)$ is seen as a 3/2-

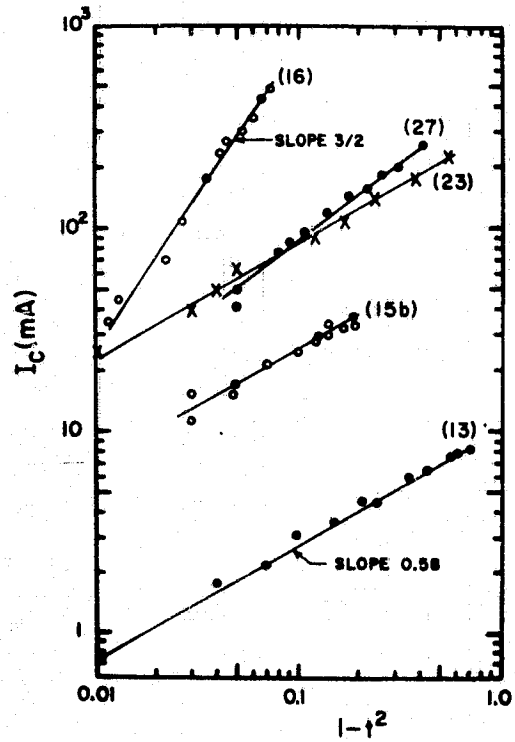

Fig. 22. Temperature dependence of I_{Cs}. Sample 15b has no N layer.

power law for sample 16 and approximately as a 0.58-power law for the other samples, including 15b.

In their work on critical currents in films of tin, Mydosh and Meissner[67] have reported a similar 3/2-power dependence on $(1-t^2)$ for low critical currents and a ~1/2-power law for higher currents.

---

67. J.A. Mydosh and H. Meissner, Phys. Rev. 140, A1568 (1965).

Phillips and Meissner[68] have made it plausible that the appearance of a voltage is due to an instability of laminar current flow. Thus, the tin critical currents observed in this investigation may also have been caused in part by the onset of the instability. While it may be more correct to call the current at the first appearance of a voltage an "instability current," the more conventional label "critical current" will be applied herein.

An additional experiment was undertaken to determine the change of the critical current of the tin when it was brought into proximity with a gold layer. First, a 9000Å tin film was vapor deposited in the shape of a "V" (see the pattern of Fig. 12). Next, a 1000Å gold film was deposited atop one of the legs of the vee, covering about one-fourth its length. These thicknesses were chosen as representative of the SNS sample. The critical currents of both tin legs were measured separately, and the results are shown in Fig. 23.

First, it is observed that the relatively thin layer of gold had its greatest effect at higher temperatures in suppressing I_{Cs}. This is expected from Eq. II. A. 7 and the temperature dependences of b (Eq. II. A. 9 and Eq. II. A. 4) and ξ_{GL} (Eq. I. B. 4. 5), for $F_s(x)$ increases with decreasing T, and the critical current of an isolated supercon-

68. H. L. Phillips and H. Meissner, Phys. Rev. B. 5, 3572 (1972).

ductor[69] varies directly as the pair potential $\Delta(x)=F(x)V(x)$. Secondly, the slope of the linear portion is once again ~ 0.58. Thus, the presence of a thin layer of gold is seen to decrease the value of I_{Cs}.

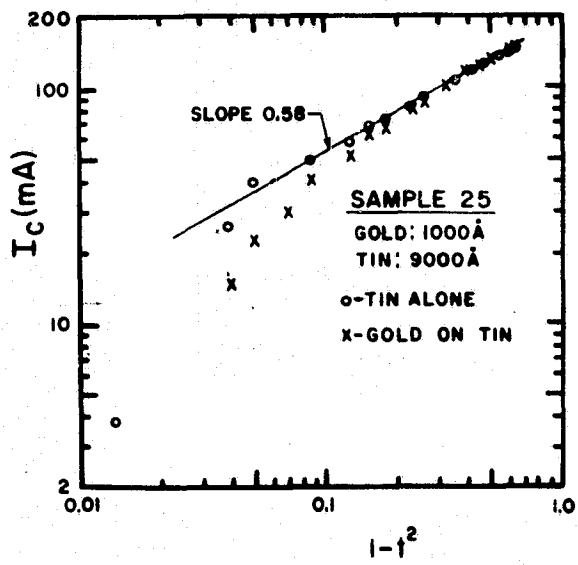

Fig. 23. Temperature dependence of critical current for S and SN films.

It would be desirable to make comparisons with other findings. However, this requires the knowledge of the intrinsic property the critical current density rather than the total current, and it is difficult to determine the tin critical current densities from the tin critical currents, because the tin probably goes normal first near the SN interface where the path of the current depends on both the penetration

69. J. Bardeen, Rev. Mod. Phys. 34, 667 (1962).

depth in the tin (Eq. I. B. 3. 3) and the Josephson penetration depth in the junction (Eq. II. C. 2. 1). As a first approximation, the critical-current carrying area of the tin was taken as either the entire cross section of the tin film or the product of the width of the tin and twice the penetration depth (Eq. I. B. 3. 3), whichever was smaller. At $T/T_C \sim 0.7$, the resulting critical current densities were of the order of $10^5 A/cm^2$. This is two orders of magnitude smaller than those obtained by Hunt[70] for isolated, very narrow tin films, where flux tubes and instabilities are absent.

In summary, the currents at which the S layers became normal conducting depended somewhat upon the proximity of the N layer - to the extent that it reduced the size of the critical currents but, apparently, did not change their functional dependence on temperature. The viewpoint of the analysis was exploratory, and it was intended to elucidate the conditions necessary to prevent the SNS device breakdown rather than determine the exact mechanism thereof.

In practice, the actual solution to the problem of relatively small values of I_{Cs} entailed (a) increasing the S-film thickness and (b) shortening ξ_N by decreasing ℓ_N through alloying the gold with copper. The former had the effect of increasing both the current-carrying area as well as the critical current density, since the depression of the order

---

70. T. K. Hunt, Phys. Rev. 151, 325 (1966).

parameter, $\Psi(x) \propto F_s(x)$, in the superconductor occurs for distances of only a few coherence lengths (see Eq. II. A. 7). Reducing ξ_N decreases the Josephson critical current exponentially (Eq. II. B. 7) and also increases the tin critical current through increasing the order parameter in the superconductor. In other words, the depression of the order parameter in the tin (Eq. II. A. 7) is affected by the normal metal only up to a thickness, t_N, of the order of ξ_N, whereas the Josephson critical current depends exponentially on the entire thickness of the N layer. Hence, reducing ξ_N allowed the reduction of I_{Csns} by increasing t_N beyond a few coherence lengths and also permitted an increase of I_{Cs}. The results of these modifications were that, with the possible exception of sample 39 at lower temperatures, the tin critical currents no longer appeared within that range of currents necessary to study the SNS device.

IV. C. The Effect of External Magnetic Field

The application of an external magnetic field, H, alters the Josephson critical current in a periodic manner described in section II. C. 1. The measurement of this effect is important for two reasons: (a) the observation of a critical current dependence on H of sin(H)/H verifies that the critical current is indeed the Josephson critical current, I_{Csns} (rather than, say, the tin critical current, I_{Cs}) and (b)

a determination can be made from the I_{Csns} vs H characteristic as to whether the junction is operating in the self-field limited region. If the junctions are self-field limited, the critical current may be significantly reduced by the self field. This is a fundamental limitation on the current-carrying capacity of the three-terminal Josephson junction device. Although the barrier current, I_N, also contributes to the self-field limitation of the device, it will be assumed to be much smaller than I_J here (i.e., a small-signal approximation) and, hence, its contribution to the magnetic field of the junction will be neglected.

The periodic behavior of I_{Csns} (hereafter called I_C for simplicity) with H was observed in two types of measurements. The first was a direct reading of I_C from the I_J vs V characteristic for various values of H. A typical I_C vs H curve obtained in this manner is shown in Fig. 24.

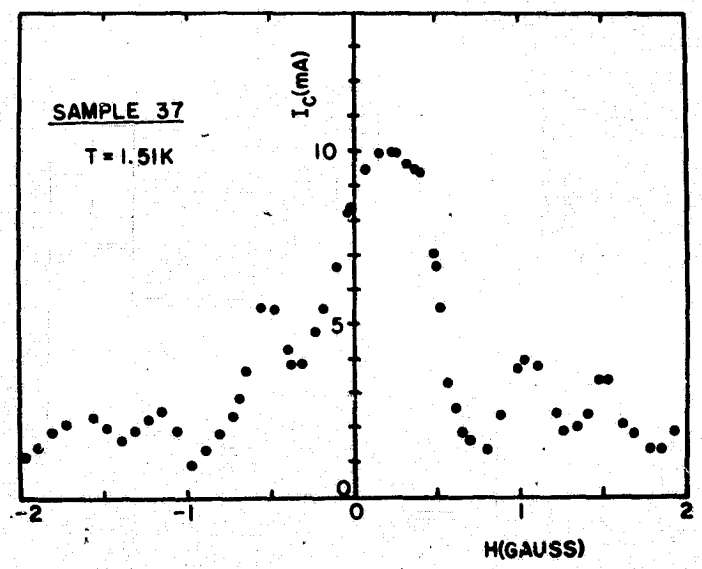

Fig. 24 I_C vs H.

The minima occur at integer multiples of H_1, the magnetic field at which the junction contains one quantum of flux. The asymmetric "skew" of the I_C vs H plot in Fig. 24 is due to the magnetic field of I_J itself (i.e., the self field)[71], and the small shift of the curve from the H=0 center is caused by stray magnetic fields. As the value of I_C increases, the junction becomes self-field limiting and the critical current varies linearly with H for small fields.[24, 39]

The second method was an X-Y recording of the variation of junction voltage with H for a fixed value of $I_J \gtrsim I_C$. Section II. C. 1 describes the theory of this approach. Although, in general, the shape of the V vs H characteristic differs from that of the I_C vs H curve due to the nonlinear relationship between I_J and V (Eq. II. D. 1. 2), the maxima of the former and the minima of the latter curves appear at the same values of $H=nH_1$ (i.e., those values of H corresponding to an integer number, n, of flux quanta in the junction). Figure 25 shows V vs H curves taken at two different temperatures and junction current levels. Curve 25b, plotted for a higher current level, shows the junction in the normal state for $|H| \gtrsim 4.7$G.

The value of H_1 can be readily determined from either type of curve, and, if the junction is not self-field limited, a theoretical value can also be determined from Eq. II. C. 1. 3. Therefore, a method to deter-

---

71. T. Yamashita and Y. Onodera, J. Appl. Phys. 38, 3523 (1967).

mine whether the SNS device is self-field limited is to compare the values of H_1 obtained both from Eq. II. C. 1. 3 and experimentally.

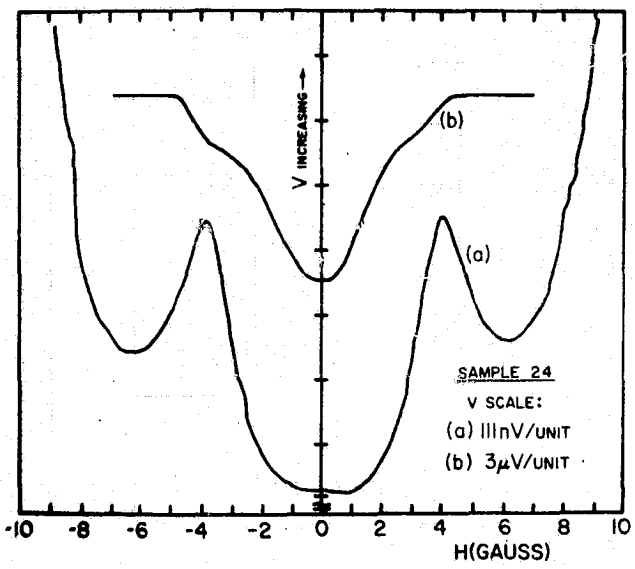

Fig. 25. V vs H plots (a) T=3.44K, I_J=2.56I_C, (b) T=3.35K, I_J=1.15I_C. The vertical scale indicates only voltage changes from V(H=0).

If there is reasonable agreement, then no limiting occurs. However, if the theoretical value is significantly smaller, the device is limiting the penetration into the junction of H and I_J to within a depth λ_J, the Josephson penetration depth[38] defined by Eq. II. C. 2. 1. For example, for sample 37 at 1.51K with λ=500Å, L=1.9x10^{-2}cm, and t_N=2580Å, Eq. II. C. 1. 3 yields H_1=0.28G which is to be compared with the experimental value found from Fig. 24 of H_1=0.53G. The degree of self-field limiting is then determined from a calculation of λ_J from Eq. II. C. 2. 3.

The result is $\lambda_J = 5.2 \times 10^{-3}$ cm, and since $\lambda_J \approx L/4$ (where L is the junction length), the device is experiencing minimal limiting due to the self field of I_J. It should be kept in mind, though, that Eq. II. C. 2. 3 is for an idealized junction geometry, and the results here are dependent upon the validity of this approximation.

Since λ_J depends on the temperature-dependent Josephson critical current density and H_1 depends weakly on λ_J, it is expected that H_1 will be weakly temperature dependent. An experimental plot of the temperature dependence of H_1 is shown in Fig. 26. The approximately linear dependence of H_1 on T is due to the linear dependence of H on I_J(Ampere's law) and the approximate linear behavior of I_C with T over a small range of T. For the example of Fig. 26 from a combination of

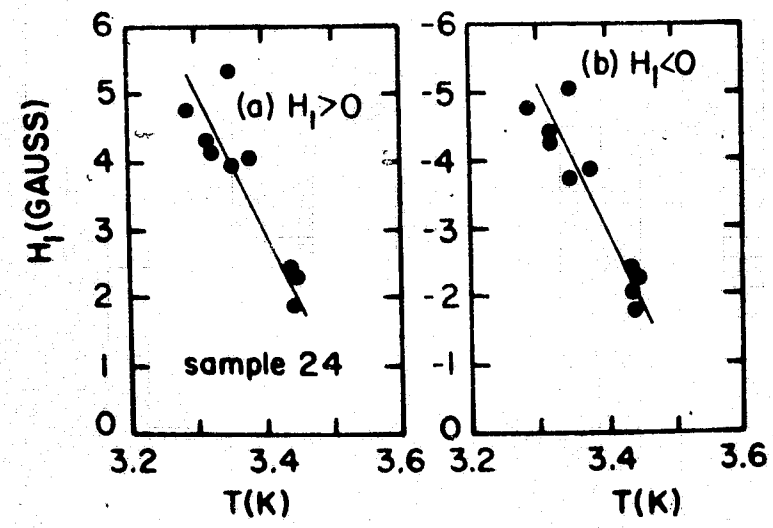

Fig. 26 Experimental temperature dependence of H_1.

Eqs. II. C. 2. 2-3 (which is equivalent to Ampere's law for the idealized geometry) an expression for H_1=(100Gauss/Amp) I_C is obtained. The value of dI_C/dT near T=3.4K is approximated from the I_C vs T plot as ~0.2A/K. The resulting theoretical variation of H_1 with T is given by $H_1=20(T_C-T)$ which is to be compared with the experimental slope of 22G/K. The agreement suggests that the idealized model for the magnetic-field effects in the junction is a good approximation.

IV. D. The Current-Voltage Characteristics of the Device

IV. D. 1. I_J vs V Characteristics with I_N=0

This section describes the I_J vs V characteristics of the SNS sandwich with only two electrical terminals (i. e., the control current, I_N, is zero), because a fundamental knowledge of the properties of the two-terminal device (viz., the usual SNS Josephson junction) is essential to the thorough understanding of the three-terminal, SNS device.

The critical current, I_C, of the SNS Josephson junction is defined as that current through the junction for which a voltage first appears across the junction. Figure 27 is a representative X-Y recording of the d. c. voltage V, across the junction. Figure 27 differs from Fig. 20 in that I_{Cs} is now sufficiently large so as not to be seen, and the voltage scale has been expanded by two orders of magnitude. The theoretical points are a fit of Eq. II. D. 1. 2, $V=R_n(I_J^2-I_C^2)^{1/2}$, to the

experimental curve with the junction resistance, R_n, as an adjustable parameter. For the curve of Fig. 27, R_n is found to be 370μΩ.

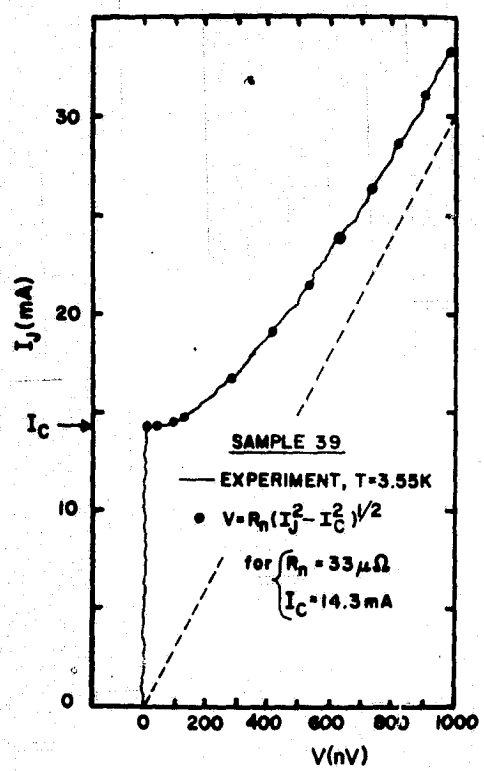

Fig. 27. I_J vs V plot for $I_N=0$.

All values of R_n were determined in this way and are listed in Table 4. As will be discussed in a later section, the values of R_n calculated from the N-metal resistivity and the junction geometry were much smaller than those values found using a best fit of Eq. II. D. 1. 2. With the exception of those early samples troubled by small critical currents of the tin films, the I_J vs V characteristics were all satisfactorily des-

cribed by Eq. II. D. 1. 2.

Recently, a Cooper pair-quasiparticle potential difference has been measured [72, 73] near an SN boundary in a nonequilibrium superconductor. Since the reported voltages have been as large as $2\mu V$[72] for a supercurrent density of $j_s = 450 A/cm^2$, a few words should be written here relating this phenomenon to the operation of the SNS device.

The pair-quasiparticle potential difference is due to an imbalance in the number of electron and hole quasiparticles in a superconductor when $\nabla \cdot \vec{j}_s \neq 0$.[74, 75] Physically, a non-vanishing divergence of j_s implies that Cooper pairs are created (quasiparticles condensed) or destroyed (pairs dissociated), and this occurs over distances extending to a few coherence lengths into a superconductor near an SN boundary. The imbalance occurs when quasiparticles are injected into a superconductor at an SN interface and pairs are extracted from it elsewhere. The quasiparticles entering the S layer produce a potential gradient for a few coherence lengths into the superconductor until they decay and condense into pairs. If the electrochemical potential of the pairs in the superconductor near the SN interface were also to experience

---

72. M. L. Yu and J. E. Mercereau, Phys. Rev. Letters 28, 1117 (1972).
73. J. Clarke, Phys. Rev. Letters 28, 1363 (1972).
74. T. J. Rieger, D. J. Scalapino, and J. E. Mercereau, Phys. Rev. Letters 27, 1787 (1971).
75. M. Tinkham and J. Clarke, Phys. Rev. Letters 28, 1366 (1972).

such a potential gradient, the supercurrent would increase in time as described by Eq. I. B. 2. 1 until bounded by some critical phenomenon (e. g., phase slippage of the order parameter). Instead, a space charge of pairs is set up[74] in order to cause the pair electrochemical potential to be constant throughout the superconductor. Therefore, the pair-quasiparticle potential difference is due just to the resistive penetration of quasiparticles into the S layer.

Since the value of the junction resistance, R_n, includes the resistance of the interface layers (as described in the following section) and is experimentally determined, the pair-quasiparticle potential need not be introduced directly into the physics of the device equations. The excellent fit of Eq. II. D. 1. 2 for the I_J vs V characteristics is evidence that the proper choice of R_n will include the effect of the pair-quasiparticle potential difference in the superconductor.

The temperature dependence of the junction critical current is shown in Fig. 28 for samples of varying thickness. The current was strongly dependent upon the thickness of the N layer, t_N, as might be expected from Eq. II. B. 7. However, some samples, (e. g., sample 38), have exhibited critical currents far smaller than those of samples with similar dimensions (e. g., sample 32 in Fig. 28). Since these samples with suppressed critical currents all had larger values of R_n than their higher-current counterparts, the effect was most likely due to

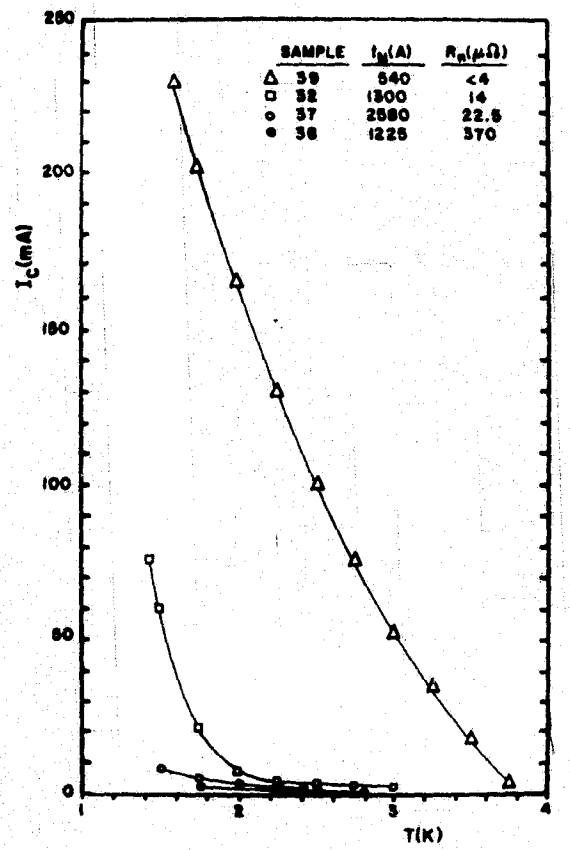

Fig. 28. I_C vs T for four samples.

a boundary-layer resistance which impeded the diffusion of pairs through N and decreased the effective value of ξ_N.* Such a boundary layer may result from too high a pressure during the vapor deposition,

---

*Rockefeller[4] has utilized such an approach in successfully explaining his results for the values of I_C for specimens of large R_n.

and it is due to the oxidation[76] of the tin layer and the general condensation of volatile impurities during the deposition. Evidence of the oxide layer and its effect on the characteristics of the three-terminal device will be presented in a later section.

In general, all the samples in this experiment experienced anomalously high values of R_n (i.e., the experimental values of R_n in Table 4 were as much as 500 times larger than that value computed from the bulk resistivity of the N layer). The high-resistance junctions experienced no self-field limiting because of the supressed values of I_C. For equivalent junctions of Pb-Cu(alloy)-Pb, Clarke[24] reported values of I_C an order of magnitude larger and R_n an order of magnitude smaller than those found here. This suggests the presence of a boundary layer dominating here but absent for Clarke's junctions which were condensed at 10^{-8} Torr.

Figure 29 is a plot of log (I_C) versus $T^{1/2}$ illustrating the types of critical current behavior observed here. The two arrows indicate temperatures where a I_C vs H curve was plotted and the amount of self-field limiting determined. Point "a" for sample 37 indicates the approximate onset for self-field limiting ($\lambda_J \approx L/4$), and point "b" for sample 38 indicates a temperature where flux still penetrates the

---

76. S. Dushman, Scientific Foundation of Vacuum Technique (Wiley, N.Y., 1949), p. 17.

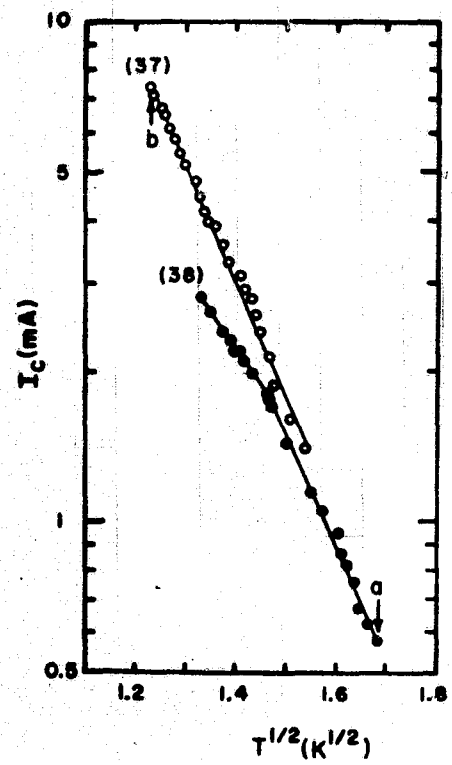

Fig. 29. Log(I_C vs $T^{1/2}$ for two samples. At point "a" H penetrates the entire junction, and at "b" $\lambda_J \approx L/4$.

entire junction area. Thus, the decrease in slope for sample 38 appears to be caused by self-field limiting. The linear portion of the curves below limiting may be expressed as

$$I_C(T) = I_{Co} \exp(-5.3T^{1/2}), \qquad \text{IV.D.1.1}$$

where I_{Co} is a positive constant. The theory (Eq. II. B. 7) is strictly valid only near T_C. Now, if it is used for lower temperatures, the

exponential term dominates; and, with the temperature dependence of ξ_N for a dirty metal (Eq. II. A. 4), it can be approximated as

$$I_C(T) \approx D \exp(-GT^{1/2}) , \qquad \text{IV.D.1.2}$$

where D is a positive constant and $G=(6\pi kt_N^2/\hbar v_N \ell_N)$. Thus, Fig. 29 suggests that the form of Eq. II. B. 7 is valid for a dirty SNS junction even for $T \approx 0.5T_C$. It also suggests that the linear behavior of $\log(I_C)$ vs $T^{1/2}$ found by Clarke[24] for $T \lesssim 0.5T_C$ was indeed dominated by self-field limiting. Sheperd[77] has verified Eq. II. B. 7 in the region $T \approx 0.1T_C$ for thick, clean SNS sandwiches.

An effective value of $\xi_N(T)$ for the combined N and boundary layers can be obtained from the above relation for G using the experimental value of G obtained from the slope of the curve in Fig. 29. The resulting values of $\xi_{Neff.}(T=3.5K)$ are 250Å and 125Å for samples 37 and 38, respectively. The theoretical value for $\xi_N(3.5K)$ obtained from the mean free path in the bulk N layer is 500Å. Therefore, if Eq. II. B. 7 is indeed valid for $T \lesssim T_C/2$, then the value of $\xi_{Neff.}(3.5)$ illustrates that the additional scattering in the boundary layer has a strong effect on the properties of the SNS devices in this investigation. This idea of an effective $\xi_N(T)$ (i. e., an empirical value) encompasses all boundary-layer phenomenon including interdiffusion between lamina.

---

77. J. G. Sheperd, Proc. Roy. Soc. (London) A326, 421 (1972).

In summary:

(a) the SNS sandwiches exhibited anomalously large values of R_n probably due to boundary layers at one or both of the SN interfaces;

(b) the I_J vs V characteristics were in excellent agreement with Eq. II. D. 1. 2;

(c) as expected, the pair-quasiparticle potential difference was not directly observed in the I_J vs V characteristics, although it did contribute to the experimental value of R_n;

(d) the SNS junctions experienced little self-field limiting because of the small values of $\xi_{Neff.}$ and, hence, small I_C;

(e) the temperature dependence of I_C was described remarkably well by an extension to lower temperatures of the theory in the "dirty" limit strictly valid only near T_C.

IV. D. 2. I_J vs V Characteristics with $I_N \neq 0$

The introduction of a control current, I_N, directly into the N layer of a SNS sandwich modifies the I_J vs V characteristics of the junction.[4] The purpose of this section is to (a) present the experimental evidence, (b) characterize the effect with empirical parameters, and (c) explain the observations with a physical model.

As illustrated in Figs. 12 and 13, I_N flowed directly into the N layer and out of the junction through one of the S layers. In the later samples

(Fig. 15), the film carrying I_N to the N-metal layer was superconducting for the purpose of reducing the input resistance of the device. However, in these experiments the superconducting I_N lead contacted the N metal sufficiently far from the junction so that only unpaired electrons were injected into the junction proper.

A typical I_J vs V characteristic obtained for various discrete values of I_N is shown in Fig. 30, where positive values were assigned to I_N when it was in the same direction as I_J in the S film common to both currents. These curves are similar to those obtained by Rockefeller[4] for crossed-wire SNS junctions, with the scaling adjusted accordingly for the larger junction areas in this investigation.

The nomenclature for the critical value of I_J with $I_N \neq 0$ (i.e., those critical-current "knees" in Fig. 30 for $I_N \neq 0$) will be $I_{JC}(I_N)$ or just I_{JC} if the particular value of I_N is assumed known. The symbol I_C shall be reserved for the critical value of the supercurrent through the N layer (i.e., the actual Josephson critical current), and it represents that value of I_{JC} for $I_N = 0$.

The result of introducing I_N into the sandwich is to shift the I_J vs V characteristics along the current scale without changing their shape. Thus, Eq. II. D. 1. 2 (Fig. 6) still describes the curves but with the zero of I_J shifted. The polarity of the current shift is dependent upon only the relative direction of I_N with respect to the

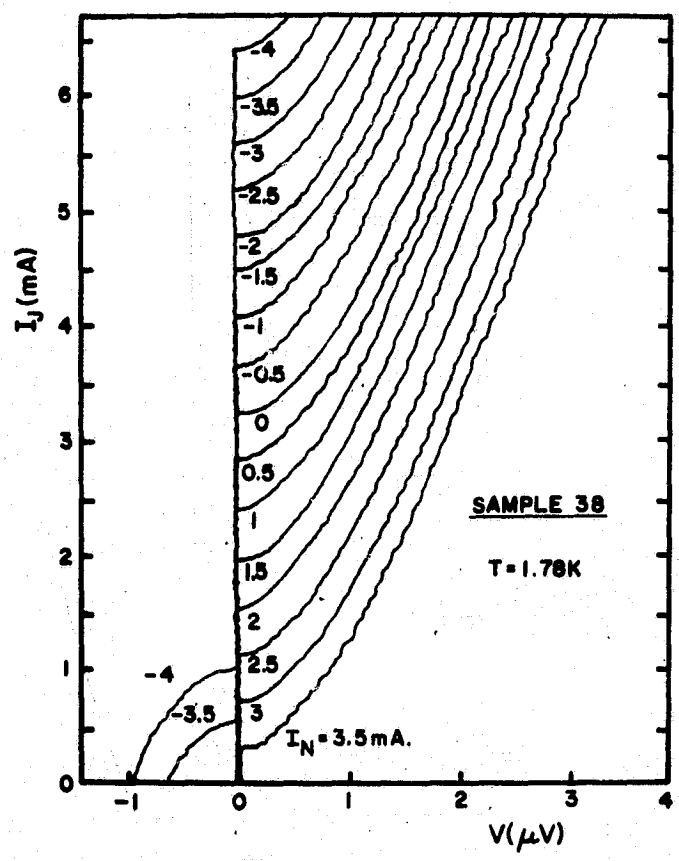

Fig. 30. I_J vs V characteristic with I_N as a parameter.

direction of I_J and not with respect to the junction. That is, the modulation of I_J by I_N is not a charge-controlled effect (as is the bipolar transistor) due to the injection or extraction of quasiparticles into or from a population of pairs and quasiparticles within the junction. Neither is the effect due to the magnetic field of I_N, for the shift in I_J with I_N is essentially independent of external magnetic fields much

C-2

larger than those generated in the junction by I_N. These arguments, as well as Fig. 30, suggest that the modulation of I_J by I_N is a current-controlled phenomenon whereby I_N, or some fraction thereof, adds to or subtracts from the Josephson current in the junction.

A measure of the modulation effectiveness of I_N may be defined by

$$\alpha_o \equiv [-\Delta I_J / \Delta I_N]_{V=\text{constant}}. \qquad \text{IV. D. 2. 1}$$

Values of α_o can be measured directly from the I_J vs V characteristics. Figures 31 and 32 illustrate the observed behavior of α_o with I_N. For

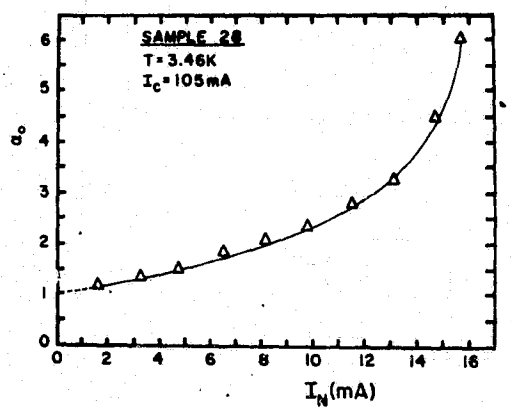

Fig. 31. α_o vs I_N for a sample in the evaporator/cryostat. $\alpha_o \approx 0$ for $I_N < 0$ until the tin went normal.

those samples measured in the evaporator/cryostat, the values of α_o are strongly dependent on I_N and are as large as $\alpha_o \approx 8$ (e.g., see Fig. 31). These values of α_o are probably related to sample heating

in the evaporator/cryostat, because both polarities of I_N suppressed I_C, and for all later samples measured in the immersion cryostat the values of α_o are essentially constant with I_N and less than unity.

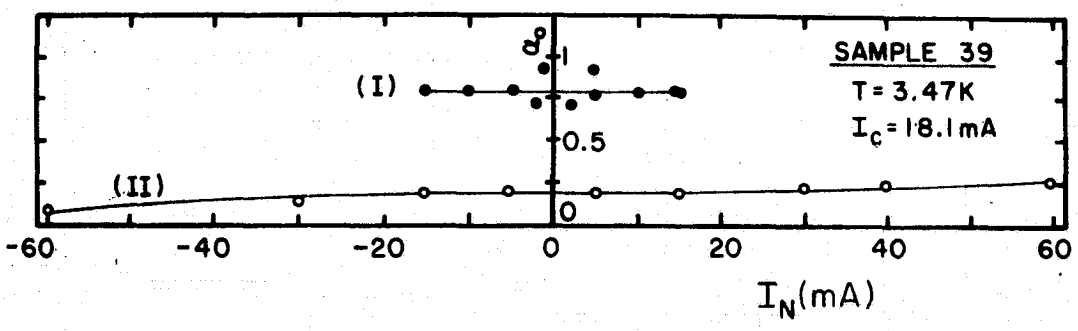

Fig. 32. α_o vs I_N for a sample in the immersion cryostat. Curve II has the return path of I_N changed to the S layer opposite that used for curve I.

Curve I in Fig. 32 illustrates a constant value of $\alpha_{oI} \approx 0.8$ for sample 39. Curve II is plotted for the same sample with a change in the return path of I_N from one S layer to the other. The resulting $\alpha_{oII} \approx 0.2$ is constant for $|I_N| < 18$ mA. For values of $|I_N| > 18$ mA, which is approximately the value of I_C, the variation of α_{oII} with increasing I_N suggests a suppression of the critical current; and since this occurs for both polarities of I_N, heating must be suspect. The reason for $\alpha_{oI} + \alpha_{oII} = 1$ will be discussed later.

If the operation of the device is indeed dependent upon a linear combination of I_J and I_N, it should not matter which current is varied

to produce the same voltage changes (with the effect of I_N being scaled by α_o, of course). Therefore, X-Y recordings of I_N vs V for various values of I_J were made. Figure 33 is one such plot for I_J= 3mA. As

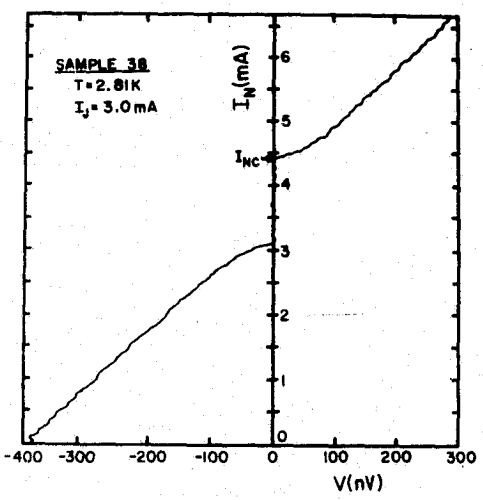

Fig. 33. I_N vs V for I_J=3mA. V=0 defined for I_N=I_J=0.

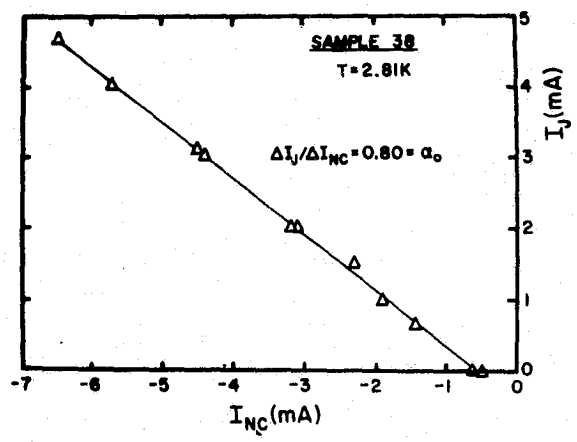

Fig. 34. I_J vs I_{NC}. (Fig. 33 defines I_{NC}.)

expected, it is of the same form as Figs. 6 and 30; and if the change in the upper critical-current knee, I_{NC} (defined in Fig. 33), is plotted versus I_J, as shown in Fig. 34, the resulting slope is indeed α_o.

A nonlinear, low-frequency, lumped model of the three-terminal SNS device is shown in Fig. 35. The model is based on that of Stewart[40] and McCumber[41], wherein the junction current is divided into (a) the supercurrent $I_C \sin\phi(t)$, where $\phi(t)$ is the phase difference of the order parameter across the junction, and it is related to the instantaneous

junction voltage v(t) by Eq. II. B. 2 and (b) the resistive current (quasi-particle current) which flows through R_a and R_b, where $R_a + R_b = R_n$.

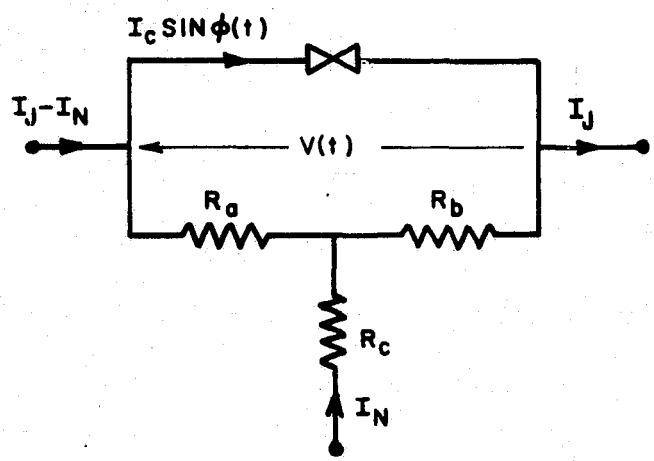

Fig. 35. A lumped, low-frequency model of the three-terminal SNS junction, shown with $I_N < 0$.

The shunt capacitance of the SNS junction is $\sim 10^{-12}$F and is neglected in this model. This is an excellent approximation since the highest frequencies experienced by the junction were of the order of 10^9Hz (viz., the characteristic Josephson frequency for a junction voltage of a few microvolts - see Eq. II. B. 3) resulting in a maximum capacitive current of $C dv/dt \sim 10^{-8}$A $\ll I_J, I_N$. Also, the $R_n C$ time constant of the junction was so short ($\sim 10^{-17}$sec) as to have no effect on the junction voltage.

The arguments for the modification of the Stewart-McCumber model to represent the three-terminal device are as follows. When

there is zero voltage across the SNS sandwich, the quasiparticles injected into the N metal from the I_N lead are expected to flow through the N metal and boundary layers to both superconductors. The expected flow patterns for a simple junction geometry are shown in Fig. 36 for $\alpha_o = 0.75$. Since the interaction potential is small in gold and copper[24]

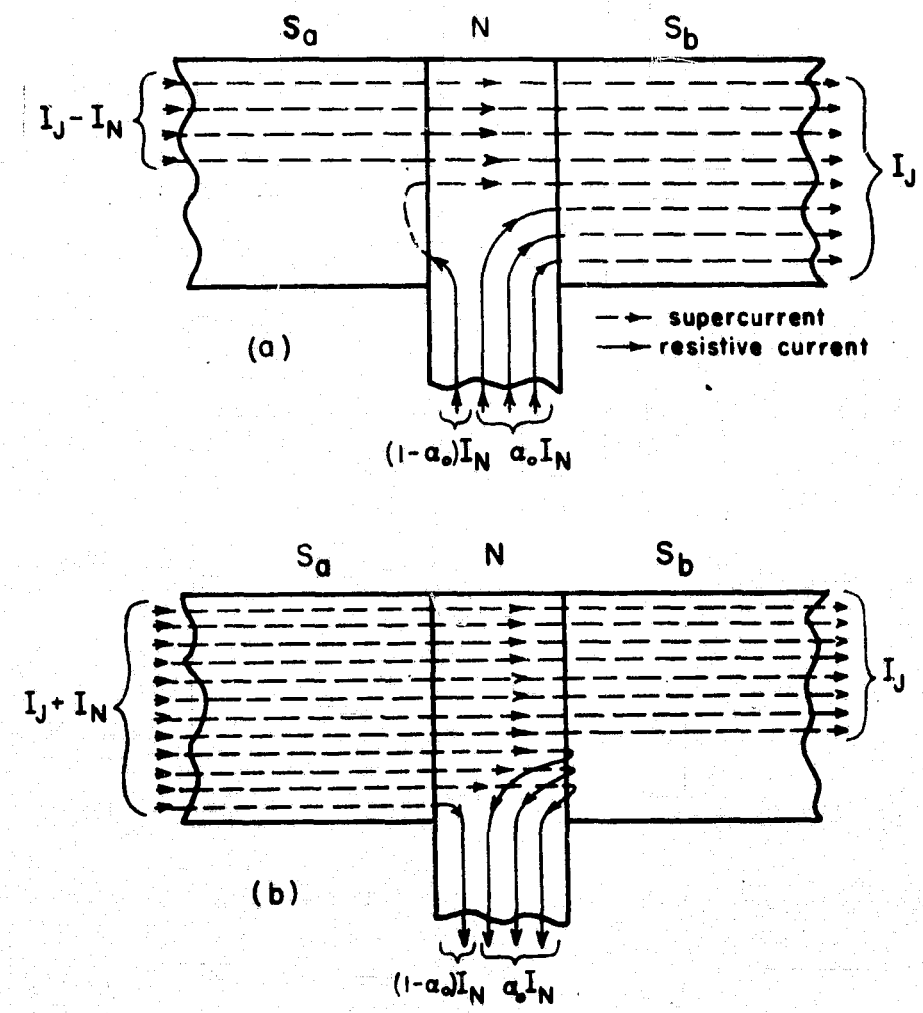

Fig. 36. Simplified junction geometry illustrating diagrammatically the paths of normal and supercurrents for $\alpha_o = 0.75$. (a) $I_N = -0.5I_J$ and (b) $I_N = 0.5I_J$.

(i. e., neither metal has been reported to exhibit superconductivity), it is expected that on the average the quasiparticles will not condense into pairs within the N layer. Thus, the current I_N will produce potential differences within the N layer. Now if $I_J = I_{JC}$, which from the definition of α_o is given by

$$I_{JC} = I_C - \alpha_o I_N , \qquad \text{IV.D.2.2}$$

then the supercurrent through the junction is at its critical value and the quasiparticle current I_N must split as shown in Fig. 36 dictated by continuity of total current. In addition, $V=0$ for $I_J = I_{JC}$; and the voltages across R_a and R_b must then be equal. Combining the requirement for the splitting of I_N with the equality of voltages across the two resistors yields the following relation between α_o and the junction resistances:

$$\alpha_o = R_a/(R_a + R_b) = R_a/R_n . \qquad \text{IV.D.2.3}$$

Equation IV. D. 2. 3 was experimentally verified through measurements of the values of R_a and R_b. This was accomplished by setting $I_N = 0$ and making X - Y recordings of I_J vs $V_a - V_N$ and I_J vs $V_N - V_b$, where $V_a - V_N$ and $V_N - V_b$ are the voltages between the N-metal contact and superconductor "a" and superconductor "b", respectively. Figure 37 is a sketch of the expected equipotentials for $I_J > I_{JC}$ and $I_N = 0$ illustrating V_a, V_b, and V_N. These current-voltage curves are similar

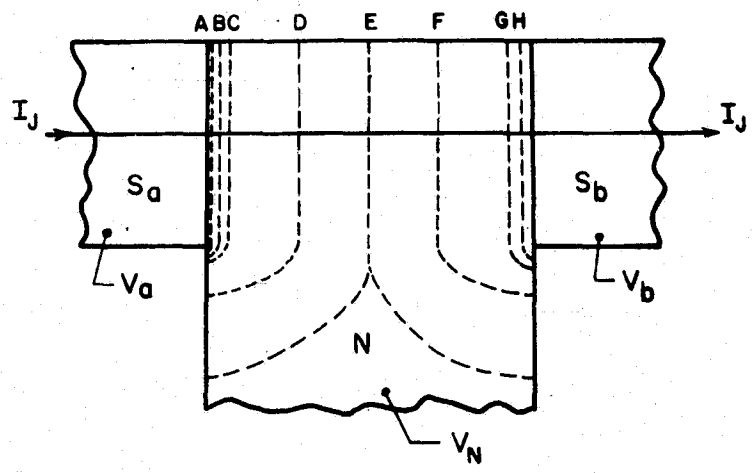

Fig. 37. Sketch of the expected equipotentials (dashed lines A-H) for $I_J > I_C$, $I_N = 0$, and $R_a > R_b$.

to the I_J vs V characteristics shown earlier (because $V = V_a - V_b$), and the values of R_a and R_b were obtained from the curves at the larger values of I_J where the curves become ohmic. For example, for sample 38 the three resistances were measured at T= 2.81K and found to be: $R_a = 305\mu\Omega$, $R_b = 65\mu\Omega$, and $R_n = 370\mu\Omega$. The sum of R_a plus R_b equals R_n as expected, and $R_a/R_n = 0.82$. This is in good agreement with the value of $\alpha_o = 0.81$ obtained from the I_J vs V curves for T = 2.81K. The disparity of R_a and R_b is thought to be due to the asymmetry in the vapor-deposition process: Superconductor "a" is the first film to be deposited, and it probably oxidizes somewhat before the N layer is deposited over it. Therefore, the value of R_a might be dominated by an oxide layer at the lower SN interface. On

the other hand, the second (upper) SN junction was formed by depositing tin atop a layer of gold, and since gold does not oxidize, the resistance of this boundary layer is expected to be smaller than that of the lower SN interface. In one run R_b was measured to be less than 1% of the value of R_a (here $\alpha_o \approx 1$). Therefore, if R_a were due to an oxide layer as supposed, the value of R_n measured in the absence of such a boundary layer would necessarily be smaller by a factor of 10^{-2} (i. e., the bulk resistance of the N layer in this case is smaller than the boundary-layer resistance by a factor of 10^2). This supports the supposition that the anomalously large values of R_n in these experiments (Table 4) were due to boundary layers at the SN interfaces.

Another test of Eq. IV. D. 2. 3 is the observation of how a change in the return path of I_N affects α_o. Figure 32 illustrates the two resulting values of α_o for the return path of I_N being either superconductor "a" or superconductor "b". The values of α_{oI} in Fig. 32 are obtained in the usual manner with the return path of I_N through superconductor "a" (e. g., Fig. 36a or b). Conversely, the values of α_{oII} are obtained with the I_N return path through superconductor "b" (which, in effect, is the same setup shown by Fig. 36 with the "a" and "b" labels interchanged). The resulting sum of these two experimental values of α_o is unity as expected from Eq. IV. D. 2. 3, since $\alpha_{oI} + \alpha_{oII} = R_a/R_n + R_b/R_n = R_n/R_n$.

Since the value of R_n varies somewhat with temperature (see section IV. E), then α_o must also if Eq. IV. D. 2. 3 is valid for all T. Experimentally, the value of α_o was found to be slightly temperature dependent (as was R_n). For example, $\alpha_o = 0.81$ for sample 38 at T= 2. 80K, whereas at T= 1. 77K the measured value of α_o increased to $\alpha_o = 0.83$. This increase in α_o is consistent with the decrease of both R_a and R_b due to the increase of Andreev[78] scattering at the SN interface for lower temperatures. For temperatures closer to T_C more of the quasiparticles impinging on the superconductor from the N metal will have energies greater than $\Delta(T)$ (where $\Delta(T)$ approaches zero with increasing temperature as $(1 - T/T_C)^{1/2}$ near T_C[79]) and, consequently, will have a finite probability[80] of propagating into the superconductor where they will decay dissipatively.[81] The result will be a larger resistance. If this dissipative process occurs equally at both SN interfaces, the change in $R_n = R_a + R_b$ need be only ~3% to produce the change in α_o observed for sample 38 from T= 1. 77K to 2. 80K. This 3% change in R_n is in reasonable agreement with the observed variation of R_n with T (e. g., see Fig. 38).

---

78. A. F. Andreev, Sov. Phys. -JETP 19, 1228 (1964).
79. e. g., ref. 19, p. 124.
80. W. L. McMillan, Phys. Rev. 175, 559 (1968).
81. A. B. Pippard, F. R. S., J. G. Shepherd, and D. A. Tindall, Proc. Roy. Soc. (London) A324, 17 (1971).

Thus far, the proposed model of the three-terminal device has agreed with the experimental results for V=0 (i.e., in the absence of an a.c. Josephson current). When a finite voltage is present across the junction, the solution to the problem becomes more complex since the d.c. currents are then coupled to the a.c. Josephson current. From the model of Fig. 35 when $v(t) \neq 0$ (i.e., $I_J > I_{JC}$), an equation can be written relating the instantaneous junction voltage, v(t), to the instantaneous values of junction current, $i_J(t)$, and control current, $i_N(t)$; and it is given by

$$v(t)/R_n = [\, i_J(t) + \alpha_o i_N(t) \,] - I_C \sin\phi(t). \qquad \text{IV.D.2.4}$$

v(t) is related to $\phi(t)$ through Eq. II.B.2. For $i_N = 0$ and for a constant-current supply whereby $i_J(t) = I_J$, the solution to Eq. IV.D.2.4 for the time-averaged voltage across the junction, $V = \langle v(t) \rangle$, as a function of I_J is given by Eq. II.D.1.2. Now, if the variation of the control current is much slower than that of $\phi(t)$ (viz., the Josephson frequency $\omega_o = 2ev/\hbar$), an approximate solution to Eq. IV.D.2.4 for $i_N \neq 0$ can be obtained from Eq. II.D.1.2 by replacing I_J with $I_J + \alpha_o i_N$. The resulting solution is given by

$$V = R_n [(I_J + \alpha_o i_N)^2 - I_C^2]^{1/2}. \qquad \text{IV.D.2.5}$$

This is a good approximation for a low-frequency control signal, since even for junction voltages as low as one nanovolt the corresponding value of ω_o is as large as $\sim 5 \times 10^5$ Hz. That the model still satisfies the experimental results when $V \neq 0$ can be seen by holding V constant and examining the right-hand side of Eq. IV. D. 2. 5. Since I_C is a constant for any one temperature, then the quantity $I_J + \alpha_o i_N$ must also be a constant for the right-hand side of Eq. IV. D. 2. 5 to be constant. However, $I_J + \alpha_o i_N$ = constant is just the integral form of Eq. IV. D. 2. 1, and, thus, the model satisfies the data for a low frequency or constant control current.

In summary-

(a) the three-terminal SNS junction is a current-controlled device in its present form;

(b) the introduction of I_N shifts the I_J vs V characteristics along the current scale in a manner described by an empirical parameter, α_o;

(c) $\alpha_o = R_a/R_n$ and, so, depends strongly on the boundary-layer resistance;

(d) α_o is essentially independent of the value of I_N, and it has a weak dependence on T (as did R_n);

(e) a low-frequency, lumped model was developed which characterizes the SNS device with the equation: $V = R_n[(I_J + \alpha_o i_N)^2 - I_C^2]^{1/2}$.

IV. E. Characteristic Resistances

This section presents the experimental values for those resistances which characterize the three-terminal SNS device: R_{in}, R_n, and r_o. The importance of these resistances with respect to the operation of the three-terminal device will be discussed in section V.

The control current I_N experiences a resistance R_{in} which is a combination of the normal-metal lead resistance R_c (see Fig. 35) and a junction resistance which, for V=0, is given by the parallel combination of R_a and R_b. As will be discussed later, R_{in} must be minimized for the effective utilization of the three-terminal device as a circuit element. Therefore, in the later samples the gold-film I_N input lead was replaced by a superconducting film of tin which effectively reduced R_{in} by three orders of magnitude (see Tables 1-4). However, because of the accuracy limitations of mechanical mask alignment, the resulting value of R_{in} was still dominated by the N-metal resistance outside the junction proper, R_c (i.e., R_{in} can still be reduced significantly by contacting the N film with a superconducting lead closer to the junction proper).

The values of R_n and its strong dependence on the boundary layers and the dissipative penetration of quasiparticles into the superconductor at the SN interface have already been discussed. A typical plot of the temperature dependence of R_n is shown in Fig. 38. At about 3.5K the

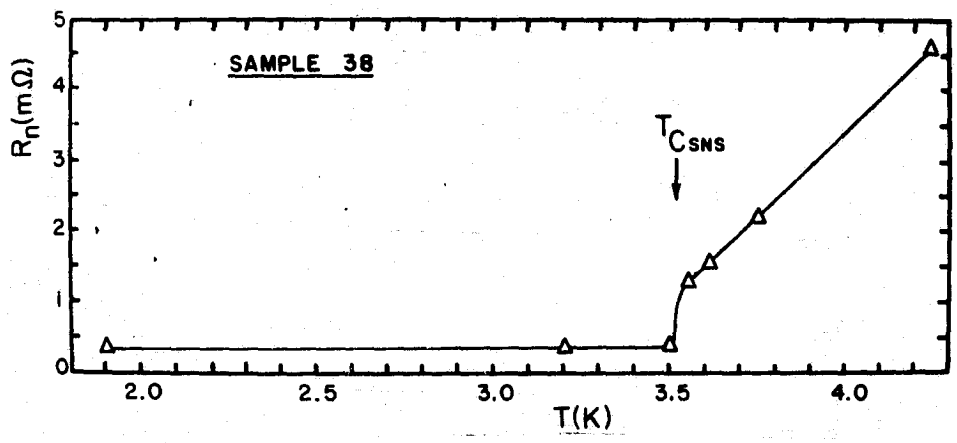

Fig. 38. Temperature dependence of R_n.

the junction becomes superconducting. The observed variation of R_n from T= 3.2 to 1.9K is ~ 3%. This decrease in R_n at lower temperatures may be explained qualitatively by the reduction of the number of quasiparticles which have sufficient energy to penetrate the S layer dissipatively at the reduced temperatures where Andreev[78] scattering becomes dominant.

The third resistance, r_o, is the dynamic resistance of the junction (i.e., the slope of the V vs I_J curve, which may be found by differentiating Eq. II. D. 1. 2). A method peculiar to the three-terminal device was employed to plot a voltage change, ΔV, proportional to r_o versus I_J. As detailed in section III. H. 4, the technique involved injecting a positive-going square-wave current $i_N(t)$ and then measuring the magnitude, ΔV, of the resulting square-wave junction voltage with the

lock-in amplifier.

As the value of $i_N(t)$ switches from 0 to ΔI_N, the voltage across the junction changes by an amount ΔV as shown in Fig. 39. Since the I_J-supply source resistance ($\sim 50\Omega$) is much larger than the sample resistance of $\sim 10^{-5}\Omega$, the jump ΔV occurs essentially at constant I_J.

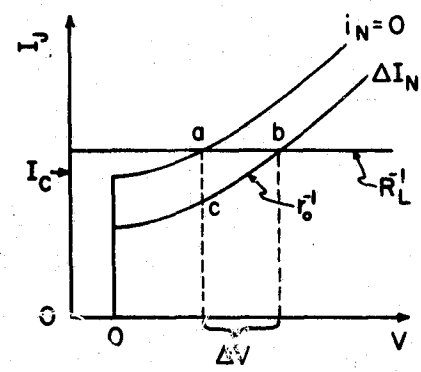

Fig. 39. I_J vs V plot illustrating the voltage change, ΔV, due to a change in control current from 0 to ΔI_N.

Therefore, if ΔI_N is sufficiently small and constant, the contour "abc" in Fig. 39 may be approximated by a right triangle where then $\Delta V \approx \alpha_o \Delta I_N r_o$. Thus, a plot of I_J vs ΔV represents the variation of r_o with I_J. Figures 40a and 40b are examples of two such I_J vs ΔV curves for different square-wave frequencies. The dashed lines in Fig. 40 are a plot of the differential form of Eq. IV. D. 2. 5,

$$V = R_n 2\alpha_o \Delta I_N \{1 - [I_C/(I_J + \alpha_o i_N)]^2\}^{-1/2} \qquad \text{IV. E. 1}$$

for a value of $R_n = 370\mu\Omega$ obtained from a best fit of Eq. II. D. 1. 2 to the I_J vs V characteristic.

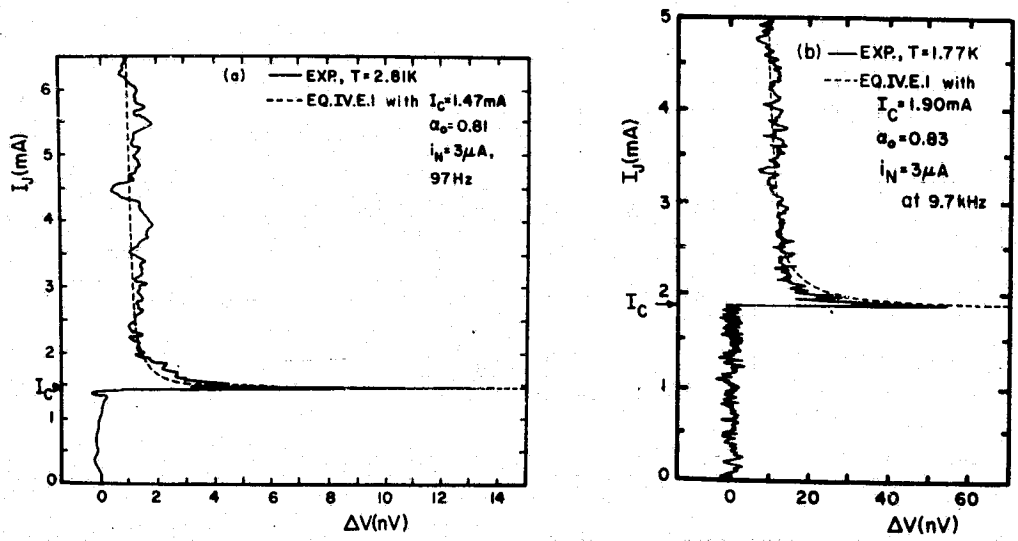

Fig. 40. I_J vs ΔV plot for sample 38 with $R_n = 370\mu\Omega$. (a) i_N is a square wave at 97Hz, (b) 9. 7kHz.

The agreement between theory and experiment in Fig. 40a suggests that the lumped model of Fig. 35 is an excellent approximation for the three-terminal device at low frequencies. The curve of Fig. 40b indicates that at higher signal frequencies the SNS junction reaches the normal-resistance state with increasing I_J somewhat faster than that predicted by the low-frequency theory. The greater significance of Fig. 40b, though, is that it provides evidence that the three-terminal

SNS device will operate at frequencies of at least 9.7kHz (i.e., it is demonstrated that the phenomenon is not restricted to constant currents). It was not tested at higher frequencies because the upper frequency limit of the lock-in preamplifier was 10kHz.

The results of this section may be summarized as:

(a) R_{in} is presently dominated by the N-metal lead resistance R_c;

(b) the observed variation of R_n with temperature for $T < T_C$ is in agreement with the corresponding change in α_o;

(c) a method was developed to plot the dynamic junction resistance, r_o, versus I_J for various control-signal frequencies;

(d) the data confirmed the validity of the low-frequency model at 97Hz and showed its limited applicability at 9.7kHz;

(e) experimental evidence was provided that the three-terminal device will operate at frequencies of at least 9.7kHz.

IV.F. Fluctuation Effects

The effect of thermal fluctuations on the I_J vs V characteristics of the SNS sandwich is to "round" the critical-current knee, the region of greatest dynamic resistance, r_o. A quantitative description of this rounding is given by the parameter

$$\gamma = \hbar I_C / kT_{noise} , \qquad \text{IV.F.1}$$

as described in section II. D. 2. T_{noise} is the effective noise temperature of the fluctuation-current generator. In the limit as γ approaches ∞, the fluctuations produce a negligible effect. Now, since the maximum value of r_o is limited by the fluctuations, a measurement of r_{oMax}, as from the I_J vs ΔV curves of the previous section, can be used to determine the experimental value of γ. This section presents such a method to determine γ and, consequently, the effective noise temperature of the sample.

A sketch is shown in Fig. 41 representing the case where fluctuations are present when the control current is switched from 0 to ΔI_N in square-wave fashion producing a change, ΔV, in the junction voltage.

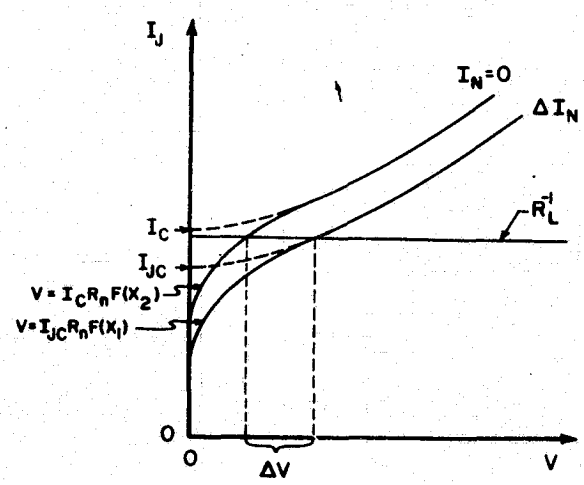

Fig. 41. Theoretical I_J vs V curves for finite γ, illustrating ΔV due to ΔI_N. Dashed curves for $\gamma=\infty$. $X_1 \equiv I_J/I_{JC}$ and $X_2 \equiv I_J/I_C$.

The dashed curves represent the case where $\gamma = \infty$. From Eq. II. D. 2. 2, $F(X_1)$ and $F(X_2)$ may be used as closed-form approximations[45] of the lower and upper curves, respectively, for $X_1, X_2 < 1$ and large γ. The reduced currents are defined by $X_1 \equiv I_J/I_{JC}$ and $X_2 \equiv I_J/I_C$, where $I_{JC} = I_C - \alpha_o \Delta I_N$.

The maximum value of $\Delta V \approx \alpha_o \Delta I_N r_o$ is clearly dependent upon both γ and ΔI_N and is given by $\Delta V_{max} \approx I_C R_n [F(X_1) - F(X_2)]_{max}$, which is the maximum voltage separation of the two curves along the load line. A computer program was written to calculate $[F(X_1) - F(X_2)]_{max}$. However, the maximum value occurred at $X_1 \gtrsim 1$, for which $F(X_1)$ is not defined. Therefore, the theoretical voltage difference ΔV was approximated by the voltage difference between $F(X_2)$ and the lower dashed curve in Fig. 41 for $\gamma = \infty$ (i. e., the curve defined by Eq. IV. D. 2. 5). This approximation will cause the computed value of ΔV_{max} to be somewhat larger than the actual theoretical value, but the resulting error should be small because of the large values of γ in this experiment. The solid curves shown in Fig. 42 are the computer calculations for $\Delta V_{max}/\Delta I_N$ versus $\Delta I_N/I_C$. The curves are truncated for small ΔI_N where γ is not sufficiently large to allow $F(X_2)$ to represent the actual curve for values of X_2 near 1.

The $\gamma = \infty$ curve was obtained from Eq. IV. D. 2. 5 using the following argument. The maximum value of ΔV occurs at $I_J = I_C$ for the dashed

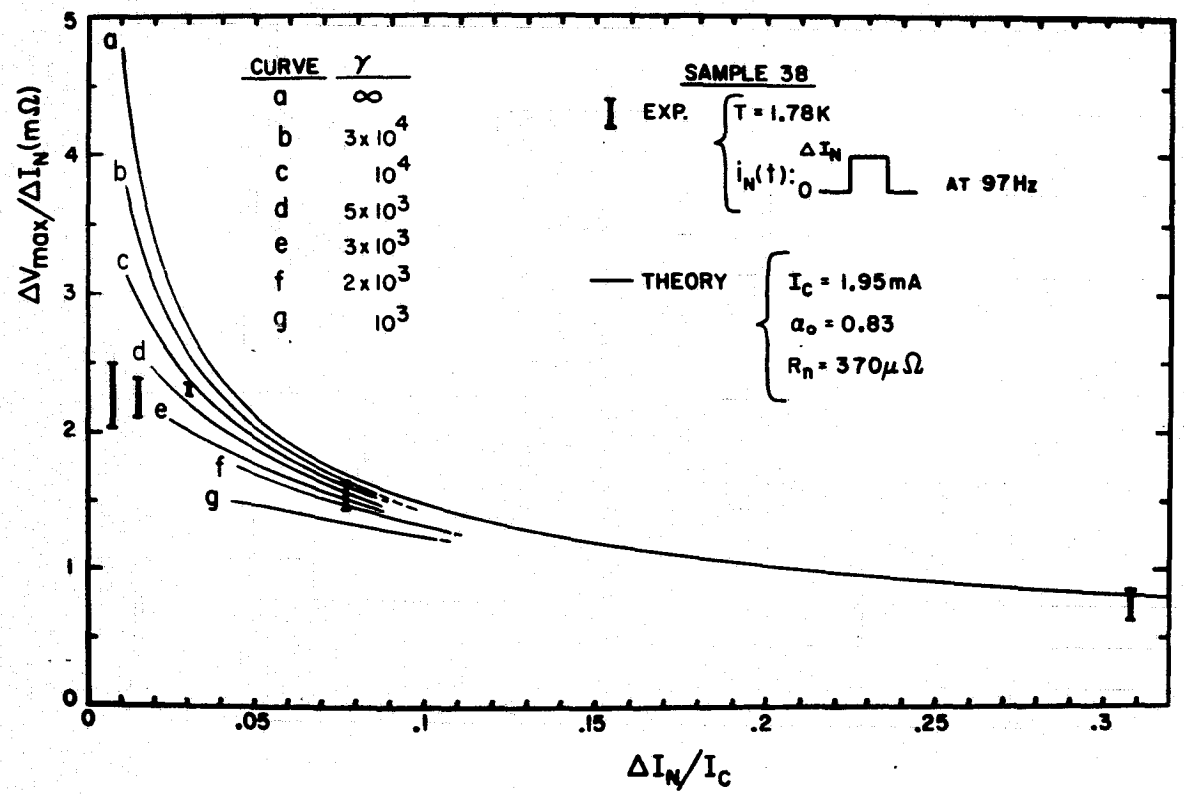

Fig. 42. A comparison of experiment and theory to determine the effect of fluctuations in terms of the parameter γ.

curves of Fig. 41, since varying I_J either above or below this value decreases the value of ΔV. Therefore, for $\gamma = \infty$, the relation for ΔV_{max} can be obtained from Eq. IV. D. 2. 5 with "I_C" replaced by I_{JC} and the value of "$I_J + \alpha_o I_N$" set equal to I_C, resulting in $\Delta V_{max} = R_n (I_C^2 - I_{JC}^2)^{1/2}$. Then using Eq. IV. D. 2. 2, the relation for ΔV_{max} becomes, for $\gamma = \infty$,

$$\Delta V_{max}/\Delta I_N = R_n (2\alpha_o I_C/\Delta I_N - \alpha_o^2)^{1/2}. \qquad \text{IV. F. 2}$$

The data bars in Fig. 42 are obtained by measuring the value of ΔV_{max} from a series of I_J vs V curves for various values of ΔI_N. Since the I_J vs V curve is extremely sharp at $\Delta V = \Delta V_{max}$, the curve is difficult to trace, and the bars indicate the uncertainty in the trace. A best fit in Fig. 42 is obtained for a value of $\gamma \sim 3\text{-}5 \times 10^3$. From Eq. IV. F. 1, this corresponds to an effective noise temperature of ~20-30K.

The final experimental run was conducted in a screened room in order to determine the effects that the ambient r.f. radiation had had on previous samples. A value of γ was obtained for this sample in a manner similar to that for Fig. 42, and the resulting curves are shown in Fig. 43. A best fit of the theory is obtained for $\gamma \sim 10^5$. This corresponds to an effective noise temperature of ~3K!

The results of this section illustrate that, although the cryostat was fairly well shielded, the r.f. radiation still penetrated sufficiently to cause fluctuations at an effective noise temperature of ~20- 30K.

The effective noise temperature for the sample measured in the screened room, however, was only ~3K, and it testifies to the effectiveness of the screened room in shielding the sample from r.f. radiation.

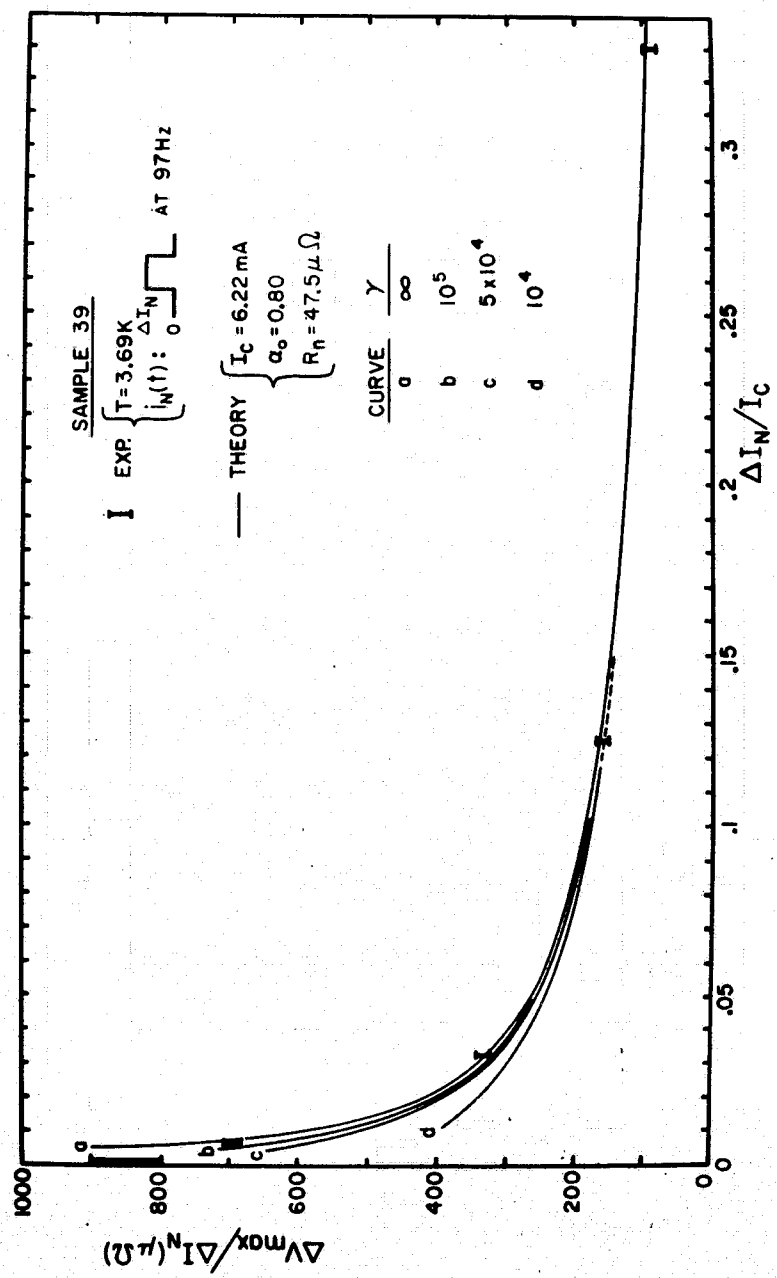

Fig. 43. Determination of γ for the sample in a screened room.

V. CHARACTERISTICS OF THE DEVICE AS A CIRCUIT ELEMENT

V.A. Linear Model, Twoport Characteristics

In this chapter the three-terminal, SNS Josephson device will be considered as a circuit element. It will be shown that under favorable conditions the theory suggests its use as an impedance transformer. Also, it is found that in its present form the device does not provide power gain. The physical realization of a useful device based on the phenomenon studied herein will be left as a subject for future investigation, and the following analyses are presented only to suggest possible device properties and act as a springboard for future study.

The three-terminal SNS device can be treated as a twoport with one of the three terminals common to both the input and output port. One such configuration, called the "common S_a," is shown in Fig. 44a,

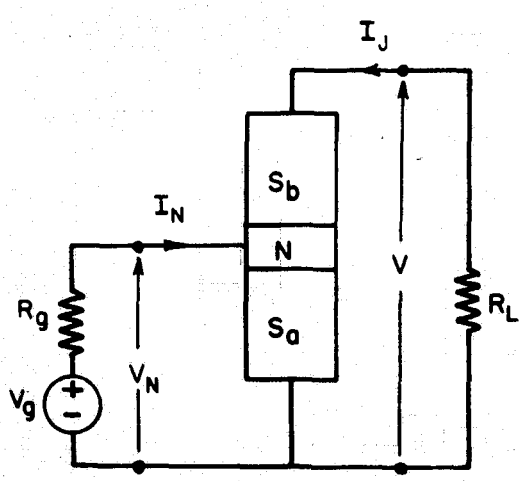

Fig. 44a. An SNS junction in the common-S_a configuration, "forward operation."

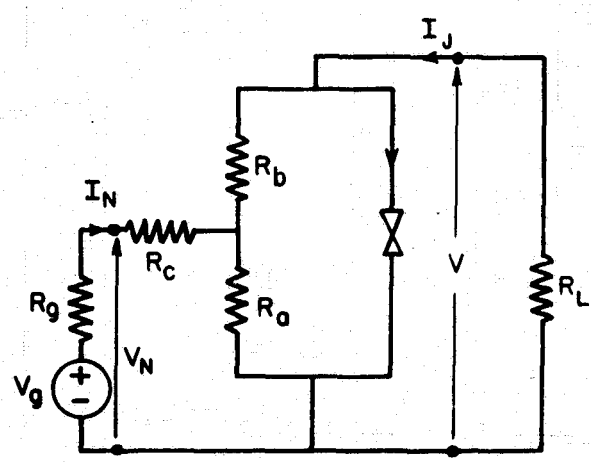

Fig. 44b. Nonlinear equivalent circuit where: $V = R_n[(I_J+\alpha_o I_N)^2 - I_C^2]^{1/2}$.

with the control-current (I_N) port being the input and the junction-current (I_J) port being the output. This and any other configuration having the signal applied across one SN junction will be defined as the "forward" operation. A load resistor, R_L, and a signal generator, V_g, in series with a source resistance, R_g, are also included in Fig. 44a. Figure 44b shows the equivalent low-frequency nonlinear circuit, developed in section IV. D. 2, for the common-S_a configuration.

A linear model can be approximated from Fig. 44b for sufficiently small signals. One such model is the h-parameter representation, which is useful here because the h parameters are readily determined from the experimental curves traced during this investigation. For signals sufficiently small (i. e., a linear approximation), the h parameters may be calculated for the circuit of Fig. 44b, and in the differential limit they are given by

$$(h_{if})_{S_a} = [dV_N/dI_N]_{V=0} = R_c + \alpha_o(1-\alpha_o)R_n \ , \qquad \text{V.A.1}$$

$$(h_{rf})_{S_a} = [dV_N/dV]_{I_N=0} = \alpha_o \ , \qquad \text{V.A.2}$$

$$(h_{ff})_{S_a} = [dI_J/dI_N]_{V=0} = -\alpha_o \ , \qquad \text{V.A.3}$$

$$(h_{of})_{S_a} = [dI_J/dV]_{I_N=0} = F/R_n = r_o^{-1} \ , \qquad \text{V.A.4}$$

where the subscript "f" indicates the forward operation of the device

and $F \equiv \{1 - [I_C/(\alpha_o I_N + I_J)]^2\}^{1/2}$, where $0 \leq F \leq 1$, is a parameter which defines a degree of "normalcy" of the junction. When F=0, the junction current equals the critical value and V=0 (i.e., the junction acts as a superconductor). On the other hand, when F=1, $V = I_J R_n$ and the junction acts ohmic. The resistance r_o is the dynamic output resistance of the device and is defined by Eq. V.A.4 (i.e., r_o^{-1} is the slope of the I_J vs V curve), and $\alpha_o = R_a/R_n$.

The h-parameter equivalent circuit for the common-S_a configuration is shown in Fig. 45. For differential changes in I_N and I_J, F is

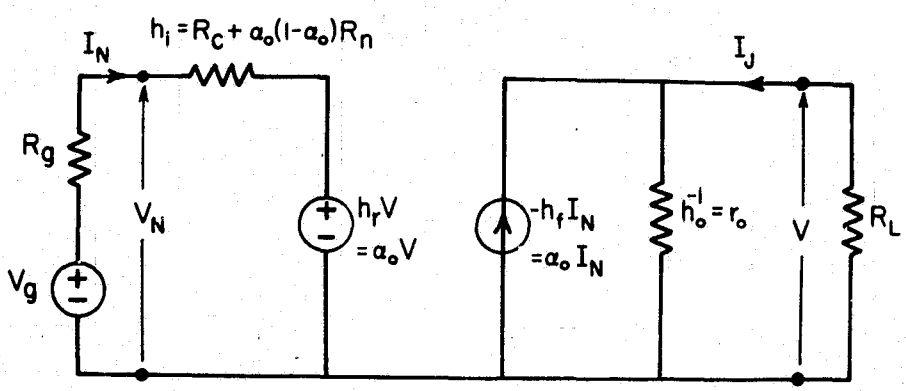

Fig. 45. Linear model for the common-S_a configuration.

constant and the model is linear. The values for the current and voltage output/input transfer ratios and power "gain" can then be calculated from the equivalent circuit of Fig. 45, and they are

$$G_{If} \equiv dI_J/dI_N = \frac{-a_o}{1+R_L/r_o} \quad , \qquad \text{V.A.5}$$

$$G_{Vf} \equiv \frac{dV}{dV_g} = \frac{a_o}{a_o^2+(R_L^{-1}+r_o^{-1})[R_g+R_c+a_o(1-a_o)R_n]} \quad , \qquad \text{V.A.6}$$

and

$$G_{Pf} \equiv |G_{If}G_{Vf}| = \frac{a_o^2}{(1+R_L/r_o)\{a_o^2+(R_L^{-1}+r_o^{-1})[R_g+R_c+a_o(1-a_o)R_n]\}} \quad . \qquad \text{V.A.7}$$

An inspection of Eqs. V.A.5 and V.A.7 reveals that G_{If} and G_{Pf} are always less than unity for this configuration. The voltage transfer ration, G_{Vf}, though, must be considered more carefully.

In the following analyses, several assumptions will be made a priori relating the resistance levels of the device. It should be emphasized that these approximations were not achieved experimentally because of limitations imposed by the available thin-film fabrication setup. However, a discussion of the realizability of these approximations is included in the next section, and there are no fundamental prohibitions on the attainment of these ends. In practice, the severity of these approximations would restrict the usefulness of the device. Therefore, the following theoretical results are to be interpreted as merely suggestive of the possible uses of the phenomenon.

Returning to Eq. V.A.6 for the case of $r_o, R_L >> R_g, R_c, R_n$, the voltage transfer ratio becomes

$$G_{Vf} \approx 1/\alpha_o \quad , \qquad \text{V.A.8}$$

and since $0 < \alpha_o < 1$, the voltage ratio can be greater than unity. A graphical description of the voltage ratio can be seen with the aid of Fig. 46, where a section of the I_J vs V characteristic near the critical-current "knee" is shown for the case of $R_L \sim r_o$. For a sufficiently

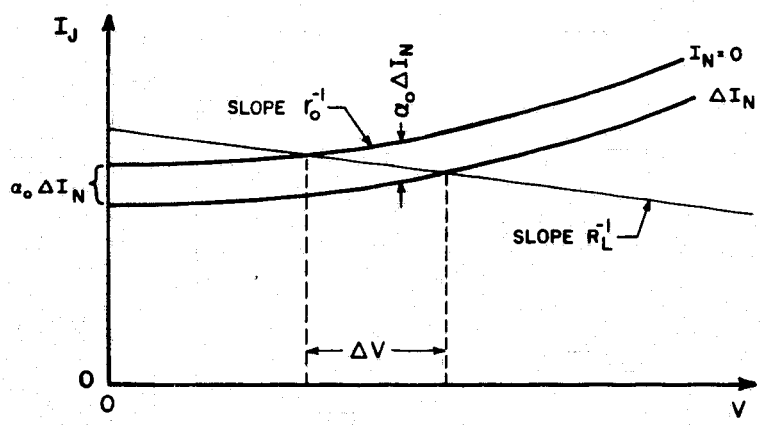

Fig. 46. I_J vs V characteristic near the critical-current knee for $R_L \sim r_o$.

small change, ΔI_N, in the control current, the curves of Fig. 46 may be approximated as linear, and the output voltage change, ΔV, can be obtained from Fig. 46 as $\Delta V = \alpha_o \Delta I_N R_L/(1+R_L/r_o)$. Now, the result of such an input current change, ΔI_N, is also to produce a change in the input voltage of $\Delta V_N = \Delta I_N R_{in}$, where R_{in} is the input resistance,

which may be found from the circuit of Fig. 45 to be

$$R_{in} \equiv [dV_N/dI_N]_{I_J=-V/R_L} = R_c + \alpha_o(1-\alpha_o)R_n + \alpha_o^2 R_L/(1+R_L/r_o). \quad \text{V.A.9}$$

For the approximation of Eq. V.A.8, the input resistance becomes

$$R_{in} \approx \alpha_o^2 R_L/(1+R_L/r_o). \quad \text{V.A.10}$$

Then, an increase ΔI_N in the input current will cause a corresponding increase in the input voltage of

$$\Delta V_N \approx \Delta I_N \alpha_o^2 R_L/(1+R_L/r_o), \quad \text{V.A.11}$$

while causing an increase of $\Delta V \approx \Delta I_N \alpha_o R_L/(1+R_L/r_o)$ in the output voltage. Thus, as in Eq. V.A.8, a smaller value of α_o produces a larger voltage transfer ratio.

Here, it is interesting to note that if the restrictions of Eq. V.A.8 (i.e., $r_o, R_L \gg R_g, R_c, R_n$) were extended to $r_o \gg R_L \gg R_g, R_c, R_n$, then the current ratio of Eq. V.A.5 becomes

$$G_{If} \approx -\alpha_o. \quad \text{V.A.12}$$

Equation V.A.12 also follows from Eq. V.A.8 with the same approximations, because the restriction that $r_o \gg R_L \gg R_g, R_c, R_n$ is simply a statement that the power dissipation within the device and the source be small so that essentially all of the input power is delivered to the

load R_L. That is, $P_{in} \gtrsim P_{out}$ or $|\Delta I_N \Delta V_g| \approx |\Delta I_J \Delta V|$, and with Eq. V.A.8, this results in Eq. V.A.12:

$$|\Delta V/\Delta V_g| \approx |\Delta I_N/\Delta I_J| \approx a_o^{-1}. \qquad \text{V.A.13}$$

Equation V.A.13 (i.e., Eqs. V.A.8 and V.A.12) is characteristic of a transformer with a "turns ratio" of a_o and a small internal dissipation.

From Eq. V.A.10, for $r_o >> R_L$, the input resistance becomes

$$R_{in} \approx a_o^2 R_L. \qquad \text{V.A.14}$$

Thus, the resistance seen by the source is that of the load "transformed" by a factor a_o^2. The output resistance may also be computed, and from Fig. 45 it is given by

$$R_{out} \equiv [dV/dI_J]_{I_N = -V_N/R_g} =$$

$$[R_g + R_c + a_o(1-a_o)R_n]/\{r_o^{-1}[R_g + R_c + a_o(1-a_o)R_n] + a_o^2\}. \qquad \text{V.A.15}$$

For the above approximations, the output resistance becomes

$$R_{out} \approx a_o^{-2}[R_g + R_c + a_o(1-a_o)R_n], \qquad \text{V.A.16}$$

which is a transformation of the source resistance, R_g, plus the internal resistances of the device.

The predicted forward voltage ratio of $\sim a_o^{-1}$, the transformation of

the load resistance to $\sim \alpha_o^2 R_L$, and the increase of the source resistance to a value given by Eq. V.A.16 (which is but a transformation of the source resistance for $R_g >> R_c$) suggests that the common-S_a, three-terminal SNS device could be used as an impedance transformer for the restriction that $r_o >> R_L >> R_g, R_c, R_n$.

If, indeed, the device has the properties of an impedance transformer, it must also exhibit them for operation in the reverse direction. Therefore, the "transformer" ratios should be calculated for the "reverse" operation of the device. Figure 47 shows the SNS device and its equivalent circuit for reverse operation in the common-S_a configuration. The current and voltage transfer ratios as well as the

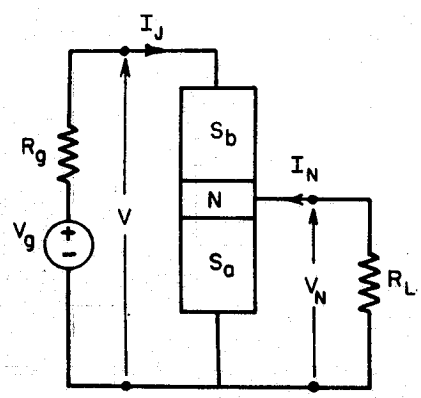

Fig. 47a. An SNS junction in the common-S_a configuration, "reverse operation."

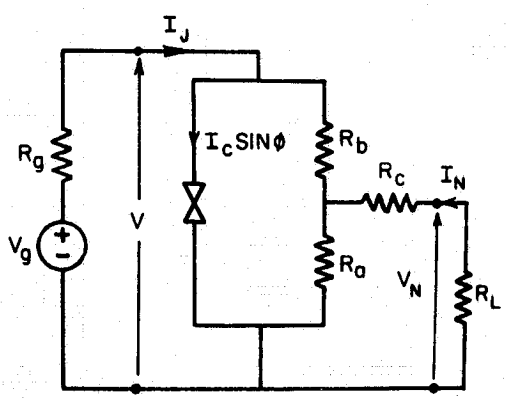

Fig. 47b. Nonlinear equivalent circuit where $V=R_n[(I_J+\alpha_o I_N)^2-I_C^2]^{1/2}$.

power "gain" can be computed for this configuration using Fig. 45 with

the signal source and the load interchanged, and they are given by

$$G_{Ir} = \frac{-a_o}{a_o^2 + r_o^{-1}[R_L + R_c + a_o(1-a_o)R_n]}, \qquad \text{V.A.17}$$

$$G_{Vr} = \frac{a_o}{a_o^2(R_g/R_L) + (1+R_g/r_o)\{1+R_L^{-1}[R_c + a_o(1-a_o)R_n]\}}, \qquad \text{V.A.18}$$

and

$$G_{Pr} = |G_{Ir}G_{Vr}|. \qquad \text{V.A.19}$$

Upon inspection of Eqs. V.A.17-19, it is found that only the current transfer ratio, G_{Ir}, can be greater than unity; and, for the restriction that $r_o \gg R_L, R_c, R_n$, it can be approximated by

$$G_{Ir} \approx -1/a_o. \qquad \text{V.A.20}$$

A graphical explanation similar to that made for Eq. V.A.8 can be made for Eq. V.A.20.

Thus, in theory for the appropriate resistance ratios, the device also exhibits a reverse current transfer ratio greater than unity. The above analysis then suggests that for the circuit shown in Fig. 44, if the conditions that $r_o \gg R_L \gg R_g, R_c, R_n$ are met, in theory the common-S_a device will operate as an impedance transformer with a small but finite dissipation, and the transformation ratio will be $\sim a_o^{-1}$. Although

necessary for large current and voltage ratios, the above restriction on the source and load resistances precludes direct cascading of the devices.

One immediate advantage of this device over the conventional transformer is that no magnetizing current is required, for its operation does not depend upon magnetic flux coupling the input and output circuits. Also, since Josephson devices operate up to the Josephson frequency (Eq. II. B. 3), this device may have the same potential.

The values of R_a and R_b and, hence, $\alpha_o = R_a/(R_a + R_b)$ may be varied by altering the device fabrication procedure (e. g., adding a thin oxide layer); and, as a result, the value of α_o can theoretically be predetermined anywhere in the range $0 < \alpha_o < 1$. Therefore, the upper limit of the transformer ratio, α_o^{-1}, depends upon how small the ratio R_a/R_b can be made.

In addition to the common S_a, two other configurations can be made of the three-terminal SNS device. One is the "common S_b" which, in effect, is the common S_a as shown in Figs. 44 and 47 but with the labels "a" and "b" interchanged. Due to the inherent symmetry of the device, the only difference between the common-S_a and common-S_b configurations is the interchange of values for R_a and R_b, which results in the

interchange of α_o in one case with $1-\alpha_o$ in the other, or vice versa. Thus, for the common-S_b configuration the current and voltage ratios become (from Eqs. V.A.20 and V.A.8)

$$G_{Ir} \approx -1/(1-\alpha_o) \qquad \text{V.A.21}$$

for $r_o \gg R_L, R_c, R_n$, and

$$G_{Vf} \approx 1/(1-\alpha_o) \qquad \text{V.A.22}$$

for $r_o, R_L' \gg R_g, R_c, R_n$. Again, since α_o can in theory be varied over the range $0 < \alpha_o < 1$, the ratios can be maximized through suitable fabrication procedures.

The third possible configuration of the three-terminal device is termed the "common N" and is shown in Fig. 48. Due to the symmetry

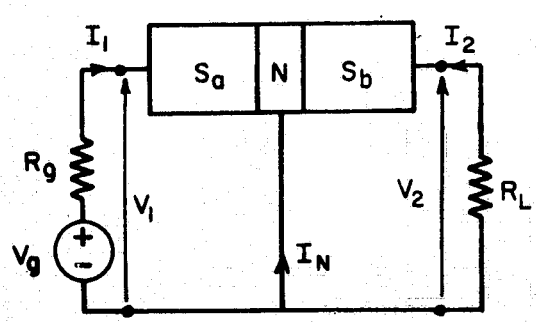

Fig. 48a. An SNS junction in the common-N configuration.

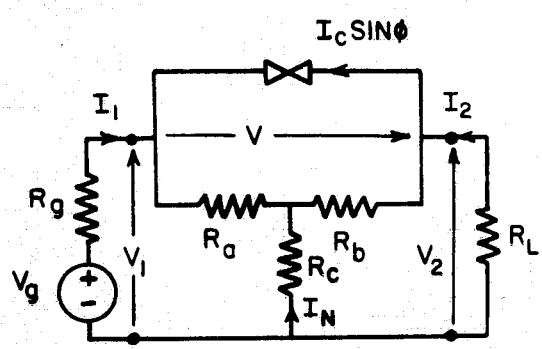

Fig. 48b. Nonlinear equivalent circuit where $V=R_n[(I_2+\alpha_o I_N)^2-I_C^2]^{1/2}$.

of the common-N configuration, the "forward" and "reverse" configurations (i.e., the interchange of S_a and S_b) differ only by the interchange of α_o for $1-\alpha_o$ and vice versa. Therefore, the following are the h parameters and transfer ratios of the common N only for the forward case shown in Fig. 48:

$$(h_{if})_N = [R_c + \alpha_o(1-\alpha_o)R_n]/B, \qquad \text{V.A.23}$$

$$(h_{rf})_N = \{r_o^{-1}[R_c + \alpha_o(1-\alpha_o)R_n] - \alpha_o(1-\alpha_o)\}/B, \qquad \text{V.A.24}$$

$$(h_{ff})_N = -(h_{rf})_N, \qquad \text{V.A.25}$$

$$(h_{of})_N = r_o^{-1}/B, \qquad \text{V.A.26}$$

where $B \equiv (1-\alpha_o)^2 + r_o^{-1}[R_c + \alpha_o(1-\alpha_o)R_n]$; and

$$G_{If} = \frac{\alpha_o(1-\alpha_o) - r_o^{-1}[R_c + \alpha_o(1-\alpha_o)R_n]}{(1-\alpha_o)^2 + r_o^{-1}[R_L + R_c + \alpha_o(1-\alpha_o)R_n]}, \qquad \text{V.A.27}$$

$$G_{Vf} = \frac{-\alpha_o(1-\alpha_o) + r_o^{-1}[R_c + \alpha_o(1-\alpha_o)R_n]}{\alpha_o^2 + (r_o^{-1} + R_L^{-1})[R_c + \alpha_o(1-\alpha_o)R_n]}, \qquad \text{V.A.28}$$

and

$$G_{Pf} \leq 1, \qquad \text{V.A.29}$$

where the current and voltage tranfer ratios have been determined with the assumption that R_g is negligibly small.

For the case that $r_o >> R_L >> R_g, R_c, R_n$, the current and voltage transfer ratios for the forward operation of the common-N become

$$G_{If} \approx \alpha_o/(1-\alpha_o) \qquad \text{V.A.30}$$

and

$$G_{Vf} \approx -(1-\alpha_o)/\alpha_o , \qquad \text{V.A.31}$$

either, but not both, of which can be greater than unity for a particular value of α_o. Again, the transfer ratios would be similar in the reverse case with α_o replaced with $1-\alpha_o$.

Thus, in theory the common-N configuration will also exhibit current and voltage transfer ratios similar to those of a transformer. The transformer ratio of the common-N, though, is smaller than that of the common-S by a factor of α_o.

The tables of h parameters above indicate that for the present device $h_f = -h_r$. This relation defines a reciprocal network*, and it exemplifies the present device symmetry which prohibits power gain. The symmetry results in an internal negative voltage feedback just

---

*defined as a network obeying the reciprocity theorem, e.g., see ref. 82, p. 307.

82. E. Peskin, Transient and Steady-State Analysis of Electric Networks (Van Nostrand, Princeton, N.J., 1961).

sufficient to negate any power gain.

In summary, from the theory developed in section IV.D.2 it is shown that under suitable conditions (i.e., $r_o >> R_L >> R_g, R_c, R_n$) the three-terminal SNS device is expected to have the properties of an impedance transformer with small internal power dissipation. The theory further indicates that the low-frequency, small-signal, transformer "turns ratio" is given by $\sim \alpha_o^{-1}$, which is adjustable through variation of the geometry-dependent parameter $\alpha_o = R_a/R_n$. However, due to the present geometry limitations, no transformer action was observed experimentally. The following section includes a discussion of the realizability of the above restrictions on the device resistances.

V.B. Improvements Necessary for Amplification

Consider an ideal amplifier as a two-port network with the input signal to be amplified supplied in the form of a current, I_N. In order for the amplifier to have high gain, the first requirement to be satisfied is that the input power consumption be as small as possible. This would mean that the resistance, R_{in}, which the current I_N sees at the input terminals be as small as possible. Fundamentally, finite values of R_{in} are unwanted here not only because of diminished power gain but also because of device heating and a possible lowering of its frequency response due to an increase in the input time constant, $R_{in}C$.

Another desirable property would be that I_N pass through the amplifier at least undiminished and exit from a high-impedance output into a moderately high impedance load.

In the case of the forward operation of the common-S_a, three-terminal SNS device, the input signal is in the form of the control current I_N. The input resistance, R_{in}, is a composite of several resistances and is given by Eq. V.A.9. In spite of a superconducting leader film, the experimental value of R_{in} was dominated by the resistance, R_c (see Fig. 35), of the normal-metal film which introduced I_N into the N layer of the SNS junction. Here R_c ($\sim 10^{-2}\Omega$) was large compared to R_n ($\sim 10^{-5}\Omega$) because of the accuracy limitations of metal-mask positioning during the fabrication of the thin-film sandwich. However, photolithographic techniques exist where thin-film patterns can be positioned to accuracies within a few microns.[83] With these methods* then, SNS sandwiches theoretically could be fabricated where R_c was of the order of R_n. For example, if an oxide layer were formed at one of the SN boundaries creating an "SIN" (superconductor/insulator/normal-metal) junction for the purpose of increasing R_b and, thus,

---

* A separation of a few microns between the superconducting input lead and the junction proper would be sufficient to prevent pair tunneling from the I_N lead into the S layers of the SNS device and, hence, preserve the applicability of the model (in particular Eq. V.A.9) to the device.

83. e.g., ref. 48, p. 7-43.

lowering α_o; then R_n would be approximately equal to R_b and, perhaps, increased sufficiently by the oxide layer to be comparable with the value of R_c. Therefore, with α_o small due to $R_b \gg R_a$, the value of R_{in} theoretically could be of the order of R_n (e.g., see Eq. V.A.9 for $R_L \lesssim R_n$ and $r_o \gg R_L, R_n$).

Another method for reducing R_{in} is to form an SNSNS sandwich whereby the center S layer acts as a low-resistance lead. An analysis has not been attempted for this device.

The second requirement for power gain is that the output resistance of the device be as large as possible (i.e., $r_o \gg R_n, R_c$). Ignoring thermal fluctuations (see section II.D.2), the value of r_o theoretically becomes infinite near the critical-current "knee." It should be stressed here that r_o is the slope of the I_J vs V curve, and it can become much larger than R_n; whereas the value of the static output resistance, V/I_J, is always less than or equal to R_n. As discussed in section II.D.1, the slope of the I_J vs V curve can be decreased (thus, increasing r_o) through shunting the junction with a suitable capacitor. Therefore, the dynamic output resistance of the device can be varied but at some expense to the high-frequency response.

In the development of the circuit model in section IV.D.2, it was assumed that the signal frequency, ω_m, was small compared to the Josephson frequency, ω_o (given by Eq. II.B.3). This is not necessar-

ily a "low-frequency" approximation, for $\omega_o = 483\ \mathrm{MHz}/\mu\mathrm{V}$ of junction voltage, and ω_o can be increased by increasing the junction bias voltage (up to a point consistent with the restrictions in section V.A for the transfer ratios to be greater than unity, i.e., $r_o(V) >> R_n$). However, the particular geometry (Figs. 12 and 13) of the SNS device studied here was not designed for high-frequency use, and the low-frequency model was found sufficient for the analysis although, in theory, the device is inherently capable of operating at frequencies approaching ω_o.

The Josephson frequency is a fundamental limitation for quasi-linear operation of the SNS device. Consider an instantaneous voltage across the Josephson junction of $v(t) = V_o + v_s \sin\omega_m t$, where V_o is the d.c. bias voltage and v_s is the amplitude of a signal voltage due to a control current at frequency ω_m. Then, from Eqs. II.B.2 and II.B.6, the Josephson supercurrent density may be written as

$$j_s = j_C \sin[\omega_o t + (\omega_s/\omega_m)\cos\omega_m t] , \qquad \text{V.B.1}$$

where $\omega_o = 2eV_o/\hbar$ and $\omega_s = 2ev_s/\hbar$. Equation V.B.1 is the equation of a frequency-modulated (f.m.) signal of center frequency ω_o and modulation frequency ω_m. Therefore, for signal frequencies sufficiently close to ω_o, the Josephson junction acts as a frequency mixer , thus

precluding its use as a quasilinear amplifier near the Josephson frequency.*

If $\omega_m = \omega_o$, a zero-frequency (d.c.) term will appear in the f.m. supercurrent (Eq. V.B.1); and if the signal is supplied from a constant-current source, the additional supercurrent will be manifested as a constant-voltage current step in the I_J vs V characteristic.[86] These current steps have also been observed in junctions with no external microwave signals but with a small constant magnetic field,[87,88] and they are due to the excitation of the resonant modes of the junction acting as an open-ended, parallel-plate resonator.

As a result, operation of the three-terminal SNS device should be restricted to frequencies well below the Josephson frequency because of the possible distortion of the signal due both to side-band frequencies and current steps in the I_J vs V curve at or near ω_o. The distortion by current steps due to the junction resonant modes can be avoided with a

---

* Josephson junctions have been used as millimeter and submillimeter frequency mixers[84] and microwave sources.[85]

84. P. L. Richards, F. Auracher, and T. VanDuzer, Proc. IEEE 61, 36 (1973).

85. B. T. Ulrich and E. O. Kluth, Proc. IEEE 61, 51 (1973).

86. S. Shapiro, Phys. Rev. Letters 11, 80 (1963).

87. D. N. Langenberg, D. J. Scalapino, B. N. Taylor, and R. E. Eck, Phys. Rev. Letters 15, 294 (1965).

88. B. N. Taylor, J. Appl. Phys. 39, 2490 (1968).

sufficiently small geometry (e.g., a junction length of 0.8mm corresponds to a first-order mode frequency of about 10GHz[88]).

The SNS device in its present form suggests its limited applicability as an impedance transformer. The requirements for a transformer ratio greater than unity have been given ($r_o >> R_L >> R_g, R_c, R_n$), and possible methods for achieving these ends have been suggested. Now, in addition to its characteristics as a transformer, there exists somewhat of a parallel between the SNS device and the bipolar junction transistor in the fact that they are both inherently three-terminal devices which amplify a signal in the form of a current and both have similar output characteristics. The essential change necessary for the SNS device to become such a "superconducting transistor" is to decrease its electrical symmetry, for it is the reciprocity (viz., $h_f = -h_r$) of the present device which prohibits power gain. A design incorporating the asymmetry of an SIN junction might be fundamental to such an amplifying device. A semiconductor analogy of an SIN junction is the tunnel metal-insulator-semiconductor diode,[89] which has a quasiparticle energy band picture similar to that of the SIN junction. The analogy, though, has its limits in that the quasiparticle forbidden band in the superconductor is occupied by Cooper pairs whereas in the semiconductor it is empty, with the possible exception of impurity levels.

---

89. for a description see S. M. Sze, Physics of Semiconductor Devices (Wiley, N. Y., 1969), p. 487.

Fisher and Giaever[90] have observed a small rectifying effect (i.e., electrical asymmetry) in an Al-Al_2O_3-Al junction at T = 77K which they attribute to possible electron donor states in the Al layer near the interface where the oxide was grown. However, when a similar tunneling experiment[91] was done on an SIN (Pb-Al_2O_3-Al) junction at temperatures below the transition point of the superconductor (Pb), no rectification was observed in the current-voltage curves. This might have been due to the "freezing out" of conduction electrons from the donor states at the lower temperatures; and if so, the electrical asymmetry of the SIN junction theoretically could be accomplished through a suitable metallurgical choice of the N and oxide layers so as to produce shallow donor energy levels, for it has been shown[92] that GaAs junction transistors can operate at 4K using very shallow impurity-level dopants.

Additional evidence of the electrical asymmetry of an SIN junction has recently been reported by Clarke.[37] He observed that the pair-quasiparticle potential difference in a nonequilibrium superconductor depended upon whether electrons were injected into or extracted from a superconductor by means of an SIN tunnel junction. The effect was

---

90. J.C. Fisher and I. Giaever, J.Appl.Phys. 32, 172 (1961).
91. I. Giaever, Phys.Rev.Letters 5, 147 (1960).
92. see ref. 89, p.295.

attributed to the asymmetry of the electron density of states at the Fermi level.

The geometry of the SNS devices in this investigation was such that $W, L \gg \xi_N, t_N$, where W and L are the width and length of the junction, t_N is the thickness of the normal metal, and ξ_N is the coherence length in the normal metal. If the size of the junction were to be reduced such that $W, L \sim \xi_N, t_N$, then the flow pattern of I_N would spread across the entire junction (as contrasted with the present case where $\ell_N, t_N \ll W, L$ and, as suggested in Fig. 36, I_N spreads little across the area of the junction). The SNS device with this proposed geometry would appear more analogous to the junction transistor since there would be two types of charge carriers (viz., pairs and quasiparticles) "interacting" across the barrier region.

VI. CONCLUSIONS

This investigation was initiated as a result of the discovery by H. Meissner and R.R. Rockefeller[3] of the control of the SNS Josephson junction with a current introduced directly into the N layer, and it has led to an understanding of the physical mechanisms and electrical characteristics of the thin-film device, in particular its potential as an amplifier.

The three-terminal SNS device is essentially a two-terminal Josephson junction with an additional electrical terminal for the introduction of a control current directly into the N layer. Its operation as a Josephson junction in the two-terminal mode was ascertained through the excellent agreement of the experimental I_J vs V curves with the theory of Stewart[40] and the observation of the characteristic sin(H)/H variation of the Josephson critical current, I_C, with magnetic field.

Although strictly valid only near T_C, the theory describing the temperature dependence of I_C for the "dirty" limit was found experimentally to be valid even near $T_C/2$. This supports the findings of Clarke[24] whose results were somewhat masked by the presence of self-field limiting at the lower temperatures. The SNS junctions in the present investigation, however, suffered little or no self-field limiting, because, in general, the junctions had relatively high

normal resistances, R_n, which reduced their critical currents. The large values of R_n were due primarily to the oxidation of the initial tin (S) film deposited prior to the gold (N) layer.

When a control current, i_N, was introduced directly into the N layer, the I_J vs V characteristics were displaced along the I_J axis in a manner described by an empirical parameter α_o. These results support the findings of Rockefeller[4] who made similar observations on crossed-wire SNS junctions.

Experimentally, α_o was found to depend upon the resistances R_a and R_b of the two halves of the N layer as $\alpha_o = R_a/(R_a + R_b)$, where $R_a + R_b = R_n$. The measured values of α_o were typically ~ 0.8, with $R_a > R_b$ due to the aforementioned oxide layer. Since the values of R_a and R_b can be adjusted through changes in the fabrication procedure, the value of α_o can be predetermined anywhere in the range $0 < \alpha_o < 1$. The value of α_o was found to be essentially constant with variations in i_N and H and have only a weak dependence on T (as did R_n).

The following low-frequency, lumped, nonlinear model based on that of Stewart[40] and McCumber[41] was proposed for the three-terminal device:

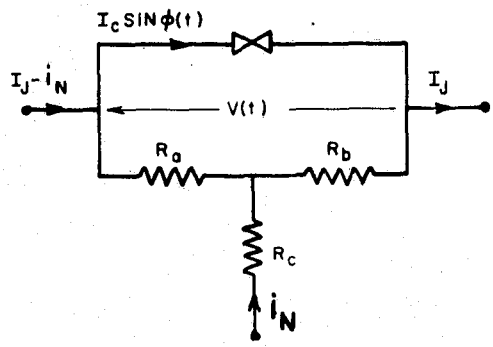

The equation

$$V = R_n[(I_J + a_o i_N)^2 - I_C^2]^{1/2},$$

which characterizes the current-voltage relationship of the device, was derived from the above model for signal frequencies well below the Josephson frequency; and it was found to be in excellent agreement with the experimental results for low-frequency variations of the control current.

A method peculiar to the three-terminal SNS device was developed to plot the dynamic junction resistance, r_o, versus I_J. With this method it was illustrated that the device could operate at signal frequencies of at least 9.7kHz, which was the limit of the lock-in amplifier. Despite (a) the low-frequency assumption implicit in the above equation and (b) the fact that no attempt was made to design the SNS geometry for high-frequency use, the data at 9.7kHz was adequately described by the equation cited above.

A small-signal linearized analysis of the device suggests its use as an impedance transformer. However, due to the limitations of the present setup for fabricating the thin-film junctions, the input resistance of the device was dominated by the relatively large I_N-lead resistance, R_c; and the resulting output/input current and voltage ratios of the present device are much less than unity in either direction of operation. In theory, though, with a suitable geometry, R_c can be reduced to of the order of R_n, which will permit the transformer ratio of the device to be approximated by α_o^{-1}. Therefore, large transformer ratios are theoretically possible through minimization of the geometry-dependent parameter α_o.

The present device is a reciprocal twoport (i.e., $h_r = -h_f$), and power gain is prohibited as a consequence of the symmetry. It is felt that power gain might eventually be obtainable through suitable metallurgical and geometrical designs.

The theoretical upper frequency limit of the SNS device as a quasi-linear transformer or "superconducting transistor" is given by the Josephson frequency, $\omega_o = 2eV/\hbar = 483\,\mathrm{MHz}/\mu\mathrm{V}$ of junction voltage.

Originally, it was intended to vapor-quench the thin-film sandwiches onto a 4K substrate and then measure them in situ in order to minimize the interdiffusion between metal laminae. However, during the course of the experiment several limitations became apparent and

the films were eventually vapor deposited onto a 300K substrate. Although some interdiffusion surely occurred with this method, it was accounted for by describing the N layer with an empirical coherence length, $\xi_{Neff.}$.

During the experiments on some of the early samples, the Josephson junction was rendered inoperable by the transition of one or both of the S films to the normal state due to I_J exceeding a critical value. A separate experiment showed that the presence of the N metal reduced the tin critical current somewhat (the proximity effect). As a result of these findings, the gold (N) layer was alloyed with copper to reduce its effect on the tin. The S layer was also thickened, and the critical current of the tin was no longer exceeded.

BIBLIOGRAPHY

1. H. Meissner and F. Bedard, Phys. Rev. 101, 126 (1956).
2. H. Meissner, Phys. Rev. 109, 686 (1958).
3. H. Meissner and R. R. Rockefeller, U.S. Patent No. 3,689,780, Sept. 5, 1972.
4. R. R. Rockefeller, Ph. D. thesis, Stevens Institute of Technology, unpublished (1970).
5. H. K. Onnes, Leiden Comm. 122b, 124c (1911).
6. H. K. Onnes, Leiden Comm., Suppl. No. 34 (1913).
7. F. B. Silsbee, J. Wash. Acad. Sci. 6, 597 (1916).
8. W. Meissner and R. Ochsenfeld, Naturwiss. 21, 787 (1933).
9. F. London and H. London, Proc. Roy. Soc. (London) A149, 71 (1935).
10. C. Gorter and H. B. G. Casimir, Physica 1, 306 (1934).
11. D. Shoenberg, Proc. Roy. Soc. (London) A175, 49 (1940).
12. A. B. Pippard, Proc. Roy. Soc. (London) A216, 547 (1953).
13. A. B. Pippard, Proc. Roy. Soc. (London) A203, 210 (1950).
14. J. Bardeen, L. N. Cooper, and J. R. Schrieffer, Phys. Rev. 108, 1175 (1957).
15. E. A. Lynton, Superconductivity (Methuen, London, 1964), p. 46.
16. Ibidem, p. 38.
17. e.g., T. E. Faber and A. B. Pippard, Proc. Roy. Soc. (London) A231, 336 (1955).
18. V. L. Ginzburg and L. D. Landau, Sov. Phys.-JETP 20, 1064 (1950).
19. P. G. deGennes, Superconductivity of Metals and Alloys (Benjamin, N. Y., 1966), p. 225.
20. e.g., for a detailed explanation see D. J. Scalapino, Tunneling Phenomena in Solids, ed. by E. Burstein and S. Lundqvist (Plenum, N. Y., 1969), p. 477-8.
21. for a discussion of the quasiparticle concept see C. Kittel, Quantum Theory of Solids (J. Wiley, N. Y., 1963), p. 84.
22. L. P. Gorkov, Sov. Phys.-JETP 10, 593, 998 (1960).

23. H. Meissner, Phys. Rev. 117, 672 (1960).

24. J. Clarke, Proc. Roy. Soc. A308, 447 (1969).

25. P. G. deGennes, Rev. Mod. Phys. 36, 224 (1964), p. 227.

26. G. Deutscher and P. G. deGennes, Superconductivity, ed. by R. D. Parks (Marcel Dekker, Inc., N. Y., 1969), p. 1006.

27. P. G. deGennes and E. Guyon, Phys. Letters 3, 168 (1963), p. 169.

28. see ref. 19, p. 233.

29. see ref. 25, p. 231.

30. N. R. Werthamer, Phys. Rev. 132, 2440 (1963).

31. B. D. Josephson, Phys. Letters 1, 251 (1962).

32. e.g., see J. Clarke, Proc. IEEE 61, 8 (1973).

33. P. W. Anderson, Rev. Mod. Phys. 38, 298 (1966).

34. B. D. Josephson, Rev. Mod. Phys. 36, 216 (1964).

35. e.g., see ref. 19, p. 238.

36. P. W. Anderson and J. M. Rowell, Phys. Rev. Letters 10, 230(1963).

37. J. Clarke, Phys. Rev. B. 4, 2963 (1971).

38. R. A. Ferrell and R. E. Prange, Phys. Rev. Letters 10, 479 (1963).

39. A. M. Goldman and P. J. Kreisman, Phys. Rev. 164, 544 (1967).

40. W. C. Stewart, Appl. Phys. Letters 12, 277 (1968).

41. D. E. McCumber, J. Appl. Phys. 39, 3113 (1968).

42. W. C. Scott, Appl. Phys. Letters 17, 166 (1970).

43. P. K. Hansma, G. I. Rochlin, and J. N. Sweet, Phys. Rev. B 4, 3003 (1971).

44. Y. M. Ivanchenko and L. A. Zil'berman, Sov. Phys. -JETP 28, 1272 (1969).

45. V. Ambegaokar and B. I. Halperin, Phys. Rev. Letters 22, 1364 (1969).

46. National Bureau of Standards Monograph 10 (June 1960).

47. P. L. Kapitza, Sov. Phys. -JETP 5, 59 (1941).

48. L. I. Maissel and R. Glang, Handbook of Thin Film Technology (McGraw-Hill, N. Y., 1970), p. 2-10

49. Ibidem, p. 2-53.

50. P.M. Chirlian, V.A. Marsocci, H.W. Phair, and W.V. Kraszewski, Rev. Sci. Instr. 35, 1718 (1964).

51. e.g., Metals Handbook (American Society for Metals, Ohio, 1961), Vol. 1.

52. Properties of Materials at Low Temperatures - A Compendium, ed. by V. Johnson (Pergammon, N.Y., 1961).

53. J.R. Clement, E.H. Quinnell, M.C. Steele, R.A. Hein, and R.L. Dolecek, Rev. Sci. Instr. 24, 545 (1953).

54. see ref. 48, p. 6-38.

55. W.F. Koehler, J. Opt. Soc. Amer. 43, 739 (1953).

56. R.F. Duffy, Ph.D. thesis, Stevens Institute of Technology, 1964 (unpublished).

57. K. Fuchs, Proc. Cambridge Phil. Soc. 34, 100 (1938).

58. E.H. Sondheimer, Adv. Phys. 1, 8 (1952).

59. H. Mayer, Structure and Properties of Thin Films (Wiley, N.Y., 1959), p. 225.

60. D.K.C. MacDonald, Encyl. Phys., XIV (Springer-Berlin, 1956), p. 188.

61. M.H. Jacobs, D.W. Pashley, and M.J. Stowell, Phil. Mag. 13, 129 (1966).

62. H.L. Caswell, J. Appl. Phys. 32, 105 (1961).

63. W. Buckel and R. Hilsch, Z. Physik 138, 109 (1954).

64. J.M. Lock, Proc. Roy. Soc. (London) A208, 391 (1951).

65. J.W. Garland, K.H. Bennemann, and F.M. Mueller, Phys. Rev. Letters 21, 1315 (1968).

66. see ref. 48, p. 22-9.

67. J.A. Mydosh and H. Meissner, Phys. Rev. 140, A1568 (1965).

68. H.L. Phillips and H. Meissner, Phys. Rev. B 5, 3572 (1972).

69. J. Bardeen, Rev. Mod. Phys. 34, 667 (1962).

70. T.K. Hunt, Phys. Rev. 151, 325 (1966).

71. T. Yamashita and Y. Onodera, J. Appl. Phys. 38, 3523 (1967).

72. M. L. Yu and J. E. Mercereau, Phys. Rev. Letters 28, 1117 (1972).

73. J. Clarke, Phys. Rev. Letters 28, 1363 (1972).

74. T. J. Rieger, D. J. Scalapino, and J. E. Mercereau, Phys. Rev. Letters 27, 1787 (1971).

75. M. Tinkham and J. Clarke, Phys. Rev. Letters 28, 1366 (1972).

76. S. Dushman, Scientific Foundation of Vacuum Technique (Wiley, N. Y., 1949), p. 17.

77. J. G. Sheperd, Proc. Roy. Soc. (London) A326, 421 (1972).

78. A. F. Andreev, Sov. Phys. -JETP 19, 1228 (1964).

79. e. g., ref. 19, p. 124.

80. W. L. McMillan, Phys. Rev. 175, 559 (1968).

81. A. B. Pippard, F. R. S., J. G. Shepherd, and D. A. Tindall, Proc. Roy. Soc. (London) A324, 17 (1971).

82. E. Peskin, Transient and Steady-State Analysis of Electric Networks (Van Nostrand, Princeton, N. J., 1961).

83. e. g., ref. 48, p. 7-43.

84. P. L. Richards, F. Auracher, and T. VanDuzer, Proc. IEEE 61, 36 (1973).

85. B. T. Ulrich and E. O. Kluth, Proc. IEEE 61, 51 (1973).

86. S. Shapiro, Phys. Rev. Letters 11, 80 (1963).

87. D. N. Langenberg, D. J. Scalapino, B. N. Taylor, and R. E. Eck, Phys. Rev. Letters 15, 294 (1965).

88. B. N. Taylor, J. Appl. Phys. 39, 2490 (1968).

89. for a description see S. M. Sze, Physics of Semiconductor Devices (Wiley, N. Y., 1969), p. 487.

90. J. C. Fisher and I. Giaever, J. Appl. Phys. 32, 172 (1961).

91. I. Giaever, Phys. Rev. Letters 5, 147 (1960).

92. see ref. 89, p. 295.

ACKNOWLEDGEMENTS

This is a brief attempt to acknowledge those many wonderful sources of fiscal, scientific, and psychic support rendered me during the course of this investigation. In particular, I am indebted to Professor Hans Meissner for his guidance which allowed me to obtain an invaluable perspective on far more than is contained within the covers of this dissertation. I should also like to thank the National Aeronautics and Space Administration for its contract support and the Electrical Engineering and Physics departments for the use of their facilities. A grateful acknowledgement must also be included here for the mechanical expertise and enthusiastic encouragement of Gunther Wirth and Walter Kraszewski. Lastly... thank you, Mother Nature, for whispering a few of your secrets into my ear during those long, cold nights with my cryostat.